ECOspec

Microplastic Identification with Raman Spectroscopy

Group 6 Members:

Sophia Adams	Landon Morjal	Logan Sullivan	Michael Rusinko
PSE	*CPE*	*CPE*	*PSE/EE*

Review Committee:

Dr. Justin Phelps	*ECE*
Dr. Suboh Suboh	*ECE*
Dr. Kathleen Richardson	*CREOL*
Dr. Arelis Colòn	*Mentor at Ocean Optics*

Advisors:

Dr. Aravinda Kar	*CREOL*
Dr. Sreeram Sundaresh	*ECE*

List of Tables

List of Figures

1. Executive Summary

Environmental contamination from microplastics has become a critical global issue. Plastics are produced at enormous scales and break down into small particles that spread throughout ecosystems and water supplies. These particles are now found in drinking water, food, soil, atmospheric dust, and even in human blood. Their long-term health effects are not fully understood, but studies already suggest possible harm to cells, organs, and hormonal systems. Detecting and identifying microplastics in water is therefore an important step toward understanding their impact and reducing exposure.

ECOspec is a compact Raman spectroscopy system designed to identify microplastics suspended in water with minimal sample preparation. The device incorporates a 785 nm laser, Raman filtering optics, a custom Czerny Turner spectrometer, and an electronic control system that manages data acquisition, temperature control, and safety interlocks. By collecting Raman spectra from particles inside a quartz cuvette, the system can determine whether microplastics are present.

The project's motivation comes from the limitations of current microplastic detection methods. Manual inspection through microscopy is slow and prone to human error. Traditional burn testing can differentiate plastic types but destroy the sample. Raman spectroscopy avoids these issues by providing non-destructive, chemically specific measurements based on the vibrational structure of molecules. Because plastics have well-defined Raman fingerprints, they can be reliably identified even when broken into small fragments.

The ECOspec system is designed around several major subsystems. The optical subsystem includes laser illumination, beam conditioning, microscope objectives, filtering, and light collection into the spectrometer. The electrical subsystem provides control through an ESP32 main controller and a CCD module. Supporting circuitry handles power regulation, cooling, laser control, and safety features. The software subsystem performs spectral calibration, preprocessing, filtering, and comparison against a reference library of plastic fingerprints. A simple graphical interface presents results to the user and could later support identification, concentration estimation, and data logging.

The system has clear goals for performance and capability. The basic goals include collecting Raman spectra from PET, polystyrene, and nylon samples larger than five millimeters, and later from microplastic pieces under five millimeters. Advanced goals expand to identify polymer type and detect particles as small as five hundred micrometers. Stretch goals outline future improvements such as support for mixed plastic samples, environmental water testing, real-time monitoring, and multi-wavelength excitation for improved fluorescence suppression.

To support these goals, the design also includes detailed specifications. These include a spectral resolution below two nanometers per pixel, integration times under forty seconds, and system temperatures below 44° C. The optical system must capture Raman shifts from

zero to thirty-two hundred inverse centimeters to cover key fingerprint regions for all three target polymers. Mechanical constraints limit the device's footprint so that it remains a compact bench-top system.

The team has also conducted extensive research into previous senior design projects, Raman spectroscopy literature, enthusiast builds, and commercial approaches. This review highlights common challenges such as detector cooling, fluorescence suppression, optical alignment, and electronic noise. Lessons from earlier projects guided the decision to use a 785 nm excitation source, infinity corrected microscope optics, long pass filtering rather than notch filtering, and a crossed Czerny Turner spectrometer layout for improved aberration control.

ECOspec has potential applications in environmental science, laboratory water quality assurance, industrial discharge monitoring, and even consumer safety. Municipalities could use the device to monitor water treatment systems. Research labs could verify water purity before experiments. Field teams could take measurements at lakes, rivers, and coastal areas to track pollution hotspots. Long-term development may lead to larger fixed installations for continuous monitoring or smaller portable versions for field work.

Overall, the ECOspec project aims to produce a reliable and accessible system for detecting and identifying microplastics in water. By combining proven optical engineering principles with practical design choices, the system addresses a growing environmental need and lays out the groundwork for future improvements in microplastic analysis.

2. Project Narrative

2.1. Project Motivation and Background

Annual production of plastic has increased rapidly since the first synthetic plastic was produced in 1907. In 2024, 413.8 million tons of plastic was produced globally. 2 million of those tons end up in our ocean, and 52 tons end up as environmental pollution [1]. One of the side effects of this plastic waste is microplastic (MP) pollution in our ecosystems. Even though these tiny plastic particles seem small, less than 5 millimeters in size, they pose a major environmental and health crisis that requires their detection [2]. Humans consume an estimated 74,000 microplastic particles a year, and its impact on our health is just beginning to be understood [3].

Microplastics are typically manually analyzed with microscopes or burn tests. This process is time consuming, leaves room for human error in visual identification, and in the case of the burn test, destroys the sample of interest. A spectroscopic measurement of a given plastic sample is a reliable method of determining its chemical composition. A type of reliable chemical identification spectroscopy is a technique called Raman spectroscopy. Raman analyzes the shifts in frequency that occur when a sample is excited with incident laser light. Raman allows for high specificity of analysis, minimal sample preparation, and is non-destructive. Certain materials are associated with unique Raman fingerprint spectra that allow them to be identified from other materials. Plastics are one such material.

Each type of plastic, ranging from PET water bottles to EPS from styrofoam, is associated with a unique Raman spectrum. This unique Raman spectrum is a consequence of the materials' molecular and atomic structures.

2.1.1. The Concept of ECOspec

ECOSpec is a compact, pre-packaged microplastic detection system that contains a laser excitation source, spectrometer, and Raman filtering components. The user can introduce a sample of interest into the system and will receive a live Raman spectrum. This configuration enables the acquisition of characteristic Raman spectra, which allows for the precise identification of microplastic polymer types based on their unique Raman fingerprint. Therefore, not only will the device tell the user if microplastics are detected, It will also provide the type of microplastic.
ECOspec would be useful for real-world applications on a large scale. Numerous companies, governments, and research facilities would benefit from having their water noninvasively analyzed for microplastics and other harmful materials. Public health can easily be compromised if water is not monitored or maintained. ECOSpec allows for a non-intrusive method to identify and characterize plastics that could be found in consumable products or drinking water. It has value in both consumer safety and regulations put in place by different agencies. Governments at all levels would benefit by using ECOspec for analysis of plastic contamination, whether it be in large water sanitation plants or small measurement stations implemented in residential buildings.

ECOspec could also be implemented at research facilities. Many labs require a certain level of purified water as the impurities in tap water could interfere with experiments and compromise results. Allowing a water source to be monitored by ECOspec would increase confidence that the purity of water in a lab is at a sufficient level. On the other hand, it could also be used by labs to research microplastics and problems caused by microplastics.

ECOspec would also be perfect for environmental water monitoring where it would detect and identify microplastics in natural water sources such as lakes, rivers, and oceans. This ability allows for pollution tracking and efforts for remediation once hotspots of contamination are located. Additionally, involving ECOspec with monitoring output of runoff and discharge from operations such as farming, plants, industrial facilities, and urban/residential areas is beneficial. Many of these produce and then introduce harmful chemicals and materials to natural water ways, damaging ecosystems.

2.2. Project Background Research

2.2.1. Environmental and Health Impact of Microplastics

Throughout history, toxic materials have been used in a wide variety of products that were commonly in close physical proximity to humans and other living creatures. Some of these

more well-known materials are lead, arsenic, and plastic. In modern times society has pushed a lot of effort into removing arsenic and lead from our environments, but there has been little pushback against plastic in comparison. Movements to remove plastic straws and bags from select areas have been popular in recent years, but they are largely limited to small areas in cities or natural parks.

Plastics are a convenient material. They do not break down easily, are resistant to many chemicals, and are hydrophobic. Overall, they provide a platform for mass production of material with desirable properties that are widely customizable for a wide range of applications and are otherwise not found in nature.

But for these very reasons, plastics are actively contributing to a decline in human and general environmental health. While they do not break down easily in bulk, plastic items are almost constantly leaving behind micro and nano plastics. These tiny particles of plastic, over the decades of their increasing prevalence, have become extremely pervasive. They are estimated to have touched almost every point on Earth. Microplastics are found in city water supplies, plants in fields miles from civilization, food, human blood, and even snow samples in Antarctica [4].

Microplastics are suspected to be toxic to the human body when built up in large quantities. They have been found to cause cell death and disturb the cellular reproduction cycle [5]. There have also been multiple studies on the adverse effects of microplastics on hormones, the thyroid, and reproductive organs of mammals in general [6].

2.2.2. Principles of Raman Spectroscopy

Raman spectroscopy is a measurement technique that is often used for material identification. This is enabled by the principles of Rayleigh and Raman scattering. Rayleigh scattering is the most common type of scattering and defines the scattered photon to have the same frequency (energy) as the incident photon. Raman scattering occurs at roughly every 100,000,000 interactions and defines the scattered photon to have a shifted frequency (energy) from the incident photon [8].

The Rayleigh cross section describes a material's tendency to scatter light. As seen in Figure _, the value of the cross section is related to the inverse of the wavelength raised to the fourth power. Thus, the intensity of scattering is related to the fourth power of the wavelength.

Cross Section of Rayleigh Scattering

$$\left(\frac{d\sigma_{ss}}{d\Omega}\right)_{Rayleigh} = \frac{4\pi^2(ni-1)^2}{N^2\lambda^4} \tag{2.1}$$

Cross Section of Raman Scattering

$$\left(\frac{d\sigma}{d\Omega}\right)_{Raman} = 10^{-3} \cdot \left(\frac{d\sigma}{d\Omega}\right)_{Rayleigh} \quad (2.2)$$

There are two outcomes for Raman scattering: Stokes and Anti-Stokes scattering. In stokes scattering, the frequency of the scattered photon experiences a reduction in frequency (loss of energy), which is perceived as an increase in wavelength. In Anti-Stokes scattering, the frequency of the scattered photon experiences an increase in frequency (gain in energy), which is perceived as a decrease in wavelength.

In a typical Raman spectrometer system, the laser spot size is minimized to focus all the optical power to as small as possible. This increases the likelihood of generating and receiving a Raman signal in the precisely selected area, increasing the confidence of obtaining a true Raman spectra associated with a known material.

2.2.3. Advantages for Microplastic Analysis

Plastic molecules are organic molecules. They are molecules made of a chain of hydrocarbons. They have unique geometries and unique energy levels associated with them. These unique molecular structures and properties give plastics unique Raman spectra associated with each type. Because plastics have uniquely identifiable Raman spectra, it is logical to conclude plastics are easily identifiable with Raman spectroscopy [9]. From polyethylene terephthalate (PET) in water bottles to expanded polystyrene (EPS) in styrofoam, the plastics commonly used in modern light each have unique Raman spectra.

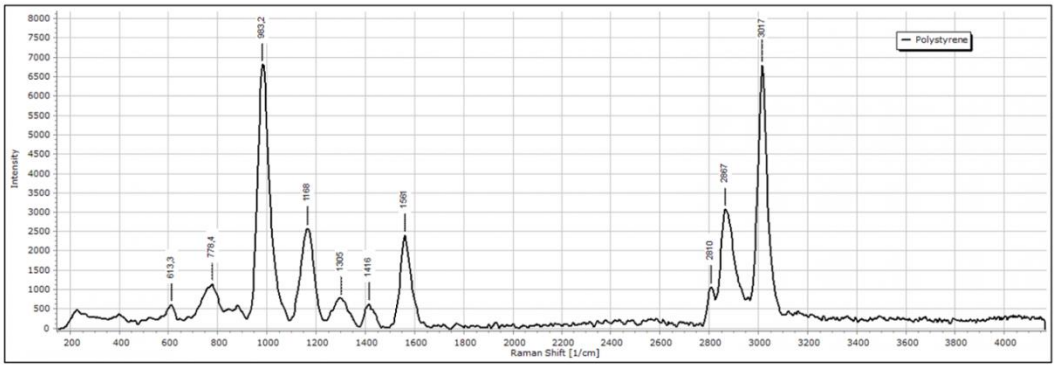

Figure 1 Expected Raman Spectra, Polystyrene

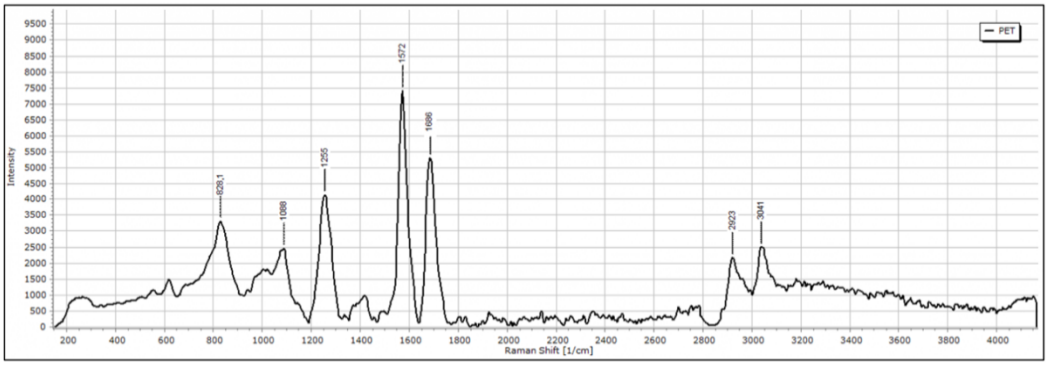

Figure 2 Expected Raman Spectra, Polyethylene Terephthalate (PET)

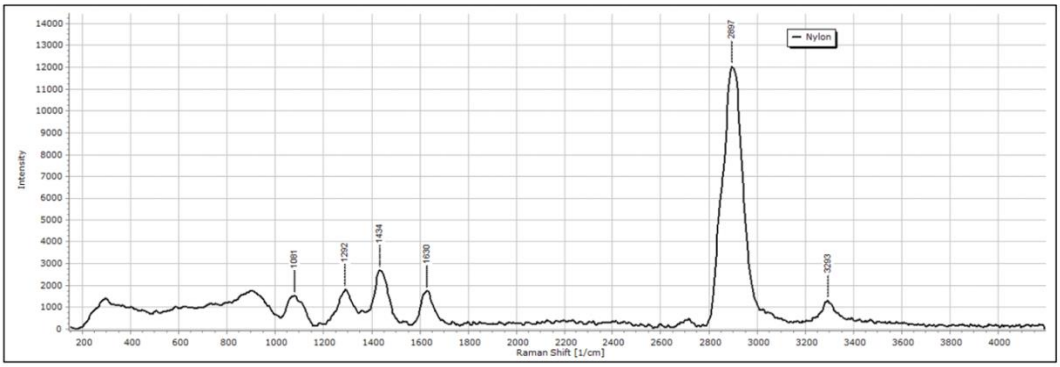

Figure 3 Expected Raman Spectra, Nylon

2.2.4. Spectrometers

Spectrometers are instruments that measure how light is dispersed across different wavelengths. It takes incoming light, separates that light into its component wavelengths, and measures each wavelength intensity. There are many different types of spectrometers including prism, diffraction grating, Fourier transform, Raman, mass, and miniature spectrometers. These broad classes mainly differentiate between how the light is being dispersed, and its application. The first spectrometer was a prism spectrometer built in 1802, where sunlight was focused through a slit, and sent through a prism. Prism spectrometers use a glass or quartz prism to refract and disperse the light into different wavelengths. It is historically important and simple in design, but it has a few limitations, such as nonlinear dispersion through the prism, and typical low resolution. Diffraction grating spectrometers use an optical component that has thousands of grooves that separate light into its component wavelengths by the principles of diffraction. Each wavelength is diffracted at a different angle, which creates the different intensities at each wavelength. Using a diffraction grating over a prism for dispersion can be beneficial because a higher resolution is possible with a uniform wavelength separation. Complications include straylight from other diffraction orders and the complex design which requires precise alignment. Fourier transform spectrometers use interferometry to measure all the wavelengths at once, and then a Fourier transform is applied to extract the spectrum. It provides a very high resolution, and high throughput, but it requires moving mirrors, which

complicates the design, and it won't work well for a demonstration because of its sensitivity to vibrations.

2.3. Existing Project/Past project/prior related work

2.3.1. Previous Senior Design Projects

2.3.1.1. TEXRAY

TEXRAY was a previous Raman spectroscopy system used for analysis of different types of fabrics. The goal was to utilize machine learning to match collected Raman spectra to previously confirmed datasets. The team used a 532 nm laser as a light source, basic optical components to focus and collect the light, a lens-grating-lens (LGL) spectrometer layout to separate the light, and a charge coupled device (CCD) to detect the spectra. (Samuels et al., 2025)

However, the final product was not a fully functioning device. The optics functioned as intended, and a Raman spectrum was able to be gathered; however, a signal from the CCD could not be resolved. This issue could have resulted from a variety of reasons, ranging from the CCD being oversaturated to a faulty signal amplification circuit. The TEXRAY system did not include cooling for the CCD, which is typically required for Raman collection. Due to the weak nature of the Raman signal, a proportionally weak current is the output of the detector. Significant care must be taken to ensure signal integrity and noise isolation for the traces and IC which this signal will propagate through.

The original design included a Czerny-Turner spectrometer configuration, but a LGL was later swapped for simplicity. This was likely due to the increased expenses with a Czerny-Turner, ranging from the curved mirrors to reflective grating. Czerny-Turners are robust to aberration and off high spectral resolutions but are notoriously hard to align. As a compensatory note: a member of the group has experience aligning Czerny-Turner's from an internship position.

While a 532 nm laser is suitable for Raman spectroscopy, sources strongly suggest longer wavelength lasers produce significantly less fluorescence. However, for TEXRAY's applications of bulk fabric analysis, the 532 nm excitation proved to be sufficient to produce a Raman signal. 532 nm approaches the shorter end of common Raman excitation sources due to the fluorescence problem. Due to the Raman scatterring profile's proportionality to the inverse of the wavelength, these peaks can be intense enough to overcome saturation from background fluorescence.

2.3.1.2. WATER

WATER was a previous Raman spectroscopy focused senior design project sponsored by Ocean Optics. It utilized a different type of spectroscopy, spatial heterodyne spectroscopy, for water contaminant analysis. Spatial heterodyne spectroscopy utilizes Fourier transform

to analyze Fizeau fringes. [5-7] The layout utilized a Michelson interferometer. Instead of two mirrors utilized for reflection and creating a spatiotemporal dependent point of interference, two fixed diffraction gratings are used to create a point of interference that is wavelength dependent. The team was successful in obtaining Raman spectra for various contaminants such as sulfur, ammonium nitrate, and potassium perchlorate, (Smith-Blanchard et al., 2023). However, discussion with previous advisors said their results had a high uncertainty.

The system was designed around a 785 nm excitation source but was later changed to 532 nm source due to too weak of a Raman signal. WATER used a scientific CMOS camera as their detection module with a sensitivity peak at 532 nm. Due to the low quantum efficiency at their initial range, performing spatial heterodyne spectroscopy with such a weak signal was likely the final reduction in power to lose an identifiable signal.

After reviewing this project, the final product was not too cohesive of a project. Much of this project was externally controlled, with the spectral analysis being performed with MATLAB and the laser sitting a top of the device. We wish to avoid

2.3.1.3. NIRSPEC

NIRSPEC was a senior design project from 2016. The NIR in NIRSPEC stands near infrared and was an NIR light source character. This project was formerly sponsored by Ocean Optics and was built without an optical engineer.

An STM32 was utilized as the primary control and analysis system of the project.

NIRSPEC used a Indium-Gallium-Arsenide (InGaAs) linear photodiode array as their detector. This type of sensor has a peak sensitivity in the infrared spectrum but a low resolution. Typical photodiode arrays have horizontal pixel counts up to 128 and are only 1 row tall. These sorts of sensors are useful for analyzing narrower bandwidths, and for detecting small shifts in wavelength. CCDs often have horizonal pixel counts up to 2048, and CCD area arrays often go up to ~500 pixel vertically. Despite the high sensitivity in the NIR, InGaAs linear photodiode arrays are not suitable for our applications due to their low pixel count.

2.3.1.4. FLAMES

FLAMES was a project designed to detect the spectral signature of fire. The spectral signature minimized the chance of a false alarm from the detection system. Furthermore, the use of light offers a near immediate detection time compared to traditional sensing methods. (Singh et al., 2025)

Several controller systems were used in this project. An ESP32, Raspberry pi _ 8 GB, and a BASYS 3 FPGA board were all computing modules of active subsystems.

2.3.2. Research Papers

2.3.2.1. Quantitative Raman analysis of microplastics in water using peak area ratios for concentration determination

This paper uses Raman spectroscopy to determine the concentration of certain microplastics in a water sample. A Nanobase XperRAM-C is used to obtain the Raman samples. A 532 nm laser is used as the excitation source. Spectra were obtained with 25 second measurement times. 800 um x 800 um images were obtained with a galvo motor scanning the laser across the sample. (Jung et al., 2024)

2.3.2.2. Constructing a Micro-Raman Spectrometer with Industrial-Grade CMOS Camera—High Resolution and Sensitivity at Low Cost

This work discusses the creation of a micro-Raman spectrometer with the use of an industrial-grade CMOS camera. They report a Raman shift resolution of 2.5 cm-1, a small footprint, and a sensitivity comparable to "research-grade confocal Raman microcoscopy systems." (Zgrablić et al., 2025)

2.3.2.3. Cavity enhanced Raman spectroscopy

This paper used a resonating cavity to enhance Raman analysis of gases. It concludes using a cavity to recirculate the light through the sample multiple times to produce more Raman scattering does improve the received signal on the detector.

2.3.3. Enthusiast Projects

2.3.3.1. OpenRaman

OpenRaman is an enthusiast project designed by _. The purpose of the project was to bring advanced material analysis systems (Raman spectroscopy) to research labs and hobbyists for a significantly reduced cost compared to conventional systems. Over the years of its development, there have been many upgrades brought to the OpenRaman platform. The standard version of the device utilizes a 3D printed alignment base, a 532 nm diode laser, a FLIR CMOS camera, cage mounts, ThorLabs optics, and a 3D printed enclosure; all while taking up a small footprint. OpenRaman is also originally intended to perform analysis of aqueous samples in cuvettes. The 3D printed enclosure includes a cuvette holder with an integrating mounting system for the focusing lenses.

The design of OpenRaman is centered around simplicity and reproducibility: no microscope objective is used, the collected light undergoes the minimum laser filtering, the light is collimated onto a reflective grating, whose spectra is then immediately refocused onto a commercial CMOS camera. However, some of the assembly processes are a bit more advanced. For example, the use of helicoils, "POLYAMIDE SLS" (Selective Laser Sintering) 3D printing

Some of the upgrades to OpenRaman include a fiber laser attachment, imaging lens upgrade attachment, an improved cuvette holder, and a solids cuvette attachment.

2.3.3.2. OtterDIY

OtterDIY is a "hackaday" hobby project. The last time this page was updated was in 2017. It documents the author's process in developing a Raman spectrometer, from lens design and component choice, to circuit design and troubleshooting. The author included equations and calculations he used to determine distances and optical component specifications.

An STM32F103 "blue pill" was used as the microcontroller for taking readout from a Toshiba TCD1304DG CCD and outputting status data to a . A 532 nm laser was used as the excitation source. A custom heatsink and TEC solution was fabricated to cool the CCD, reaching a reported temperature of –0.6 C. (Esben Rossel, 2017)

In the FAQ section, the author claims "a slit is a waste of light" and that he chose to use a fiber optic as the "point source" incident on the grating. The width of the slit is directly correlated to spectral resolution. A circular "point source" would create a distorted spectrum, which varies vertically as the circular source varies in thickness.

2.4. Goals and Objectives

2.4.1. Goals

2.4.1.1. Basic Goals

1. Collect Raman spectra of 2 – 5 mm sized plastic samples in water, polyethylene terephthalate.
2. Collect Raman spectra of bulk plastics of interest in water.
3. Utilize a 785 nm laser .
4. Detect the presence or absence of specified microplastics in water using Raman spectral fingerprints. Refer to Appendix B for a collection of the peaks of interest. These samples will be prepared without mixes of plastic types. Maintain a CCD operating temperature of sub 40° C.
5. Obtain full control of the laser system through external electrical means.

2.4.1.2. Advanced Goals:

1. Identify the type of plastic a specific not-mixed water sample has in it, between polyethylene terephthalate, polystyrene, and nylon.
2. Identify microplastics down to 500 micrometers in length and 100 micrometers in width.

3. Addition of a database server to connect to the device, which would be able to host records of previous identification runs and utilize the data for more robust known material libraries.

2.4.1.3. Stretch Goals: Mixed MP Samples < 5 mm and Imaging of MP

The device will:

1. Detect and identify microplastics of mixed pre-made water solution samples, rather than individual polymer samples.
2. Detect and identify microplastics from a sample from the environment, such as tap water, or lake water sample.
3. Detect and identify microplastics in powdered form.
4. Implementing an additional system to image microplastics in addition to detection and identification to give the user a more accurate view of what they are measuring.
5. A larger scale version of ECOspec that could be set up for stationary real-world uses. It would be established in waterlines and natural bodies of water to detect high concentrations of harmful materials in the water.
6. Portable, battery powered, field deployable version instead of a bench system. It would be useful for outdoor environmental sampling, or for personal use for microplastic detection in your home.
7. Integrate a second 1064 wavelength source for Raman spectra with reduced fluorescence.

2.4.2. Objectives

2.4.2.1. Basic Objectives

- Basic alignment of Raman spectrometer with white light source.
- Calibration of spectrometer so the pixel spaces accurately map to nanometer space.
- Obtain Raman spectra using our system with large pieces of common plastics > 5 mm in size.
    - Plastics of interest: Polyethylene terephthalate (PET), polystyrene (PS), and nylon
- Confirm that Raman spectra collected matches known fingerprint peaks of those polymers
- Using our samples of interest, we will create microplastic samples in DI water. These samples will each only contain one type of microplastic.
- Obtain Raman spectra using our device with individual microplastic samples.
- Obtain Raman spectra of the water for reference comparison during the output processing.
- After collecting the needed references, we can use the device to detect if microplastics are present or not in more individual microplastic water samples that we made at varying concentration levels.

2.4.2.2. Advanced Objectives

- Create more individual microplastic samples that include a broader range than the initial samples of interest.
- Collect a reference library of known fingerprint peaks of the samples we intend to test.
- Create microplastic samples of various types and sizes, confirmed by visual inspection with a microscope.
- Take Raman measurements of our individual, pre-made microplastic samples.
- Implement software changes needed to include identification, in addition to detection.

2.4.2.3. Stretch Objectives

- Implement software changes to include mixed-microplastic detection.
- Create known mixed pre-made samples to test our post-processing.
- Collect environmental samples to detect microplastics, including tap or lake water.
- Test if identification is possible with the environmental samples.
- Direct the reflected 785 nm light into a CCD or infrared camera after back reflection off the dichroic mirror
- Implement another mount, lens systems, and dichroic mirror to stabilize, collimate, and direct a secondary 1064 nm laser source into the pre-established path of the 785 nm source.
- When establishing the known material library, inclusion of a small, non-linear, regression model. This model would require a more intensive calibration to allow the model to establish the required relationships between Raman shift intensity, material, and material concentration in a fluid sample.
- A website/app connected to a database where the results could be stored so a multitude of people have access to the data. This could also replace the basic GUI we included previously. This would also allow for crowdsourced data collection. Crowdsourced data can provide more detailed material libraries, enabling more accurate identification.
- Real-time monitoring that allows for continuous sampling of water. For example, using it in a waterline that would trigger alerts if a certain concentration threshold were to be exceeded. This would be beneficial for labs or municipalities to maintain clean water for their facilities.

2.5. Major Subsystems

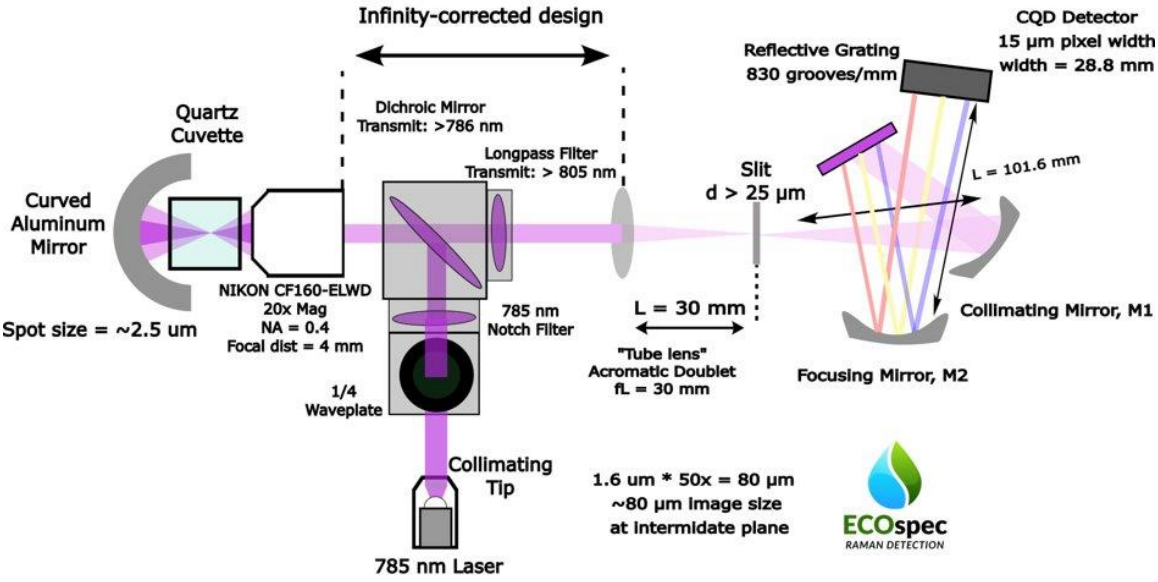

Figure 4 Optical Diagram

Optical design concept for collimation, illumination, and collection optics, along with task delegation.

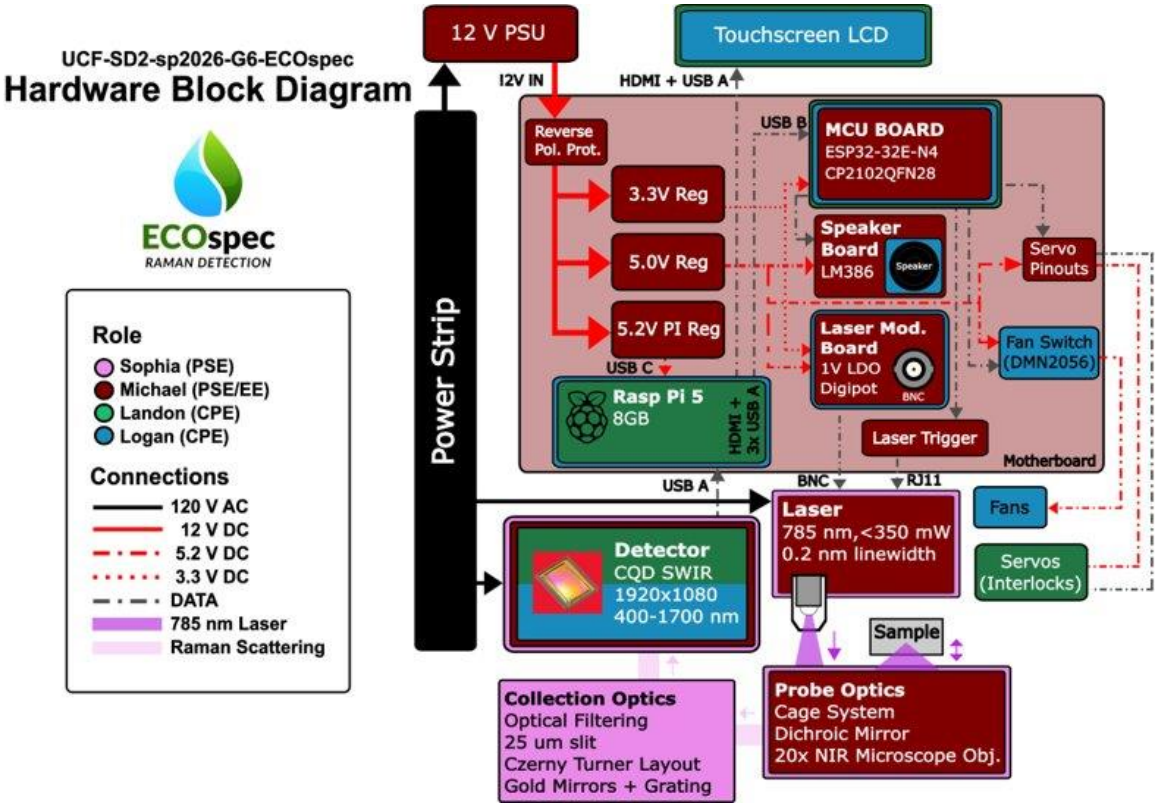

Figure 5 Hardware Block Diagram

Hardware block diagram visualizing larger components and PCBs for primary subsystems.

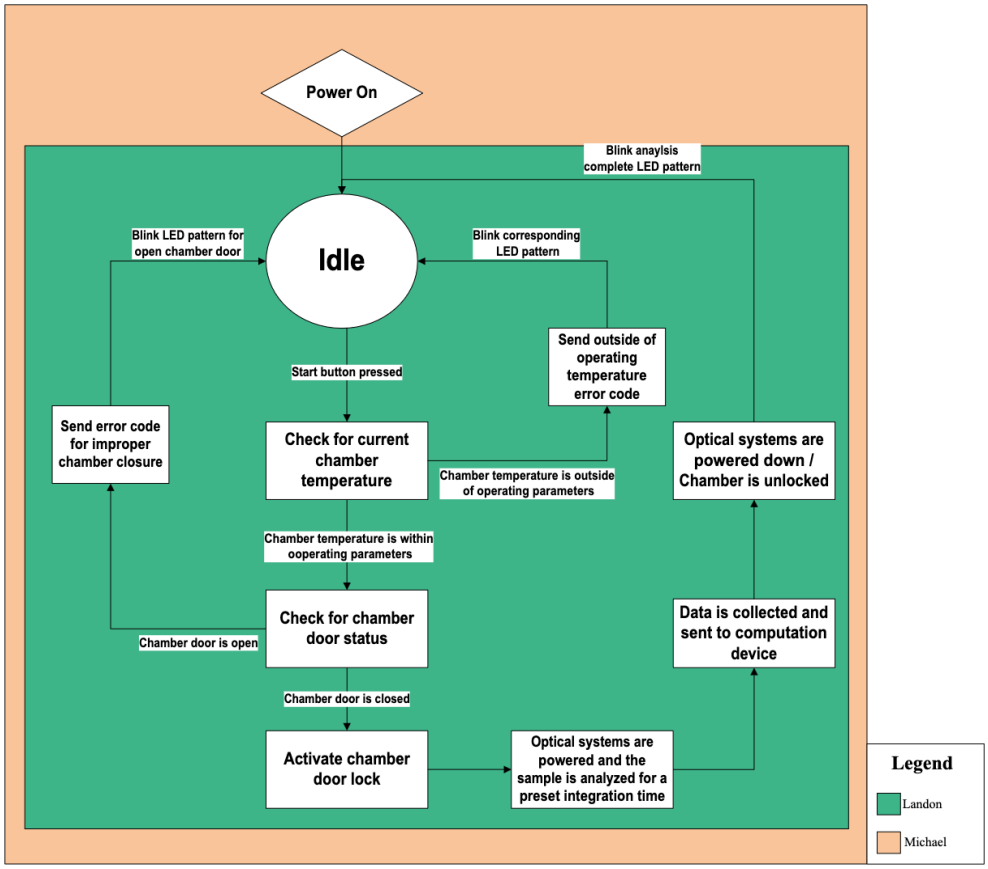

Figure 6 Software Block Diagram

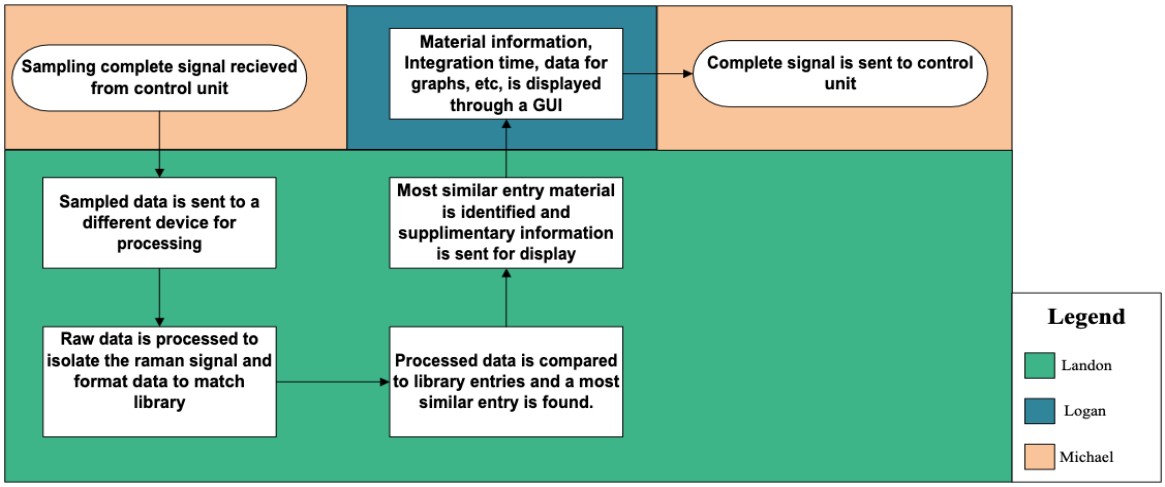

Figure 7 Signal Processing Software Block Diagram

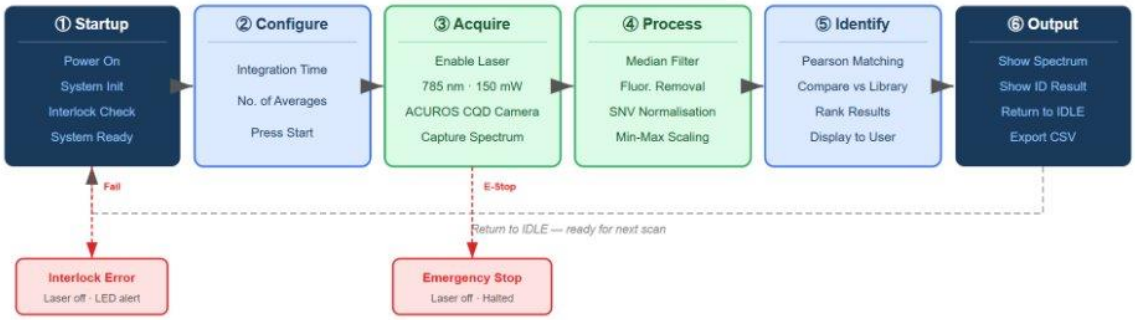

Figure 8 User Interface Flowchart

Figure 9 User Interface

2.5.1. Software

2.5.1.1. Raman Spectra Comparison Library

To achieve the expected functionality of ECOspec, an advanced suite of spectral processing must be employed. This included conversion of raw spectral data into raw Raman spectra,

through equipment baseline correction and the Raman shift formula. Following this, the data is run through a pre-processing pipeline, which includes removal of dark noise and fluorescence, rescaling Raman shift intensity values, and interpolation of the data to align x-axis for comparison. With the processed data, ECOspec will be able to compare the spectra of the unidentified sample with a pre-established spectra library of known materials using a similarity metric such as Pearson correlation of cosine similarity to classify the material present in the water sample.

2.5.1.2. GUI

Data collected by ECOSpec is displayed in real time through a touchscreen interface running directly on the Raspberry Pi 5. The interface was built using HTML5 and JavaScript, rendered as a native desktop application using PyWebView, so no browser is needed.

The screen is divided into four sections that are all visible at once: a live Raman spectrum display, an identification result panel showing the best material match and Pearson similarity score, a real-time system log, and a hardware control column on the right. The scan button stays locked until both the ESP32 and camera are detected, so the system can't be triggered without everything connected.

After a scan completes, the operator can export the results as a CSV file with the real wavenumber data, normalized intensity values, and match result included. Laser power and integration time are adjustable through sliders, and direct commands can be sent to the ESP32 for servo control, laser modulation, and other hardware functions through a built-in control panel.

2.5.1.3. Calibration and Safety

X-axis pixel to wavelength calibration will be necessary to confirm the repeatability of measurements and so the true Raman shifts can be recorded. Y-axis intensity calibration could be implemented so that no peaks appear weaker than they really are due to how the detector responds to different wavelengths.

Safety checks for interlocks and device temperature will be in place before allowing for collection of Raman signal can occur.

Raman Shift

$$\Delta v\left(Raman\ Shift\ (cm^{-1})\right) = \left(\frac{1}{\lambda_{Laser}} - \frac{1}{\lambda_{Scattered}}\right) \cdot 10^{-7}$$

2.6. Required Specifications

Table 1 Optical and Hardware Component Specification

Optical Prototype Specifications		
Component	**Parameter**	**Value**
Spectrometer	Short integration time	< 40 seconds
	High Spectral Resolution	< 2 nanometers per pixel
Laser	Wavelength	785 nm
	Laser Power	150 mW
	Beam Diameter	3 mm
Microscope Objective	Magnification	20x
Quartz Cuvette	Size	3.5 mL, 12.5 mm x 12.5 mm x 45 mm
Component	**Parameter**	**Value**
Dichroic Mirror	Cut-on Wavelength	805 nm
	Reflection Wavelength	400 - 785 nm
	Transmission	825 – 1300 nm
Long pass filter	Rejection Wavelength	<= 785 nm
	Transmission	1%
Extra filters	Rejection Wavelength	TBD
	Transmission	TBD
Spectrometer Optical Components		
Diffraction Grating	Groove Density	1200 lines/mm
	Blaze Angle	800 nm
Slit	Slit Width	25 um
Concave Mirror 1	Off-axis parabolic	Gold coated
Concave Mirror 2	Off-axis parabolic	Gold coated
Laser Alignment Components		
Mirror 1	TBD	TBD
Mirror 2	TBD	TBD
Polarizer	TBD	TBD
Waveplate	TBD	TBD
Lens 1	TBD	TBD
Lens 2	TBD	TBD
Hardware Component Specifications		
Component	**Device Name**	**Parameters**
Main MCU	ESP32	240 MHz
CCD MCU	Teensy 4.1	600 MHz
CCD Sensor	ESPROS Photonics AG EPC901-CSP32-033	1024 H x 1 V
ADC	MCP3008	10-bit resolution
TEC	TBD	TBD
3.3 V Voltage Regulator	TBD	TBD
5.2 V Voltage Regulator	TBD	TBD
9-12 V Voltage Regulator	TBD	TBD

CCD Amplifying Transistor	TBD	TBD
12 V PSU	TBD	Handles up to 10 A

Table 2 Engineering Requirements for the Performance and Physical Features of the Envisioned System.

Overall System Specifications	
Parameters	**Target Value**
Detection Accuracy*	± 10 nm
Total Integration Time	< 10 minutes
High Spectral Resolution	< 2 nm per pixel
Lowest Concentration Detected	*Requires further research
Microplastics Measured Size	< 5 mm
System cooling	Maintain temperatures < 40° C
Wavelength Range	> 150 nanometers
Dimensions of Device	< 50 cm x 100 cm x 100 cm

*Refer to Appendix B for peaks of interest for each plastic type

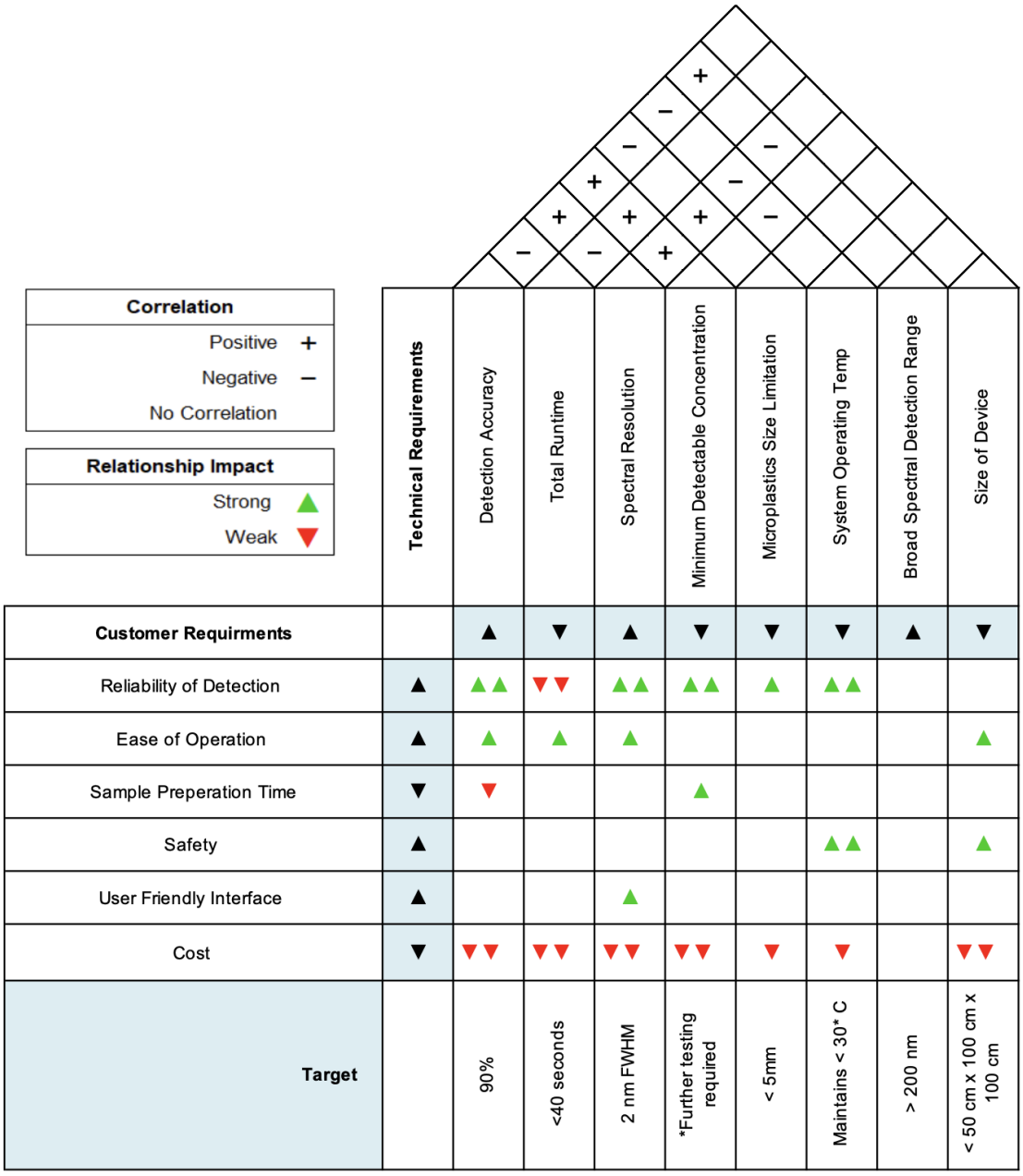

Figure 10 House of Quality

Diagram that displays the relationship between customer and technical requirements, as well as demonstrates the correlation between the technical requirements.

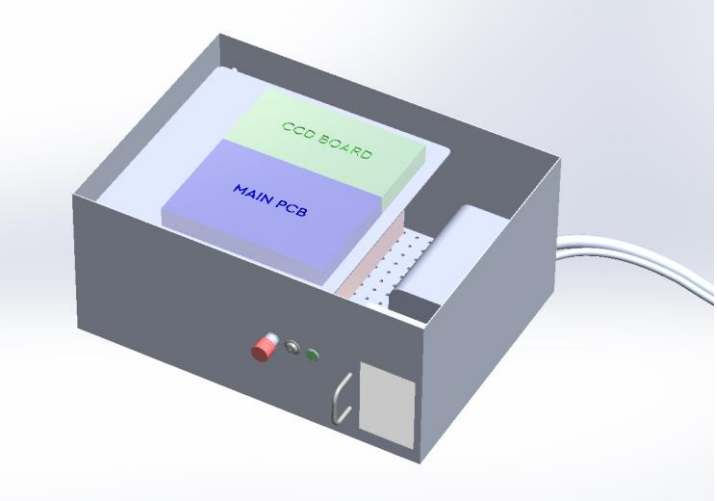

Figure 11 Prototype Illustration

Isometric top view, illustrating potential board placement. A hinge system will be employed for placement of the electrical boards and compactness of the device.

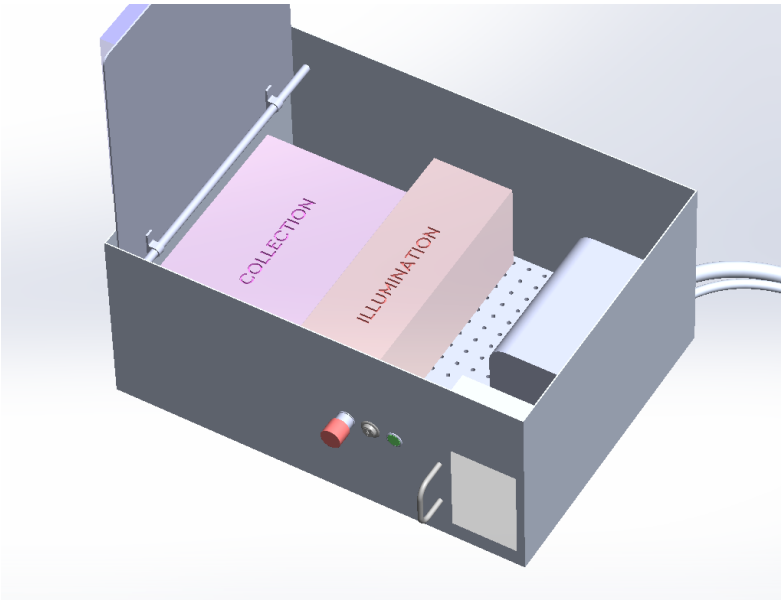

Figure 12 Prototype Illustration 2

Dimetric top-down view displaying the optical subsystems placed underneath the hinge system.

3. Research on Current Technology

3.1. Optical System

3.1.1. Spectroscopy Overview

3.1.1.1. What is spectroscopy, what is a spectrometer?

Spectroscopy is a measurement powerhouse, and it describes the study of interactions between matter and light, which provides a powerful way to analyze the composition and structure of materials. These measurements are done with a spectrometer, an instrument that separates light into its component wavelengths, and measures their intensity. Before diving into how a spectrometer can be designed, how the measurement done by the spectrometer works is vital. Atoms or molecules are thought to exist in certain quantum states, where each state has a specific, discrete amount of energy, and transitions between the states are possible when specific light is shown on the molecule. When the molecule changes state from a higher to lower energy, emission occurs, and a photon is released. Comparatively, absorption occurs when the molecule transitions from a lower to a higher energy by absorbing a photon. The total change in internal energy that a molecule can go through is the sum of its rotational, vibrational, and electronic energy. These specific energy change intensities are measured by spectrometers, which split up the incoming light into its component wavelengths, and detect the intensity of the incoming light at each wavelength. This wavelength versus intensity plot is referred to as a spectrum. The spectrum produced from the measurement is then further analyzed, based on the peak positions, spacing, and linewidth. For example, a reference spectrum of polystyrene absorption is illustrated in figure 3.2. Most spectra demonstrate the same thing: how intensity or brightness varies with wavelength, but the light-matter interactions on a molecular level vary with the specific excitation wavelength, and what is being measured. In addition to absorption and emission, there are many other measurement techniques that employ spectroscopy that provide light data to identify molecular presence, including mass-spectroscopy. Raman and spectroscopy, fluoresce, reflectance, and measurements across the electromagnetic spectrum, including infrared, x-ray, UV, and visible ranges. One would choose the type of spectroscopy based on the type of information needed, the nature of the material, and experimental constraints such as cost, speed, if the sample needs to be preserved, and location.

Diving into the different types and their limitations, UV-visible spectroscopy is typical for absorption in the UV-Vis range, and is commonly used for concentration determination, or analyzing pigments or dyes. It is limited to samples that absorb in the UV-Vis range and is not the correct choice for identifying molecular structure. Infrared spectroscopy detects molecular vibrations, which is used for identifying functional groups in molecules. These functional groups can identify organic compounds, analyze polymers, and verify certain materials. Some of its limitations include its requirement fo r pure samples, and the strong absorbance of water, which can get in the way of getting results in wet environments or samples in water. Mass spectroscopy measures a mass-to-charge ratio of ions and is best

for identifying and quantifying molecules. It comes in handy for chemical analysis, drug testing, and environmental monitoring, but can destroy samples because it requires ionization. Another method of spectroscopy is fluorescence spectroscopy, which measures the light emitted by excited molecules when an energy transition occurs, and the atom falls back to its original state. Fluorescence can be spontaneous and stimulated, which requires an excitation state. Fluorescence spectroscopy can detect trace compounds and is used in medical diagnostics, but the material tested must have fluorescent properties and can be very sensitive to the environment it is in, which can quench the signal.

After careful analysis of our application, detection and identification of microplastics in water samples, our group selected Raman spectroscopy as our measurement of choice.

3.1.1.2. Raman Spectroscopy

Before understanding why we choose Raman spectroscopy, some background on how the process works is required. Raman spectroscopy is based on how molecules scatter photons. Compared to absorption and emission, a certain energy level is not required for scattering to occur. Absorption requires light at a certain frequency or wavelength, whereas scattering can occur at any point. Raleigh scattering is the elastic scattering component and describes light scattering without a change in energy. On the other hand, Raman scattering is a measure of the inelastic scattering that is occurring. Because molecules are not rigid, vibrations, made up of stretching and bending, rotations and constantly occurring. The vibrations and rotations have certain quantum energy levels. When incident light hits a molecule, Rayleigh scattering, scattering with no energy change, occurs, but sometimes the light will interact with the vibrations and rotations, and exchange energy with the molecule, and produce scattering at different energy level. This is described as a change in polarizability when the laser light's electric field tries to distort the molecule's electron cloud. This change is the ground rule for Raman scattering to occur, and it is dependent on the molecular structure, because molecular symmetry determines if the electron cloud distribution is easier or harder to distort by the laser light. Symmetric vibrations usually do change polarizability, whereas asymmetric vibrations tend to change the dipole instead, which describes the charge of separation, and is different from polarizability. Polarizability is highly dependent on what phase the molecule is in, its crystal orientation, and any strain or defects in the materials, which could possibly change the symmetry. Some examples of molecules with strong polarizability include double bonds, single carbon bonds, aromatic rings such as benzene.

A simple light scattering experiment can be described with a focused laser beam across some volume of material, and a lens to focus the scattered light onto a detector. The light that is scattered will contain both Raleigh and Raman scattering at certain wavelengths. Raleigh scattering wavelength is equal to that of the incident light, and Raman scattering is either increased or decreased in wavelength. This increase or decrease is referred to as anti-stokes, a positive shift, or stokes, which would result in a negative shift. (Eq. 3.1)

$$\begin{aligned} \textbf{Rayleigh} \quad & E(elastic) \\ \textbf{Anti-Stokes Raman} \quad & E + \Delta E(inelastic) \end{aligned} \tag{3.1}$$

Stokes Raman $E - \Delta E(inelastic)$

Equations comparing the energy and frequency of Raleigh versus Raman scattering, and the difference between Anti-Stokes and Stokes is displayed. E is the energy of the incident photon, $\Delta E = \Delta E_{rot,vib}$, which is the energy from rotations and vibrations within the chemical compound because of its bonds and chemical makeup, which is the inelastic aspect of Raman.

In terms of the spectra that is produced, the vibrations define the major Raman peaks and reveal the most specific chemical information such as specific bonds and structure. Each bond vibrates at a specific frequency, and Raman spectroscopy identifies those frequencies as peaks in the Raman spectra. Because Raman spectroscopy measures the vibrational frequencies as shifts in the scattered light, bonds will always appear around the same approximate Raman shift value (wavelength dependent). For instance, double carbon bonds always appear at an approximate Raman shift of ~1600 cm^{-1}. because each molecule has its own unique movement pattern, the Raman spectrum can become a molecular fingerprint for identification of specific bonds in materials. The peak intensity can show how strong or present the bond is, implying more of that bond type in the measured material, a stronger polarizability change, or better alignment of your system. The shape of the peak sheds light on the structural information. Sharp peaks identify a crystalline, ordered material, whereas broad peaks define the opposite- typically amorphous, disordered samples. Seeing issues with the peak shape in the spectra, such as split peaks, can be due to molecular symmetry changes, and shifts in peak position are a result of environmental changes, such as a highly fluorescent environment. The cross section of expected Raman scattering is much smaller than that of Raleigh scattering, which means the signal of Raman is very weak. This weak signal is a major drawback of Raman spectroscopy as a measurement technique, but its advantages make it worth it to mitigate.

There are various reasons we chose Raman spectroscopy as our spectroscopic method of choice compared to other technology options for our project, the first being the advantage Raman spectroscopy holds for samples of microplastics in water. Microplastics can be analyzed in situ, suspended in liquid, without a strong signal from water overpowering the signal from the microplastic. Water has a very weak Raman cross section due to its weak vibrational bands in the fingerprint region that is relevant to polymer detection. Although IR spectroscopy could have been used for microplastics not in water, it would not work for our application of microplastics in water because water has IR absorption bands that overpower the polymer signals. Additionally, microplastics are mostly made of hydrocarbon-based polymers, their C-C, C=C, and C-H vibrational modes exhibit high Raman signal, from their high polarizability, so sharp peaks, for detection, with distinct spectra for Nylon, Polystyrene, and PET for polymer identification, because each of the 3 microplastics are made of their own amounts of differing polymer compounds that have their own peaks, and peak heights. Raman is also able to detect small particles, perfect for our micro-scale application. Minimal sample preparation is another advantage of Raman spectroscopy. In terms of future applications, such as taking water samples from the environment or sink taps, microplastics will undergo oxidation and surface modification in the water. But with Raman, we can still receive the chemical makeup of the plastics, while also not destroying the sample. Raman spectroscopy can also detect the addition of

pigments in polymers, and weathering signatures. High chemical specificity is enabled by the narrow Raman bands, so similar polymers, such as PET and PBT can still be distinguished. The expected Raman fingerprint spectrum of our 3 chosen microplastics, nylon, polystyrene, and PET are shown below. (Fig. 3.4-6)

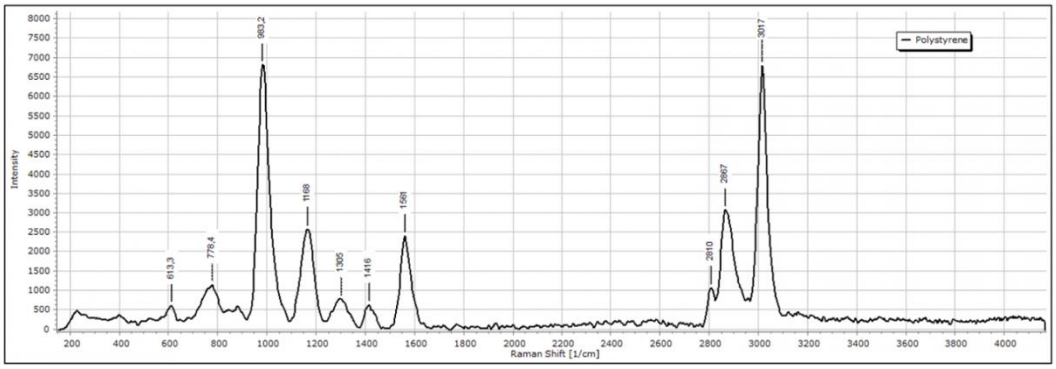

Figure 13 Expected Raman$ Spectra, Polystyrene

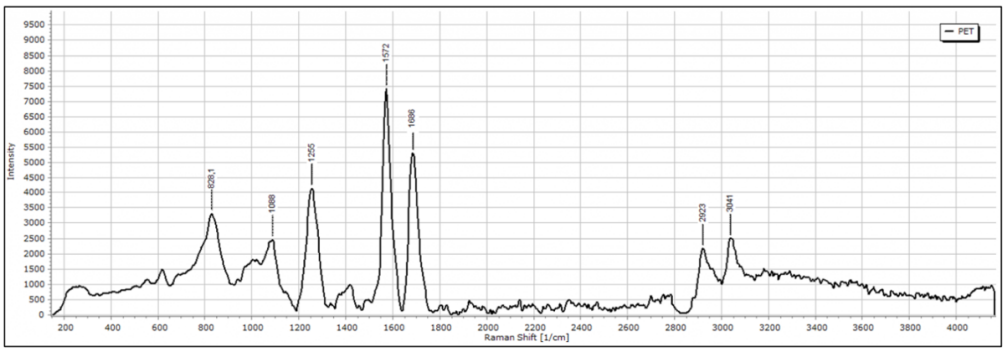

Figure 14 Expected Raman Spectra, Polyethylene Terephthalate

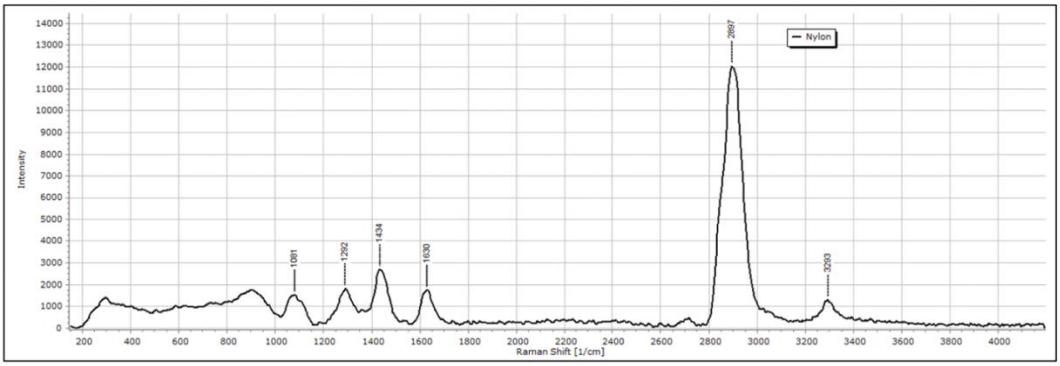

Figure 15 Expected Raman Spectra, Nylon

3.1.1.3. Raman Spectrum Details of Polystyrene, Nylon, and PET

Table 3.2 goes into detail reviewing the expected peaks of Polystyrene, Nylon, and PET, and the vibrational bonds and molecular activity that cause those peaks. For polystyrene, C-H vibrations have a higher frequency than C-H vibrations because hydrogen is lighter than carbon. Nylon is made of polyimides, such as nylon 6 and 66, which are macromolecules that are characterized by the CO-NH amide group.

Table 3 Raman Technique Comparison Applications, Strengths, and Limitations

	Bond	Location (cm^{-1})
Polystyrene	1. High frequency C-H vibrations aliphatic 2. High frequency C-H Vibrations aromatic 3. Low frequency C-C vibrations 4. C=C vibrations 5. Expansion and contraction of benzene ring	1. 3000 cm^{-1} 2. 2900 cm^{-1} 3. 800 cm^{-1} 4. 1600 cm^{-1} 5. 1000 cm^{-1}
PET	1. Stretching of C-H 2. C=O vibrations 3. C-C bound in aromatic ring	1. 3000 cm^{-1} 2. 1700 cm^{-1} 3. 1600 cm^{-1}
Nylon	1. C-H connected to N-H vibrations 2. C=O connected to N-H	1. 3300 cm^{-1} 2. 1250 cm^{-1}

3.1.1.4. Raman Spectroscopy Methods

Within the branch of Raman spectroscopy, there are several techniques that extend the basic Raman effect, each to optimize different performance goals. Spontaneous Raman provides broad vibrational fingerprints but has very weak signal intensity. It can provide information across the full vibrational fingerprint spectrum and has high chemical specificity. Its advantages include label-free, non-destructive, and applicable to a wide range of materials, with little to no sample preparation. The signal can suffer from background fluorescence. FT-Raman (Fourier Transform) uses NIR excitation around 1064 nm combined with a Michelson interferometer to reconstruct the diffraction patterns using FT mathematical reconstruction techniques to recover the signal. It provides a greatly reduced fluorescence interference from the NIR excitation, and in turn increases the signal to noise ratio. Unfortunately, excitation at that long of a wavelength already enables a decreased Raman scattering efficiency, and it is less suited for microscale imaging. Raman spectroscopy can also be combined with microscopy, with a diffraction-limited, high numerical aperture (NA) microscope. This combination enables a very low spatial resolution, which works well for very small samples, such as microplastics. It can also be added into an imaging system simply by having a secondary white light source, which can provide the user with an increased ease of finding the sample for excitation. Another well-known technique is SERS (Surface-enhanced Raman scattering). With this method, the Raman signal and sensitivity is enhanced with nanostructured metallic surfaces. The interactions between the sample molecules and the metal surfaces enabled by plasmon resonance produce local electromagnetic fields that amplify the Raman signals of

molecules on the metal surface. Metal surfaces are used because they don't produce strong Raman signals. SERS is extremely sensitive for trace molecules, but it requires sample prep of the metal nanostructures, which can increase the price of the experiment.

After comparison of the many Raman enhancement techniques, our project employs a combination of spontaneous Raman and microscopy. This configuration offers a reliable balance between cost, spectral sensitivity for polymer detection and identification, and high resolution for our micron scale application. While methods such as SERS offer a higher sensitivity, it increases the cost, and introduces sample preparation, which our project is avoiding due to the potential application. FT-Raman also is appealing because of its low fluorescence, but a 1064 nm laser is very expensive, and we have access to a 785 nm laser instead. Also, vibrations in the water sample could introduce instability in the interference patterns that are collected. Fluorescence will be an issue we will have to navigate with our optical design, but can be mitigated with post processing, and optical design optimization to reduce fluorescence.

Table 4 Raman Technique Comparison Applications, Strengths, and Limitations

	Spontaneous Raman	**Raman Microscopy**	**SERS**	**FT- Raman**
Laser Requirements	Single monochromatic CW laser	Same as spontaneous but with high-NA optics	Visible lasers, near plasmon resonance	NIR excitation (typically 1064 nm)
Signal Strength	Weak (~10^{-6} of incident photons)	Same as spontaneous at each pixel	10^4–10^8× enhancement (or higher)	Weaker intrinsic Raman but reduced fluorescence interference
Fluorescence Interference	Significant issue	Same as spontaneous Raman	Can suppress if plasmon surfaces quench fluorescence	**Very low** (NIR excitation avoids fluorescence)
Chemical Specificity	Excellent	Excellent spatially localized	Excellent for surface-adsorbed species	Excellent
Advantages	Universal Raman technique	Chemical + spatial mapping, confocal depth	**Massive enhancement, single molecule detection, trace analytes**	Fluorescence suppression, excellent S/N in NIR
Limitations	Weak signal → long acquisition time	Slow for large scans; fluorescence	Reproducibility issues; substrate-dependent	Lower scattering efficiency, bulky interferometer
Instrumentation	Low–moderate	Moderate–high	Moderate–high depending on substrate	High (interferometer + NIR detector)
Complexity + Cost	$$	$$-$$$	$$–$$$$ depending on substrates	$$$
Typical Excitation λ	532, 633, 785 nm	Same as spontaneous; high-NA objective	Visible (532–785 nm) near plasmon resonance	**1064 nm** (avoids fluorescence)

3.1.2. Probe Optics

3.1.2.1. Excitation Source

The excitation wavelength used will be 785 nm. This wavelength was selected for a variety of reasons: a decreased level of fluorescence, less detector saturation, and more prominent peaks. 532 nm laser would also be viable, but it is known to produce a lot of excess fluorescence which can saturate the detector and decrease the SNR. A 1064 nm laser is capable of producing Raman spectra with a very high SNR; however, they are a very costly item. In traditional Raman spectroscopy setup, the laser spot size is minimized to increase the likelihood of generating a Raman signal. However, our goal is to retrieve a Raman signal from illuminating a large portion of a quartz cuvette. To ensure a Raman signal is generated, the laser will be set at a higher power than typical to compensate for dispersion over a larger area.

Table 5 Excitation Wavelength Comparison

	532 nm	**785 nm**	**1064 nm**
Use Cases	Inorganics	Organics	High fluorescence materials
Raman Peak Intensity	High	Medium	Weak
Fluorescence	High	Low	Minimal
Cost of Compatible Optics	Cheap	Expensive	Very expensive
Cost	Cheap	Expensive	Very expensive

Our excitation source will be the Ocean Optics LASER-785-LAB-ADJ-S, lent to us by Ocean Optics. It is a multimode laser with a narrow linewidth (FWHM) of ~0.2 nm. It is a pre-existing laser module with dedicated current and temperature control. The light source is a diode laser that has SMA output coupling for use with SMA coupled fibers.

The output light of an unmodified fiber quickly diverges. This is due to the numerical aperture (NA) of the fiber. It is a measure of how wide of an angle a fiber (or lens) is capable of collecting light from in front of it. It is a function of the refractive index of the core and cladding layer, as seen in Equation _.

$$Numerical\ Aperture\ =\ NA\ =\ \sqrt{n_{core}^2 - n_{cladding}^2} \quad (3.)$$

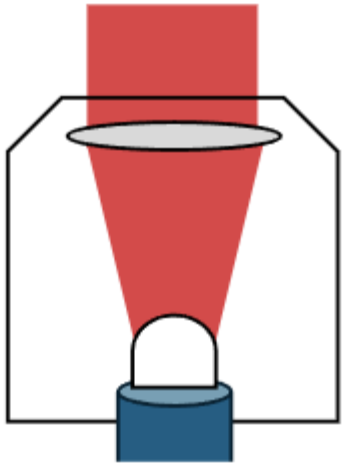

Figure 16 SMA Collimating Attachment

The SMA coupled output fiber has a collimating attachment. This collimating attachment uses a lens that matches the divergence (or NA) of the fiber output.

3.1.2.2. Focusing optics

After performing a literature review, we found that a majority of Raman analysis uses some focusing system. This is largely done to compensate for the low signal generated from the Raman phenomenon. To increase the likelihood of generating a useful Raman spectra, high power light is focused down to a small area. Focusing a larger number of photons into a smaller area increases the number of Raman interactions in that area, thus increasing the signal strength, improving SNR. It enables a larger confidence in the accuracy of the Raman signal generated from a smaller area.

ECOSPEC aims to identify microplastics, with a minimum of under 5 mm and a target goal of 500 microns. With the use of a microscope objective, our laser spot size is capable of reaching under 10 microns in diameter.

Table 6 Microscope Objective Comparison

	Newport M-10x	**Olympus LCPLN20XIR NIR**	**Nikon CF160 TU Plan Epi ELWD**
Magnification	10x	20x	20x
NA	0.25	0.45	0.4
Wavelength range	400-700 nm	400-1600 nm	N/A
Working Distance	5.5 mm	8 mm	19 mm
Effective Focal length	16.5 mm	9 mm	N/A
Parfocal length	N/A	45 mm	60 mm

Transmission @ 785	N/A	87%	N/A
Rear Conjugate Correction	160 mm	Infinite	Infinite

The minimum spot size is determined by the airy disk, as seen in Equation 3._. It is a theoretical limit of how focused a monochromatic aberration free image can be. It essentially achieves the highest intensity (W/m^2) at a given power for a laser of a certain wavelength.

$$r_{airy} = 0.61 \cdot \frac{\lambda}{NA} \qquad (3.)$$

3.1.2.3. Alignment and Beam Expander

In the final design, a beam expander was not used due to microscope objective of choice having a small rear aperture. However, to minimize the spot size created by a microscope objective, the input beam must be expanded to ~80% of the rear aperture and match the rear conjugate correction of the microscope objective (Fellers & Davidson, n.d.) . Both overfilling of the microscope objective and incorrect conjugate matching can lead to aberration, compromising the calculated airy disk (minimum spot size radius).

Our selected microscope objective has a rear entrance aperture of 14 mm in diameter. To optimize the use of the objective and minimize aberration, the collimated input beam should be 12 mm in diameter. Considering the collimated laser output is 3 mm in diameter, the required magnification will be 4x. A simple infinite conjugate beam expander follows a magnification formula of: $M = f_2/f_1$, where f_1 is the first incident lens, f_2 is the second incident lens, and the distance between the lenses is the sum of the focal lengths. The beam expansion should also occur over as short of a distance as possible to fulfill the sizing requirement of the ECOspec system.

However, a combination of commercially available lenses which create a 4x magnification would increase the size of the optical system beyond the intended scope. Another magnification size must be selected, as well as a modification of the collimated laser output size. An adjustable iris would enable the beam spot size to be reduced to 2 mm, as well as provide additional beam clean up. If a 2 mm diameter beam spot is used, a magnification of 12x would meet the 12 mm objective entrance requirement. Two lenses which fit this requirement are the Thorlabs AC050-008-B and AC254-045-B. They are AR coated for our laser wavelength, have focal lengths of 7.5 and 45.0 mm respectively, and combine to make the shortest possible beam expander with commercially available lenses. The AC050-008-B is 5.0 mm in diameter, enabling us to use a 2 mm spot size without aberration.

Table 7 6x Magnification Beam Expander Lenses

	Thorlabs AC050-008-B	**Thorlabs AC254-045-B**
Focal Length	7.5 mm	45 mm
AR Coating Range	650 – 1050 nm	650 – 1050 nm

Diameter	5.0 mm	25.4 mm

3.1.2.4. Dichroic Mirror

The dichroic mirror serves two purposes in a Raman microscopy setup. It first a majority of light within a certain band, determined by whether the dichroic is a notch filter or a cut-off filter. Our target reflected band contains our excitation wavelength, essentially acting as a mirror for our laser. This dichroic will direct the laser light onto the sample, but allow the Raman scattered light to pass through without redirection.

Table 8 Dichroic Mirror Comparison

	ThorLabs DMLP805	**Thorlabs DMLP760**	**Thorlabs DMLP900**
Transmission > 90% Wavelength Range	825 - 1300 nm	775-1600 nm	932-1300 nm
Reflection > 90% Wavelength Range	400-785	400 – 740 nm	400-872 nm
Reflectivity @ 785	90%	<5%	>95%
Thickness	3 mm	3 mm	3 mm
Cost	$331.76	$331.76	$252.95

The dichroic with the highest reflectivity at 785 nm should be used as the dichroic mirror. This will ensure minimal laser light is lost during the reflection interaction or allowed to pass into the collection optics. The Thorlabs DMLP805 fits this description. The 760 cut off mirror may be used as additional filtering to mitigate any transmit fluorescence. The 900 nm cut off mirror would reflect a large band of the Raman peaks we seek to detect.

3.1.2.5. Quartz Cuvette

Our samples under test will be stored in a quartz cuvette. The quartz cuvette is chosen for its low Raman response. It is a common piece of equipment for many Raman analysis systems. The quartz cuvette is capable of holding both solids and liquids, allowing for analysis of both material phases.

3.1.2.6. Power Management

The laser source is capable of outputting up to 350 mW of optical power. However, this power level far exceeds the saturation level of the detector. Furthermore, such high-power levels have a chance of damaging plastic components and optical films. To compensate for this, a hardware limit in the laser modulation circuit will limit the maximum power to 200 mW. Furthermore, power adjustment and retroreflection compensation is implemented with a polarized notch filter and quarter waveplate.

Table 9 Optical Power Management Scheme Comparison

	Polarizers	**ND Filter**	**Iris**
Complexity	Complex	Simple	Simple

Adjustable	Yes	No	Yes
Cost	High	Medium-low	Low

3.1.3. Collection Optics

3.1.3.1. Raman Filtering Comparison

In our research, the laser itself is strong enough to oversaturate the detector and wash out the Raman shift peaks. After the laser illuminates the sample, but before the light is collected and focused into the spectrometer setup, the laser light must be filtered out. To do this, a dichroic mirror will be employed to reflect the laser light away from the collection optics and allow the Raman shifted light in. The dichroic mirror is not enough on its own to suppress the residual laser light, and requires additional filters, or multiple filters stacked together to reduce the Rayleigh scattering of the laser light as much as possible. Additional filtering, such as a long pass filter, will be used to block the broadband fluorescence. This long pass filter is used to block wavelengths shorter than the laser wavelength. Raman shifts in this region (Anti-Stokes scattering) are less numerous and have lower intensities and work well for broadband Stokes collection. It does not work for anti-Stokes. Notch filters are another option. They reject a narrow band around the laser wavelength and enable both Stokes and anti-Stokes Raman. They tend to be used when both Stokes and Anti-Stokes scattering is required. A third option includes a bandpass filter, which rejects all light outside of the band the filter is designed for. It passes a very narrow band, but is useful for fluorescence removal, and if you are only looking to detect frequencies near the excitation frequency, or a certain range of peaks that fall within the bandpass filter region.

Our group decided to go with longpass filters rather than notch filters because not only are they less expensive, but also our application is not investigating the anti-stokes region, so longpass filters are a perfect fit.

Table 10 Notch Filters Comparison

	NF03	**NF785-33**	**ZER785F**
Vendor	Semrock	Thorlabs	Chroma
Description	785 notch filter	785 notch filter	785 nm notch filter
Transmission >90% Wavelength Range	400 – 742.1 nm and 827.9 – 1600 nm	590 – 760 nm and 810-1040 nm	500 – 760 nm and 805 – 1000 nm
Reflectivity @ 785	N/A	N/A	NA
Optical Density @ 785	>6	>5	> 5
Diameter	25 mm	25 mm	25 mm
Material	Fused Silica	Fused Silica	Fused Silica
Cost	$ 959.18	$ 635.55	$ 495

Table 11 Longpass Filters Selection

	FELH0800	FELH0775	10LWF-800-B
Vendor	Thorlabs	Thorlabs	Newport
Description	800 nm longpass filter	775 nm longpass filter	800 nm longpass filter
Transmission >90% Wavelength Range	812 – 2510 nm	787 – 2150 nm	815 – 1200 nm
Rejection Region	200 – 789 nm	200 – 763 nm	N/A
Optical Density @ rejection region	>5	>5	>3
Diameter	25 mm	25 mm	25.4 mm
Material	UV Fused Sillica	UV Fused Sillica	N/A
Cost	$ 169.26	$ 141.38	$142

3.1.3.2. Spectrometer Type Comparison

Just as there are many different types of spectroscopy methods based on your application, environment, and cost, there are multiple types of typical spectrometer designs as well. Different spectrometers exist based on the engineering need, such as resolution, noise level, size of the device, if it needs to be portable, and high throughput. Some of the different types include LGL (lens grating lens spectrometer), Littrow, Czerny-turner, and echelle. LGL spectrometers are very simple, containing a single beam optical path, including an entrance fiber, a collimating lens, a diffraction element, a focusing lens, and a detector. It is a two-lens system that provides a compact design and is typically very fast. Based on the design and lens choice, aberrations can occur, and stray light is common if the system is not baffled. The Littrow configuration has a grating that both disperses and reflects, and a collimated beam that hits the grating and returns along the same axis. It has high optical efficiency, high spectral purity, and resolution. On the other hand, it is limited because mechanical movements based on the rotation of the grating that is needed to scan the wavelengths can cause vibrations, which decreases the sensitivity, and could introduce noise. Another spectrometer layout is the Eschelle spectrometer, which combines a high-blaze echelle grating and a prism with a 2D detector, such as a camera. It uses high diffraction orders to achieve extremely high spectral resolution, and its speed is very fast, but limited by the camera's readout. It is expensive, requires larger optics, and a complex calibration technique.

We plan on employing a Czerny-Turner layout for the spectrometer design. The Czerny-Turner is a common layout employed in many commercial spectrometers. It describes a classic benchtop spectrometer geometry, and with the right design, the device can have a very high resolution. It is also very customizable and works with multiple slits and detectors. The M-Type configuration (Fig. 3.7) of the Czerny-turner is limited by its optical aberrations, induced by its off-axis mirrors. Coma and astigmatism are both possible, which are both unwanted aberrations that will reduce our resolution, and influence alignment negatively. Aberrations can be minimized with careful mirror selection and positioning.

This issue can be corrected by utilizing the crossed configuration (Fig. 3.7) instead. The crossed configuration results in very high aberration correction and has a better performance for high-NA collection optics, but it requires more complex alignment. The Czerny-turner includes a slit, a collimating mirror, a diffraction grating, focusing mirror, and a detector. Typically, the slit width controls the spectral resolution, and it ranges from 25-200 um. Good design practice for alignment includes starting with a larger slit and adjusting as we go. The first mirror is an off-axis parabolic mirror that collimates the light, leaving the slit onto the grating. The beam f/# directly correlates to the diameter and focal length of this mirror. The diffraction grating controls the dispersion of light. The blaze wavelength needs to be near our laser wavelength to maximize the dispersion efficiency at our chosen laser wavelength. The second mirror focuses on the dispersed light onto the detector array. The focal length of this mirror controls the linear dispersion at the detector.

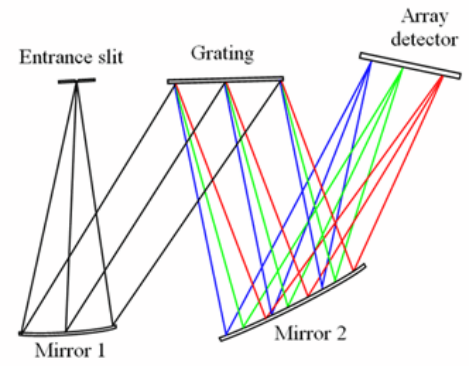

Figure 17 M-Type Czerny-Turner Spectrometer Configuration

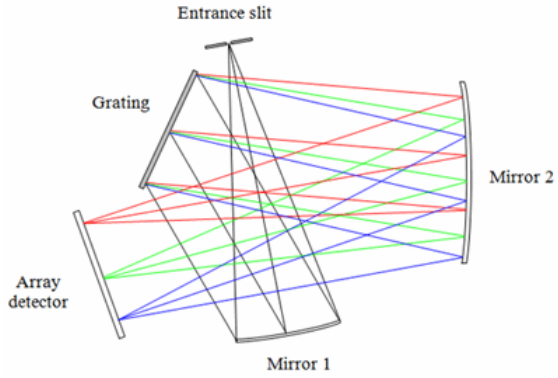

Figure 18 Crossed Czerny-Turner Spectrometer Configuration

Figure 3.7 – M-Type vs Crossed Czerny-Turner Spectrometer Configuration

3.1.3.3. Spectral Range

To begin the design of the spectrometer, a wavelength range must be selected based on the Raman shift requirements for your application, so in our case, we looked into databases

containing known Raman spectra for polystyrene, PET, and nylon [Fig. 3.4-3.6] to determine which peaks we would want to include, and wide of a range of wavelengths the spectrometer must be designed for. We choose 0 to 3200 wavenumbers, to capture the peaks we want to use for identifying the plastics. The range is so large because nylon and polystyrene have very high intensity peaks around 3000 wavenumbers, and we specifically do not want to leave high intensity peaks to make eventual identification and detection of the microplastics possible. With a goal Raman shift of 0 – 3200 wavenumbers, equation 3.2 enabled us to find a wavelength range of 780 – 1040 nm.

Raman Shift

$$\Delta v\ (Raman\ Shift) cm^{-1} = \left| \frac{1}{\lambda_{laser}} - \frac{1}{\lambda_{scattering}} \right| * 10^{-7} \quad (3.2)$$

Table 12 Summary of Wavelength Range of Spectrometer

Raman Shift Range	0 – 3200 cm^{-1}
Calculated Wavelength Range	780 – 1050 nm
Center wavelength	915 nm

3.1.3.4. Collection Optics – Focusing Optics into Spectrometer

There are 2 main microscope optical systems used with objectives, which are an infinity-corrected optical system and a finite corrected optical system. Once the light passes through the objective lens, it converges a point at the intermediate image plane, which then diverges back through the eye piece. With an infinity-corrected optical system, (Fig 3._) the light the passes through the objective does not focus down until it passes through the tube lens, which provides for a space between the objective and the tube lens, the infinite conjugate space, which offers advantages for our Raman setup. Our choice of using an infinity corrected microscope objective for the Probe Optics was with the goal of having a design that supports the necessary spectral filtering and beam conditioning in our system without degrading quality or focus. The parallel beam path that occurs in the infinite conjugate plane enables the placement of flat optics, such as filters and beam shaping optics while minimizing chromatic and spherical aberrations. This setup also provides the support needed for a high-NA objective that is required to collect the low levels of Raman scattering.

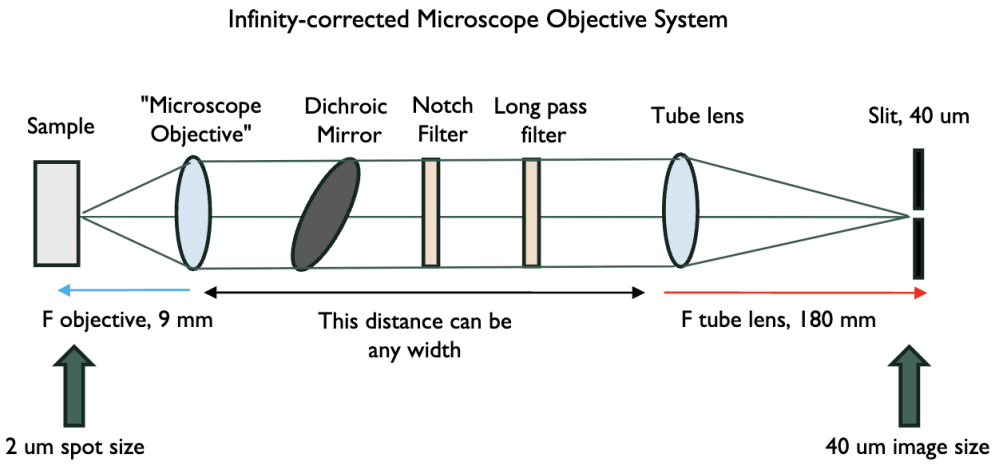

Figure 19 Infinity Corrected Microscope Objective System

The tube lens will focus the filtered Raman signal into the spectrometer's slit. In most cases, the tube lens is required, because infinity objectives produce a collimated beam, and the tube lens converts that collimated beam into a real image. The microscope objective is designed to work with the tube lens, and using anything else can introduce aberrations, decrease image quality, and vignetting. There is a drawback to using a tube lens, and that would be the price. (Table 3) For a 10x lower price, a high-quality achromatic doublet can replace the tube lens and focus the beam through the slit. This only works if the doublet has an AR coating near 785 nm. There are some risks, such as astigmatism, and the risk of a magnification mismatch- the focal length of the doublet much approximate the objective design tube focal length to preserve the stated magnification of the objective, or recalculations to find the actual magnification that is occurring need to be done.

Table 13 Tube Lens vs. Achromatic Doublet

	Tube Lens	**Achromatic Doublet**
Vendor	Edmund Optics	Thorlabs (AC254-080-B-ML)
Description	Olympus NIR single port tube lens	NIR Mounted Achromatic Doublets
Wavelength Range	400 – 100 nm	650-1050 nm
Focal Length	180 mm	Fa = 80.3 mm Fb = 73.5 mm
Coatings	N/A	AR Coated
Cost	$ 1,187	$ 141

3.1.3.5. Slit Size Selection

The slit of your spectrometer typically determines the resolution of your system; a narrower slit means a higher spectral resolution, and vice versa. The slit width defines the initial beam width that gets dispersed, and a narrower slit will produce a smaller image on your detector plane, which

would indicate a higher resolution. It also controls the signal intensity that gets through to the spectrometer. Especially for Raman spectroscopy, this tradeoff is very important. If the signal is too low, SNR is too low, and the noise dominates your system, and you might get no result. The slit also sets the entrance image height and width that goes into the dispersive optics.
In that way, the slit acts like a spatial filter, where if the slit is too wide, the spectral lines can overlap and blur, whereas if they are too narrow, the signal may be too weak to see clearly, even if the image is sharp, and at a high resolution.

To balance those tradeoffs, it is good practice to optimize the light entering your spectrometer by matching the image size from your focusing optic to the width of your slit or make it slightly smaller. After the diffracted limited spot size from the output of the microscope objective was calculated earlier, resulting in 2 um, that spot size can be used to find the resultant image size at the focal point of the tube. The equation below for the image size resulted in a 40 um image size based on the magnification of the objective and tube lens system, Therefore, a slit that is 30 um – 50 um should be selected, to match the image size as much as possible. Once the prototype is complete and we are still getting high signal, but want to improve our resolution, we can make the choice to decrease our slit, improve our resolution but decrease the signal getting to the detector. Once the light enters the slit, it hits mirror one, which is the collimating mirror. It then projects the collimated signal onto a diffraction grating, which splits the signal into its separate wavelengths, and is then reflected onto a focusing mirror which focuses each split up wavelength onto a certain pixel on the detector.

Table 14 40 um Slit Comparison

	S40k	**S40LK**	**VA100CP**
Vendor	Thorlabs	Thorlabs	Thorlabs
Description	High Precision Optical Slit	High Precision Optical Slit	Cage system Adjustable slit
Width	40 um	40 um	0 to 0.24 inches
Height	3 mm	10 mm	N/A
Diameter of Housing	1 inch housing	1 inch housing	30 mm Cage System
Cost	$ 119.33	$ 130.24	$338.11

3.1.3.6. Collimating and Focusing Mirrors Comparison

The collimating mirror converts the divergent light from the entrance slit into a parallel beam that uniformly illuminates the diffraction grating. This ensures that each wavelength strikes the grating at a well-defined incident angle, directly affecting the spectral resolution, dispersion uniformity, and throughput. After diffraction, the focusing mirror re-images the dispersed beam onto the exit detector plane, determining spot size, aberration levels, and image quality. These two mirrors together control the systems resolving power, optical efficiency, aberration budget, and stray-light performance. The coating, gold for NIR, and focal length, where a longer focal length improves the resolution, and reduces aberrations, but increases instrument size. Common mirror types include spherical, aspheric, and flat plane mirrors. Spherical mirrors provide both reflection and focusing power, whereas flat mirrors only redirect the beam- they do not collimate or focus. Using spherical mirrors

creates the necessary optical power for proper grating illumination and image formation, which directly affects the spectral resolution of spot size, line shape, and throughput. Flat mirrors only affect the beam direction, alignment, and do not contribute to resolution or focusing performance. Spherical mirrors are a compact way to collimate and focus but introduce aberrations with off-axis use, which occurs in our Czerny-turner spectrometer design, but are worth dealing with because flat mirrors cannot improve the image quality or resolution. The spherical mirror shape is essential to collect Raman spectral information at the level of detail that is required. Flat mirrors would be appropriate if our system size needs to be reduced to further condense and fold the system.

As our mirror type for the spectrometer design, spherical mirrors were selected to make sure that our system can also focus and help to improve the image quality, as the signal is passed through the spectrometer, and for the spectrometer to work correctly, the mirrors must have certain properties. To make sure that they perform optimally, the mirrors were chosen with a focal length that balances resolution and system size, a surface quality that minimizes scatter and aberrations, and a reflective coating appropriate for the wavelength range of interest. Gold coatings were selected for the NIR range to maximize reflectivity and reduce losses, while the curvature of the spherical mirrors ensures proper collimation of the incoming light and accurate focusing onto the detector plane. These considerations collectively allow the mirrors to maintain high throughput, minimize stray light, and preserve the spectral resolution necessary for precise Raman measurements.

Table 15 Collimating Mirror Comparison

	Thorlabs, CM750-200-M01	**Torrent**	Edmund Optics #37-242	Thorlabs, CM508-050-M01
Reflectance	>94%	>94%	>94%	>94%
Focal Length	-200 mm	101.6 mm	50.8 mm	50 mm
Diameter	75 mm	1 inch	25 mm	½ inch
Substrate	N-BK7	N-BK7	NA	N-BK7
Type	Concave	Concave	Off-axis parabolic	Concave
Coating	Gold	Gold	Gold	Gold
Price	$217.73	Borrowed	$291.50	$137

3.1.3.7. Grating Selection

The diffraction gating is one of the most important components for defining the range and resolution of your Raman spectrometer. It is responsible for separating the Raman signal into its constituent wavelength components. This separation allows us to discern each Raman shift that corresponds to the vibrational mode, which is used for identification and detection of plastics. This separation is done by the optical properties of the diffraction grating. The grating has a series of

closely spaced parallel grooves that separates light into its individual wavelengths by diffracting it. They work following the principles of interference and diffraction. There are many different types of gratings, each with their own advantages and disadvantages, depending on the spectrometer design. The first type to be discussed is transmission gratings, a transparent substrate patterned with periodic grooves or slits. Diffraction occurs by phases of changes between the slits. Light enters on one side, and the light diffracts as it passes through the grating. They provide a compact optical path, and alignment can be simpler, and are useful for compact spectrometers, but they can lose light due to transmission through the substrate, which results in absorption and scattering. Another example is reflection gratings, where light reflects off the grating surface, and diffraction occurs due to path differences between the grooves. These grooves are finely spaced and etched or ruled onto a reflective substrate. The efficiency of a reflective grating is governed by the blaze angle, which is a design parameter that determines how efficient energy is directed into a particular angle, at a specific wavelength. It is the physical tilt of the grooves on a diffraction grating. When the grating is operated near its blaze angle, the diffracted order at the diffraction angle is at its maximum. Reflection gratings cover broad spectra ranges and can provide a high spectral resolution due to the capability of an increase in groove density. Their disadvantages include their alignment complexity, as the incidence and diffraction angles need to be precisely controlled, and their efficiency drops sharply outside their blaze angle optimization range.

Table 16 Grating Comparison

	Newport GTI125-03A	**Optimetrics G830R800GGAC**	Edmund Optics #55-261	Edmund Optics #42-847
Groove Density (grooves/mm)	1200 grooves/mm	830 grooves/mm	1200 grooves/mm	1200 grooves/mm
Blaze Wavelength	750 nm	800 nm	750 nm	750 mm
Blaze Angle	26°	19.39°	26.73°	26.73°
Wavelength Range	700 – 3000 nm	400 – 2400 nm	700 – 3000 nm	700 – 3000 nm
Efficiency	60 – 80 %	60 – 70%	50 – 70 %	50 – 70%
Size	25 mm x 25 mm x 6 mm	25 mm x 25 mm x 9.5 mm	30mm x 30 mm x 6 mm	12.7 mm x 12.7 mm
Coating	Bare Gold	Bare Gold	Bare Gold	Bare Gold
Price	$137.27	$128.00	$210.94	$ 146.28

For our project, we have chosen a ruled reflective diffraction grating that has a high groove density to benefit from the high resolution offered, so the individual narrow Raman peaks can be deciphered as resolvable spatial separations. Additionally, we are planning to implement rotation stages for the precise alignment and find a grating that has a blaze angle optimized at our excitation wavelength for maximum efficiency. Overall, our final decision was between the Newport GT125-03A and the Optimetrics G830R800GGAC, as the Newport GT125-03A grating provides the highest efficiency at the 750 nm blaze angle while also being a proper size and being a performance and cost-effective match for our project, while the Optimetrics provides a grating at a blaze angle that is closer to the wavelengths we will be dealing with, and a comparable efficiency, at a lower price. Because we have been lent the Optimetrics grating for this project, it is the most cost-effective choice, even as the groove density is lower, the spectrometer portion can still be designed to provide the high resolution needed to decipher individual peaks.

The grating equation governs the expected diffraction from a diffraction of grating. [Eq. 3._] M describes an integer value describing the order of diffraction, λ describes the lights wavelength, describing the incident angle of light, and B describes the diffracted angle of light leaving the grating. For example, our selected grating at an incident angle of 0 degrees, would

Grating Equation

$$n * \lambda = d(\sin\theta_i + sin\theta_m) \tag{3.3}$$

Light incidents on a grating is diffracted by this equation. M is the diffractive order, λ is the lights wavelength, d is the spacing between grooves on the grating, a is the incident angle of light, B is the diffracted angle of light leaving the grating.

Resolving Power of Diffraction Grating

$$R = \frac{\lambda}{\Delta\lambda} = nR \tag{3.4}$$

The above equation describes the resolving power of a diffraction grating, where n is the order of diffraction, N is the number of grooves on the grating that is illuminated by the source, delta λ is the spectral resolution, in wavenumbers, and λ is the Raman shifted wavelength.

The resolving power of a diffraction grating by the Rayleigh criteria is defined above. [Eq. 3.__] n is the order of diffraction; N is the number of grooves illuminated by the source, Δλ describes the spectral resolution, in wavenumbers, and is the Raman shifted wavelength. The theoretical resolving power of our 800 lines/mm grating is about 800, and considering we illuminate our entire 25 mm grating, the resolving power would be 20,000, describing our best-case optical limit. As the size of the grating increases, resolving power increases. Resolving power scales linear with the number of illuminated grooves, so a larger grating or a larger illuminated area can help with a higher resolution. The resolving power relationship to resolution can be described in Equation 3.___. So, in our best-case scenario, from 800 nm up to 1300 nm, sub-micron resolution is possible.

Resolution and Resolving Power Relationship

$$\Delta\lambda = \frac{\lambda}{R} \tag{3.5}$$

3.1.3.8. Reflective Coatings Comparison

Table 17 Reflective Optic Coating Comparison

	Characteristics	Common Wavelength Range
Aluminum	Broad band	UV-IR
Silver	High Visible reflectivity	Visible-NIR
Gold	Best IR performance	NIR-IR

Within the spectrometry design, both the mirrors and the grating will be chosen to have a reflective coating. We chose gold coatings for our design because they typically have high reflectivity at 785 nanometers, and excellent reflectivity in the NIR range, higher than aluminum and silver. This ensures that there will be strong laser delivery, efficient signal collection, and higher SNR in weak

Raman signals. The gold coating also produces Minimal stray light, in comparison to using a dielectric coating. This is crucial because Raman signals are easily overwhelmed by background noise.

3.2. Electrical

3.2.1. Detectors

There are many different types of optical detectors. Depending on the physics used to obtain the optical signal, each type of detector has an optimal environment of use. Complimentary-metal-oxide-semiconductor (CMOS) are common options for imaging purposes. They are cheap, offer high performance in the visible spectrum, come in many prepackaged solutions, and some are robust enough for scientific applications.

CCD detectors are a common choice in Raman spectroscopy applications. They have quantum efficiencies above 50% in the infrared (IR) region. The IR region is a popular excitation source for Raman spectroscopy due to its low fluorescence response. High intensity values caused by fluorescence often overpowers the stokes shifted light. However, a Raman signal is still notoriously weak. In order to detect the Raman signal, both strong cooling of the CCD and amplification of the CCD output will be necessary. A heatsink and thermoelectric cooler (TEC) are the primary mechanisms to maintain operating temperature of the CCD. A very sensitive and noise resistant signal amplification circuit must be also utilized to amplify and digitize the weak CCD output.

The type of CCD sensor itself must also be taken into consideration. There are front-illuminated and back-illuminated sensors. Back-illuminated sensors are typically more sensitive and have lower noise than front-illuminated sensors. In these devices, the bulk silicon substrate the sensor is been fabricated on is etched thin, allowing more photons to come in contact and absorb within the actual active region of the CCD sensor. However, because of how thin these structures can be, longer wavelengths, like some of the Stokes-scattered signals we want to detect, may pass through the active region. This light can then reflect off the insulator layer, creating an etalon-effect within the semiconductor layers themselves, creating noise and distortion in the output of the CCD.

Table 18 Detector Comparison

Detector	Source	Wave-length Range	QE at laser	QE at Δ+200 nm	Pro	Con	Cost
CQD SWIR | ACUROS 1920-	**785**	700-1400	50%	25%	Has SDK USB Interface	Very big Difficult interfacing	Borrow

USB3-001 (2.2 MP)					Integrated Stage-1 TEC for 15 C		
CCD| Hamamatsu S10141 (2000 x 500)	**785**	200-1100	75%	20%	High sensitivity in NIR Stage 1 Integrated TEC for –14 C	Would need to design and fabricate electron control, TEC control, signal amp.	Borrow
CMOS | Sony STARVIS IMX327 (2 MP)	**785**	VIS-NIR	70% relative response	12% relative response	Easier than CCD	Not cooled, Typically has IR filter,	$180
CMOS | OSRAM OS05A20 (5 MP)	**785**	VIS-NIR	N/A	N/A	Easier than CCD	Not cooled	$80
CCD | Toshiba TCD1304DG	**532**	VIS	100% relative	10% relative response	More resilient to noise than 785	Would need to design and implement... Not sensitive enough	$13
CMOS | BlackFly FLIR Sony IMX265 (3.2 MP)	**532**	VIS	68.5 %	40%	Shown to work with OpenRaman project SDK CMOS are easier to interface with than CCDs	Not cooled	$1000 New, $250 used
CMOS | Raspberry Pi Cam (8 MP)	**532**	VIS	95% relative response	40% relative response	Easier than CCD High resolution, could use binning to boost signal	Not cooled Has IR filter	$50

We have decided on using a premade camera module. Ocean Optics is allowing us to borrow an ACUROS CQD SWIR camera. This is not a traditional CMOS sensor. The readout structure which converts the obtained optical signal into an electrical signal and transmits it to a processing unit is fabricated with CMOS technology, however the light absorbing layer utilizes thin film colloidal quantum dots (CQD) instead of fabricated semiconductor-crystal based pixels. Quantum dots are nanostructures in semiconductor material capable of absorbing and emitting photons of very specific energies. SWIR stands for “short-wave infrared” and occupies the 0.9-1.7 nm wavelength band.

Figure 20 ACUROS SWIR CQD

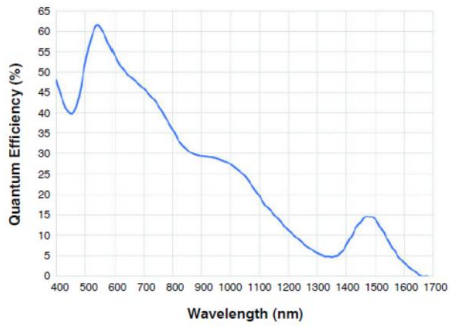

Figure 21 Detector Quantum Efficiency Plot

Figure 3. - ACUROS CQD 1920 USB3 SWIR Camera and Quantum Efficiency.

This detector offers a quantum efficiency of ~37% at 785nm, dropping off to ~27% at 1000 nm. These values far surpass other considered detectors, with efficiencies at ~10% and 2% at the target wavelengths.

The ACUROS camera has a built in 1-stage TEC, low signal amplification circuit, noise filtration, outputs to USB-B, and has a software development kit (SDK). The camera can reach temperatures as low as 15 C, has a dynamic range of It also has an OEM power cable with a split for a BNC input for trigger control.

This module interfaces with a USB-B and a Hirose 12-pin HR10 connector. The HR10 connector is for the OEM power cable which supplies power and a trigger signal. The power cable splits off into a wall power supply and a BNC input for trigger. The USB-B input is used for the camera to interface with a control PC. The SDK for the camera module supports Windows, Mac, and Linux operating systems.

The camera module supports integration times between 100 µs and 30 ms, has a dynamic range of 70 dB,

3.2.2. Processing Computer

A processing computer will be necessary to perform data processing of the received spectra. The camera module has an SDK and imaging software that allows for control of the TEC temperature, integration time, and access to individual pixel values. However, the imaging software is only compatible with the Windows operating system. If a Raspberry Pi or other "mini-computer" with a Linux based operating system is used, a virtual machine must be run to use the OEM software. This can be circumvented with the of the SDK, which supports custom Linux GUIs and UART commands which allow for control of the camera module.

Table 19 Processing Computer Comparison

	Raspberry Pi 5	**NVIDIA Jetson**	**External PC**
Processor	Broadcom BCM2712 Arm Cortex-A76	ARM Cortex-A57	N/A
Clock Rate	2.4 GHz	1.43 GHz	2.4+ GHz
RAM	8 GB	4 GB	8 GB+
Storage	Custom with microSD	Custom with microSD	Custom with SSD/HDD
Operating Voltage	5 V	5 V	N/A
Max Current	5 A	2 A	N/A
Max Power Draw	25 W	10 W	N/A

A Raspberry Pi 5 will communicate with the camera module and perform spectral analysis of the acquired data. The Raspberry Pi 5 is capable of hosting the Linux operating system, which the ACUROS SDK supports. This enables ECOspec to perform analysis of the obtained spectra without the need for an external computer. Communication with an external computer would introduce work outside of the scope of the project including TCP/IP and SSH protocols.

3.2.3. Safety and Status Control

Table 20 MCU vs FPGA Comparison

	MCU	**FPGA**
Typical Speed	Fast	Faster
Application	General Purpose	Application Specific
Configurable	Software	Hardware + Software
Programming	C	Hardware Description Language (HDL)

There are two main types of ICs used for larger system control: Microcontroller Units (MCU) or Field-Programmable Gate Arrays (FPGA). MCUs are very cheap, low power, easily programmable, and general-purpose processors. The hardware configuration included in these chips are permanent, but the nature of the device allows it to be used in a wide variety of applications. FPGAs boast lower power consumption and higher achievable operation speeds. They also offer the ability to configure the hardware through hardware description languages (HDL), meaning the logic paths which data physically propagates through can be customized. This allows them to operate at higher data rates than typical MCUs. However, FPGAs are primarily used in specific applications, where the input data will be repeatedly processed in the same manner. Furthermore, FPGA configuration is a difficult and time-consuming task.

Table 21 MCU Selection

	ESP32	Teensy 4.1	STM32
Max Clock Rate	240 MHz	600 MHz	168 – 250 MHz
Dual Core	Optional	Optional	Optional
Flash Memory	4 MB	8 MB	16 – 128 KB
I/O Ports	36	40	40
Operating Voltage	3.3 V	3.3 V	3.3 V
Max Current Draw	1.3 A	500 mA	200 mA

An MCU is best suited for control of the status and safety systems of ECOSPEC. While an FPGA may enable faster processing speeds, the design necessary to implement the system is unnecessarily difficult when compared to an MCU. With the ever-increasing prevalence of microelectronics, there is a wide selection to choose from. For the purposes of ECOSPEC, the MCU will not perform heavy calculations or experience strenuous loads. Thus, it does not need a high-performance processor. It simply needs enough bandwidth to monitor all systems of the device, control laser power, control the safety interlocks, and turn on LEDs.

The MCU serves as a status monitoring system separate from the Raspberry Pi. This is done to ensure the reliability of the safety subsystems. In case the Pi experiences some failure during processing or communication with the camera, the MCU will be able to actively monitor the system regardless.

An ESP32 will act as the primary controller of the safety interlocks, status indicators, and laser power. The ESP32 is a dual core processor, enabling two parallel actions to run at once. One core will be dedicated to always monitoring the status of the safety interlocks and laser power. The second core will perform all other functions necessary, such as engaging the locks, engaging the laser power, modulating the digital potentiometer to control the laser power, and controlling the status LEDs.

If any of the access doors are open, or the safety interlocks are not engaged, the laser will not be able to turn on. If the enclosure is somehow opened during operation, the MCU will disengage the laser as quickly as possible. If the runtime of the system exceeds a predetermined time limit, the laser will also immediately shut off.

3.2.4. Safety Interlocks

To comply with the safety regulations surrounding the use of a class 3B laser, the system enclosure must implement safety interlocks. This is to ensure that no harm is caused during operation of the device. There are many different types of safety interlocks, ranging from mechanical actuators to electromagnetic relays. Electromagnetic locks offer higher force output, non-contact applications, longer lifespans, and are more tamper proof. ECOSPEC is planned to be a smaller device where the use of 1000s of newton's of force would be redundant.

Table 22 Safety Interlock Comparison

	Banner SF-RA	**Honeywell 22AC2**	**Pheonix 2702973**	**Custom Lock w/ Servo**
Actuation Time	100 ms	100 ms	100 ms	200 ms
Mechanism	Push actuator	Push actuator	Non-contact	Linear Actuator
Supply Voltage	24 V	125 V	24 V	5 V
Cost	$56.98	$28	$20.20	$12.99

The Ocean Optics LASER-785-LAB-ADJ has a "Remote Interlock" trigger input on the back panel with an RJ-11 connector. This "Remote Interlock" input is designed as an open circuit. Without this input being occupied with an RJ-11 connector with a "closed loop" circuit, the laser will be forced into a "standby" mode. This laser comes with a modified (shorted) RJ-11 connector to enable operation without an external input.

The "Remote Interlock" is a safety feature that automatically shuts down the laser when a trigger such as a door or an enclosure opening occurs... The laser functions normally when is senses a closed circuit, but it will disable laser output when it detects an open circuit. To re-enable the laser function, you must make sure that the interlock is a closed circuit, and then manually reset the laser by toggling the Laser On switch on the front panel to the ON position." [Ocean Optics Laser manual]

3.2.5. Cooling

Table 23 Cooling Technology Comparison

	TEC	**Coolant-Based**	**Fans and Heatsink**
Feasible Cooling Area	Selective	Very selective	Cools large volumes
Complexity	High	Very high	Low

Risk	High	Very high	Low
Cost	Medium	High	Low

Another of ECOspec's software goals is thermal stability, primarily in the form of cooling systems for sensitive components within the test environment. The precision required to perform reliable Raman spectroscopy means that temperature control of both the sensor, laser, and environment is paramount. While the detector has an integrated stage-1 TEC capable of cooling the sensor to 15 C and the laser has a dedicated cooling system, the surrounding subsystems and ambient air must also not undergo considerable thermal shift. A simple ventilation system will be set in place to maintain air circulation and assist in lowering the equilibrium operating temperature.

When the cooling system is active, several measurements will be taken to determine the resilience of the device to temperature fluctuations. If the system's accuracy is disturbed with simple air flow, larger consideration will be taken into the thermal isolation of the measurement systems. Calibration of any measurement should be taken with the fans active, after the device has reached an equilibrium temperature, for repeatability purposes.

3.2.6. Laser Control

The laser offers external control through two inputs: "Remote Interlock" and BNC control. The "Remote Interlock" input uses an RJ-11 plug and takes in a trigger input from a signal such as an opened door. The laser will not begin emission unless the RJ-11 port has a "closed-loop" connection.

This laser supports an "External Power Control Mode." [OceanOptics 785 manual] This external control is implemented through a "Remote Interlock" RJ-11 plug interface and power control BNC interface.

The laser driver circuit will control the power output of the Ocean Optics LASER-785-LAB-ADJ. The BNC control takes in DC input of 0-1 V, and can modulate the laser from 0% to 100% up to ~300 KHz. We will not be modulating the laser during operation, so frequency of no concern. The digital potentiometer should act as a simple voltage divider, and be capable of being set to a 0 V point.

Table 24 Digital Potentiometer Comparison

	AD5220	**AD5160**	**AD5231**	**TPL0501**	**X9C104**
Resolution	128	256	1024	256	32
Supply Voltage	5.5 V	2.7 - 5.5 V	2.7-5.5 V	5 V	5 V
Still manufactured	No	Yes	Yes	Yes	Yes
Comm Protocol				SPI	N/A
Cost	$3.12	$4.15	$10.24	$4.58	$3.96

3.2.7. Display

Table 25 Display Comparison

Specs	Geeekpi 10.1" Touchscreen	Waveshare 7" LCD	Raspberry Pi Official 7" Touchscreen
Screen Size	10.1 inches	7 inches	7 inches
Resolution	1024 x 600	1024 x 600	800 x 480
Touch Capability	Capacitive Touchscreen	Resistive Touchscreen	Capacitive Touchscreen (10 finger)
Interface	HDMI	HDMI	DSI (Ribbon)
View Angle	178 degrees	170 degrees	170 degrees
Power Supply	5 V DC	5 V DC	5 V DC (GPIO)
Raspberry Pi Compatible	Yes	Yes	Yes
Dimensions	9.25" W x 5.59" H	6.5" W x 4.5" H	6.5" W x 4.25" H
Cost	$60	$45	$80

With using a Raspberry Pi, we focused on making ECOspec more of a standalone device. Much consideration was taken regarding the need of an external PC for data acquisition. It was decided the use of an LCD display would enable easier integration with the system rather than configuring communication protocols with external devices.

The GeeekPi 10.1" Touchscreen was selected over the more expensive Raspberry Pi Official 7" Touchscreen despite the official display's optimized integration and 10-finger capacitive touch capability. While the official Raspberry Pi display offers seamless compatibility and uses the DSI ribbon cable interface, which frees up the HDMI port, it has a smaller 7-inch screen with a lower 800 x 480 resolution compared to the GeeekPi's 1024 x 600 resolution.

For ECOspec's application, the larger screen size and higher resolution are more important than the advanced multi-touch features. Displaying detailed Raman spectral plots requires adequate screen real estate and pixel density to show fine peaks and variations in intensity. The 10.1-inch display provides approximately 40% more viewing area than a 7-inch screen, making it easier for users to interpret spectral data without straining to see small details.

The HDMI interface on the GeeekPi, while occupying the HDMI port, is a widely supported standard that simplifies troubleshooting and provides flexibility if the system needs to be connected to external monitors during development or demonstrations. The official display's DSI interface, though elegant, is proprietary and offers less flexibility for alternative configurations.

The 10-finger capacitive touch on the official display is more advanced than needed for ECOspec's interface, which primarily requires simple single-touch interactions for menu navigation and button presses. The standard capacitive touch on the GeeekPi is more than sufficient for these tasks. The cost savings of approximately $20-30 compared to the official display also allow the budget to be allocated to other critical components, such as optical elements or cooling systems.

Overall, the GeeekPi 10.1" Touchscreen provides the best balance of screen size, resolution, and cost for ECOspec's specific needs, making it a more practical choice than the smaller, more expensive official Raspberry Pi display.

3.2.8. Voltage Regulators

Table 26 Voltage Regulating Technology Selection

	Linear	**Switching**
Efficiency	Low	High
Heat generation	High	Low
Power tolerance	Lower	Higher
Output Noise	Near noise-free	Possible from switching frequency

Multiple major components throughout the system require various levels of a stable voltage and current draw. The ESP32 requires a 3.3 V up to 1.3 A, the Raspberry Pi 5 requires 5 V up to 5 A, and the safety interlocks require 24 V. In order to generate stable sources of these specific voltage levels, the use of regulators must be employed.

Linear regulators function largely through resistive means. They dissipate heat through a resistive component, ensuring a voltage output with minimized noise. Linear regulators would be best applied for components who need stable voltage supplies of lower voltage levels. A linear drop-out (LDO) regulator is commonly internally integrated in many MCUs such as the ESP32. An LDO would be the optimal source for the 1 V external BNC control of the laser.

Switching regulators include more complex circuits, involving transistors, filters, and pulse width modulation (PWM) to adjust the output voltage. They boast much higher efficiency, higher output currents, lower operating temperature, and reduced EFI. For our applications and to prioritize thermal management, switching regulators are a better fit than linear regulators. Switching regulators will be used to generate the supply voltage for the controlling electronics.

Table 27 1.0 V Buck Regulator Comparison

	AP7366-W5	TI LP5910-1.0	TI TPS78501
Min/Max Input Voltage	2.2 - 6.0 V	3.3 V	6 V
Output Voltage	0.8V - 5.0 V	1.0 V	1.2 V - 5.5 V
Max Output Current	0.6 A	1 A	1 A

Table 28 3.3 V Buck Regulator Comparison

	AP63203	LM2679T-3.3 / ADJ	LD1117V33
Min/Max Input Voltage	3.8 V - 32 V	8 V - 42 V	3.3 V - 15 V
Min/Max Input Current	4 A	8 A	800 mA
Max Output Voltage	3.3 V	3.3 V	3.3 V
Max Output Current	2A	7 A	800 mA
Switching Frequency	1.1 MHz	260 kHz	N/A (LDO)

Table 29 5 V Buck Regulator Comparison

	AP63205	LM2679T-5.0 / ADJ	TPS54331
Min/Max Input Voltage	3.8 V - 32 V	8 V - 42 V	3.5 V - 28 V
Min/Max Input Current	4 A	8 A	4 A
Max Output Voltage	5.2 V	5.0 V	25 V
Max Output Current	2A	7 A	3 A
Switching Frequency	1.1 MHz	260 kHz	570 kHz

T

The TI LM2679T-ADJ was selected as the buck converter for both the 3.3 V and the 5 V regulator boards. The output voltage of this regulator can be adjusted with a set of resistors on the ”feedback” pins of the regulator. The specific variation of the regulator is in a 7-pin NDZ package. The regulator can output up to 5 A of current, which is required for the maximum 5 A draw of the Raspberry Pi. (However, without changes in the software, or a “power-delivery” (PD) controller, the Pi will limit itself to a 3 A draw). A “softstart” feature is also included in the package, enabling the use of capacitors to protect against strong fluctuations in voltage such as during start up or heavy electrical load.

3.2.9. Power Supply

The power supply must provide enough wattage to satisfy the voltage and current requirements of all components. Consideration of max draw of all components should be taken into account when determining the minimum wattage.

Table 30 Power Draw Table

	Voltage	Current
ESP32	3.3 V	1.3 A
Raspberry PI	5 V	5 A
Safety Interlocks	12 V	30 mA
Fans	5 V	500 mA
Laser Control	1 V	20 mA

Considering the largest required voltage for the electrical system is 12 V, a 12 V main power supply will be sufficient. However, it must be capable of providing a large current draw to supply all the individual components. A main 12 V 120 W PSU will be used to supply power to the whole system. High amperage draw is expected due to Raspberry Pi, multiple sensors, fans, safety interlocks, and MCUs. Voltage regulators, mainly buck converters, will be used to supply power to devices requiring a lower voltage from the original power supply. This includes 3.3 V for the MCUs and fans, 5V for the laser and CCD, and 12 V for the safety interlocks.

Table 31 DC Power Supply Comparison

	SUPERNIGHT 360 W PSU	ALITOVE 240 W PSU	ALITOVE 120 W PSU	ALITOVE 180 W PSU
Power	360 W	240 W	120 W	180 W
Voltage	12 V	12 V	12 V	12 V
Max Current	30 A	20 A	10 A	15 A
Recommended Max Current	26 A	18 A	8 A	10 A
Type	Switching	Switching	Switching	Switching
Connector	Screw terminal	Screw terminal	Barrel jack	Barrel Jack

There will be three components which need 120 V AC wall power: the 12 V power supply, the ACUROS CQD SWIR camera module, and the 785 nm laser source. As the camera module and laser source are borrowed pieces of equipment, risk must be minimized when working with them. Creating custom power delivery schemes for these highly sensitive devices not only risks damaging them, but would also extend the scope of the project beyond its original intention. These three devices will have their power cords hidden and neatly plugged into an enclosed power extension strip. Only the cable of the power extension strip will exit the device's case.

The ALITOVE 180W power supply unit will be used to supply power to the voltage regulators. This power supply provides a voltage between the required levels of 3 V and 12 V to ease the load on each subsystems voltage regulator. It also provides plenty of current for all peripherals to operate as intended.

3.3. Software

3.3.1. Programming Language

One of the most fundamental questions to be asked when developing any kind of system or application is programming language selection. This choice can drastically shift the overall design structure of the system, as every language has its differences in syntax, execution, memory management, standard library ecosystems, and more. When selecting the language for ECOSpec, many of the primary objectives for our software system we consider are the ease of implementation for large dataset processing, as well as low level control of system hardware. These goals allow us to focus on creating a system with a high degree of functionality when acquiring and analyzing Raman spectra, while also maintaining a robust control scheme of our underlying embedded system. With these goals in mind, we are able to consider languages such as Python, MATLAB, Rust, Java, and CC.

One of the fastest-growing languages in modern system design is Python. This reason for this being is its simplicity in syntax, making rapid prototyping and development easier to access. More importantly, Python has an expansive ecosystem of libraries for multiple scientific and data-processing applications, such as NumPy and SciPy. These tools provide us with a simple way to perform complex transformation on our acquired Spectra, such as filtering, correction, peak detection, and similarity comparison, achieving core components of ECOSpec's software pipeline. Python is also incredibly portable, being an interpreted language run on its own virtual machine, making it great for prototyping across multiple devices and architectures. Due to this overall ease of use when developing Python code, one primary tradeoff is speed of execution. Compared to other languages, especially lower-level languages with more system-level control, Python can be orders of magnitude slower and therefore suboptimal for high-performance systems. This makes Python a strong choice for data-analysis but makes it difficult to justify for the embedded requirements of ECOSpec.

One language that places much more emphasis on engineering and scientific applications is MATLAB, especially when considering signal processing and analysis. Much of this functionality is provided through its numerous toolboxes that provide pre-established algorithms for data handling, many of which can be applicable in Raman spectra analysis. However, MATLAB is a proprietary language, with a heavy cost burden to obtain a license. Additionally, MATLAB is not built for use on embedded platforms, due to its lack of flexibility and system-level functionality.

In a similar vein to Python, Rust is a modern systems language with an emphasis placed on memory safety, without requiring the implementation of a garbage collector. This allows Rust to provide performance similar to languages that operate much closer to the hardware, such as C/C++. Rust also presents compile-time guarantees against memory corruption, as well as a strong type system and borrow checker. At the current moment, Rust lacks much of the scientific library support that Python has, making it less flexible for large dataset operations and transformations. Additionally, its tooling for embedded applications is still in its infancy and therefore not ideal for applications of this scale.

Another option for our application to be considered is the implementation of Java. Similar to Python, Java is platform-agnostic, running on its own virtual machine (JVM), once again providing a portable, predictable runtime. Unlike Python, Java is strictly object-oriented, which promotes organization and modularity within the application; it can also impose restrictions on design flexibility. While Java does still have a large collection of standard libraries with integrated functionality, it lacks the quantity of the scientific and data-analysis tools that Python provides. This would require a much higher code cost to perform the advanced transformations on spectra that ECOSpec requires. This alongside Java's much more rigid programming style makes it less optimal for our data-processing and system control requirements.

Contrasting both Java and Python, C provides a much lower-level set of controls for system resources. Since C operates on a level much closer to the hardware, it is able to have direct influence on memory through concepts such as pointers. Giving the developer access over these interactions allows C to excel in embedded applications, where interfacing multiple devices effectively is paramount. Additionally, C has a much lower runtime overhead compared to languages that run within their own VM, making it ideal for critical tasks within ECOSpec, such as safety systems and laser control. The cost of this much higher degree of control correlates to a much higher degree of complexity within the program itself, requiring the developer to perform manual management of systems such as memory.

For our application, each language offers traits that align with the numerous system components of ECOSpec. Python provides a simple way of implementing high-level data processing on large datasets for spectral analysis. C gives low level control of hardware components with low overhead, making it suitable for our critical embedded control. Java, while offering some of the benefits from both C and Python, does not provide enough to fully align with the requirements of the system. Through these insights, we concluded that a mix of both Python and C would allow us to fully fulfill all ECOSpec's core specifications.

Table 32 Compare Programming Languages

	Python	**Java**	**C**	**MATLAB**	**Rust**
Execution Method	Interpreted	Interpreted/Compiled Hybrid	Compiled	Interpreted	Compiled
Performance	Slow	Moderate	Fast	Fast	Fast
Memory Managment	Automatic	Automatic	Manual	Automatic	Manual

3.3.2. Communication Protocol

When designing systems in the modern era, the ability to interface multiple subsystems together becomes paramount. This can be anything from multiple controllers interacting or even connecting a system to a computer for additional control or processing. All these possibilities require the employment of communication protocols, allowing devices to communicate with each other to transmit information. These are used due to their standardized nature, ensuring usability across numerous applications, from both off-the-shelf and custom-made parts. As our application consists primarily of communication between controllers, as well as communication to a computer, three of the most common communication protocols come to mind. These are Universal Asynchronous Receiver/Transmitter (UART), Serial Peripheral Interface (SPI), and Inter-Integrated Circuit (I2C).

One of the simplest communication methods employed with embedded and integrated systems is the Universal Asynchronous Receiver/Transmitter (UART) method. This technique works between two devices, both with a transmit (Tx) and a receive (Rx) pin, enabling full-duplex communication. Data is sent serially between these two devices through their respective pins, then being read and utilized by the CPU or any other processing devices on the chip. The asyncronicity of UART references the lack of a unifying clock signal between the chips, with the alternative used being a start and stop bit placed on either side of a data packet. To ensure that data is received as intended, and no bits are misunderstood or lost, UART requires an identical (with ~10% margin of error) baud rate to be configured on both chips. UART also comes with the additional ability to interface with a computer system using a USB-to-serial adapter. This approach provides a very simple way to enable chip to chip communication in a system, but this simplicity comes at a cost, that being that a misconfiguration of the baud rate can cause data to be unusable, and therefore hinder any major subsystems that rely on these lines of communication. Additionally, UART has a relatively low ceiling in terms of data transfer speeds.

Beyond UART, another interface that can be used for communication between ICs is the serial peripheral interface (SPI). This protocol is most often used for communication between microcontrollers and peripheral ICs such as ADCs, shift registers, and many others. The most obvious difference between SPI and UART is the fact that SPI is a synchronous interface, with a shared clock line between SPI devices. It is also full-duplex and is able to be configured for rising or falling edge synchronization. Alongside the clock line, SPI interfaces require master-out slave-in (MOSI) and master-in slave-out (MISO) on the main node, and slave data-in and slave data-out (SDI/SDO) on each sub-node. Finally, SPI setups can require chip-select (CS) line for every sub-node, but this can be cut down to one when utilizing a daisy chain configuration, which connect the output of every sub-node to the input of the following node, allowing less lines to be used overall. SPI's overall design allows it to support much higher speed compared to UART, as well as supports multiple devices in the same SPI connected environment. These benefits come at a cost however, with SPI requiring a large number of pins as the number of devices increases, as well as requiring the components to be located close together to prevent signal loss or corruption.

The third protocol to consider is Inter-Integrated Circuit (I2C) communication. I2C combines many of the positives of the previously mentioned protocols to strike a balance that creates a flexible and powerful method of communication between chips. Similar to UART, I2C uses only 2 wires to handle its data transmission. Unlike UART however, one of these wires is entirely dedicated to the clock signal defined by the master, similar to SPI, making it a synchronous protocol. I2C transfers data serially through messages broken into data frames. These frames contain a start, followed by an address to select the correct sub-node. The sub-node will then send an ACK/NACK bit. Assuming ACK is received, the data is then transferred in multiple frames, each followed by an ACK/NACK, until the stop bit is received. As mentioned earlier, I2C has a lower hardware cost compared to SPI, with only two wires being required, as well as confirmation during data transfer through the ACK/NACK bits. Unfortunately, I2C cannot reach data transfer rates as high as SPI, but still higher than UART, as well as has an 8-bit limit for each data frame, which can cause large data transfers to be long.

For our application, two of the three protocols fit the requirements we have set out. The first one is UART, which can be used primarily for communication with computers, such as a Raspberry Pi or PC, through a USB-to-Serial adapter. This gives us access to high level control of lower-level systems through a uniform control center. Alongside UART, we can utilize I2C to enable easy communication between numerous peripherals, such as locks, detectors, and various other peripherals, while maintaining a lower hardware cost and simple implementations.

Table 33 Communication Protocol Comparison

	UART	**SPI**	**I2C**
Maximum standard Speed	115200 bps	16 Mbps	400 Kbps
# of wires	2	N + 3	2
Duplex	Full-Duplex	Full-Duplex	Half-Duplex

3.3.3. Spectrum Data Processing

In the goal of processing the raw spectral values into something usable for identification and utilization, numerous steps need to be taken to ensure every reading is put on a level playing field. Without this, it would be difficult to find consistent results when comparing acquired spectra with our library reference spectra. When determining a processing pipeline that would be the most effective for the application, noise/cosmic ray removal, fluorescence removal, normalization and scaling, and finally, comparison. Elaboration on the options for each of these steps will be discussed as we continue.

3.3.3.1. Noise / Cosmic Ray Removal

One of the most essential aspects of working with sensor data is removing or reducing the amount of external noise within the data. This noise can get in the way of accurate readings and cause the system to make wrong assumptions about the data. In the case of Raman

spectroscopy, one of the most common forms of noise is cosmic rays, which can appear as thin, random spikes.

To remove these artifacts from the acquired spectra, there are numerous algorithms that can be implemented within the processing pipeline. One of these methods is to rely on the localized nature of cosmic ray interference. Since the spectral span of these artifacts is usually very small, it is possible to remove them utilizing interpolation, which is the process of estimating unknown data that falls between known points based on a constructed curve. The downsides of this approach is that you lose true data, in exchange for an inferenced point, as well as the possibility of creating artificial features, dependent on the interpolation method used.

Another possible method is to use the random nature of cosmic ray interference. Since the chance of cosmic ray interference at the same wavelength across two spectral acquisitions is infinitesimally low, you can compare two different acquisitions of the same sample, and identify any major disparities between the two that would be indicative of cosmic ray interference (thin, tall, peak not matching the general shape of the spectra). The most obvious negative to this approach is the requirement of multiple readings of the same sample to be effective, which may not always be available.

The methodology that we elected to utilize sits as an alternative to the previously mentioned ideas that taking advantage of the nature of cosmic ray interference, this method being the usage of a median filter. A median filter works by replacing each point with the median of its neighbors based on a given window size. This filter is especially effective for our application of Raman spectroscopy, as it allows us to remove noise from cosmic rays and replace it with data based entirely on the shape of the spectra. This algorithm allows us to remove spikes that are not a part of the sample, while maintaining the overall shape of the spectral reading, removing the possibility of creating artificial features.

Table 34 Cosmic Ray Removal Method Comparison

	Interpolation	**Multi-Spectra Comparison**	**Median Filtering**
# of required spectra	1	2+	1
Time complexity	O(N)	O(MN)	O(N)
Space complexity	O(N)	O(MN)	O(N)

3.3.3.2. Fluorescence Removal

Another common enemy in the realm of analysis of Raman spectra is the presence of fluorescence. Fluorescence is the phenomenon in which a material, upon being exposed to light such as a laser, absorbs and then emits light at a longer, lower-energy wavelength. In the context of Raman spectroscopy, this interference can appear as a sort of "offset" within the spectra.[21] Fluorescence can cause the introduction of distortion or the burying of

Raman peaks, as well as causing a "sloping" baseline to appear, making analysis inconsistent between samples. To remedy this, numerous processing algorithms can be implemented, allowing us to achieve consistent spectra across materials.

One of the commonly utilized methods for fluorescence removal when working with Raman spectra is the method of derivative spectroscopy. This method can be implemented in numerous ways, but all follow the same principle. This technique focuses on utilizing the mathematical concept of derivation on a set of points to remove broad background features, such as those caused by fluorescence, while enhancing peaks. The consequences, however, include amplification of noise from the detection hardware, as well as distortion of some peaks, making intensity analysis unreliable, which could in turn make comparison and identification difficult.

A second method that could be developed is wavelet filtering. Wavelet filtering takes the properties of wavelets, a short oscillating waveform with an average value of zero. The properties of these wavelets are used to perform a discrete wavelet transform to decompose the signal into approximation and detail coefficients [22]. The components representative of the fluorescence background can then be suppressed or removed entirely, and the spectra can be reconstructed using the remaining coefficients. This technique provides a much more adaptive fluorescence removal, not assuming a specific baseline shape that other methods might. Wavelet filtering is not perfect, however, as this filtering can introduce artifacts as it tries to extend the data for use, as well as can be computationally intense, leading to longer processing times.

In contrast to the previously mentioned technologies and methodologies, baseline correction serves as a simple method for the removal of fluorescence. Baseline correction functions by utilizing one of many possible algorithms to fit the raw spectra, such as polynomial fitting, asymmetric least squares, and many others that achieve the same goal. These fitted models are then subtracted from the raw spectra values, both removing the fluorescence background, as well as enhancing the features defined by the Raman peaks. This method has much lower compute requirements but can scale quickly depending on the model used for fitting; however, bad parameter selection can cause over or under fitting. For our application, we elected to use a polynomial fitted baseline correction to handle fluorescence. We chose this due to its ease of implementation, as well as flexibility in terms of model parameters, allowing us to adjust only the degree of our polynomial model to enhance or reduce the amount of fit.

Table 35 Fluorescence Removal Method Comparison

	Derivative Spectroscopy	**Wavelet Filtering**	**Baseline Correction**
# of required spectra	1	1	1
Time complexity	O(N)	O(N log N)	O(N log N)
Space complexity	O(N)	O(N)	O(N)

3.3.3.3. Normalization

Continuing with the goal of utilizing our preprocessing pipeline to create consistent, comparable spectra, we need to ensure that all the data is screened to remove any possible variations due to external factors, such as laser fluctuations, sample positioning, and detector sensitivity drift. Our primary tools against these environment-based fluctuations lie within our normalization step. There are many different methods of normalization available to utilize. We will discuss these options as we continue.

One common method used in Raman spectroscopy to address normalization is the concept of Multiplicative Scatter Correction (MSC). MSC attempts to remove baseline shifts as well as scale differences between samples, by addressing both additive and multiplicative effects. When executed correctly, MSC gives a smoother and more physically consistent normalization effect on the spectra.

Unfortunately, MSC cannot achieve this quality of results on its own. A pre-requisite to performing MSC normalization is the presence of reference spectra. These spectra are used to create the regression model that is at the heart of the MSC technique. For our application, requiring multiple spectra goes directly against our goal of usability, and therefore makes it unfeasible for the application at hand.

An option that does not require reference spectra is vector normalization (L2 normalization). This method works by making the total magnitude of each spectrum equal, attempting to account for any global intensity differences. With this technique, the peak ratios are preserved across spectra, but the values become normalized across acquisitions, which accounts for many of the possible sources of variation mentioned previously. One benefit of this algorithm compared to MSC is the simplicity of implementation, making it easy to experiment and tune. On the other hand, vector normalization is unable to remove any baseline offsets, and it can also be very sensitive to noise when peaks are weak, which is impractical for Raman applications, as the signals received tend to be inherently weak, making this method suboptimal for our goal.

The method we have selected to use -- Standard Normal Variate Normalization (SNV) combines the best parts of both vector normalization and MSC. SNV can remove both additive and multiplicative effects of a spectrum, like MSC, while only using data from the spectrum itself, not requiring any reference, akin to vector normalization. It does this by both subtracting the mean, recentering the data around zero, as well as dividing the standard deviation, bringing everything to a unit variance. This algorithm proves to be the best choice to meet our goal, allowing us to have simple to implement, yet easy to use and powerful processing tool available to ensure our data is in a form that is usable downstream.

Table 36 Normalization Method Comparison

MSC	L2 Normalization	SNV

# of required spectra	2+	1	1
Time complexity	O(N)	O(N)	O(N)
Space complexity	O(N)	O(N)	O(N)

3.3.3.4. Scaling

The final step in our preprocessing pipeline before our data is ready for comparison is scaling. At its most basic level, scaling adjusts the range or magnitude of all the intensities across the spectrum. This makes sure that all values contribute accordingly when performing further analysis, ensuring that differences in scale do not skew the downstream analysis of the acquired spectra. To achieve this, there are multiple methods we could employ, including mean centering, autoscaling, and min-max scaling.

The first of the methods mentioned, mean centering, is commonly employed before multivariate analysis. Mean centering works by computing the mean intensity across multiple spectra and subtracts this mean from every wavenumber's intensity value. This technique has a very simple implementation, that emphasizes variation while preserving the relative scale. However, this technique can be vulnerable to outliers, and most importantly, requires multiple spectra, making it suboptimal for our application.

Another commonly utilized method for scaling Raman processing is autoscaling. This method functions as an extension of mean centering, after subtracting the mean from all intensity values such as in mean centering but continues by dividing the standard deviation from each wavenumber's corresponding intensity. This ensures that all peaks equally contribute to overall analysis. The downsides of this approach include a higher sensitivity to noise, as well as maintaining the multiple spectra requirements.

The third and our selected method for scaling is min-max scaling. This method rescales the data to a fixed range, which in our case is 0 to 1. This maintains the shape of the data but adjusts the scale for easier analysis. This method is still sensitive to outliers, but as we have placed this step far downstream our processing pipeline, we can expect that any pertinent outliers are already addressed. Additionally, min-max scaling does not require multiple spectra, allowing us to minimize the amount of time needed to be spent on data acquisition,

Table 37 Scaling Method Comparison

	Mean Centering	**Autoscaling**	**Min-Max Scaling**
# of required spectra	2+	2+	1
Time complexity	O(N)	O(N)	O(N)
Space complexity	O(N)	O(N)	O(N)

3.3.3.5. Spectral Comparison

As the final step in our data pipeline, we finally utilize the processed data to make conclusions as to the composition of the sample. The ideas behind this are to utilize a pre-established library of Raman spectra corresponding to the materials we ae trying to identify. The goal of our selection is to have a robust method to capture similarities between our acquired spectrum, and each spectrum we compare it against, hoping to correctly identify the material based off the most similar material from the library. There are three primary methods used to achieve this: Euclidian distance, Cross-correlation, and Correlation Coefficient (or Pearson Similarity).

The simplest of the aforementioned methods is the usage of Euclidian distance to calculate similarity. Euclidian distance works by measuring the distance between intensities for every wavenumber between our acquired spectrum, and the reference spectra. The L2 norm of these values is then found to find a since distance value, representing the amount of dissimilarity between the two spectra. This method can be implemented quite simply, with only 1-2 lines of code with library assistance. This simplicity comes with a cost, however, as Euclidian distance can be very sensitive to any irregularities within the data not caught during preprocessing.

A comparison method that could be utilized to compare spectra is cross-correlation. This technique works by "sliding" one spectrum across the other along the wavenumber axis. Cross-correlation will produce a value representing the similarity of the spectra. This method is able to compare two spectra, regardless of any inconsistencies in wavenumber/intensity pairs, assuming the shape of the spectrum is the same. Compared to Euclidian distance, however, this method is much harder to implement, and can be computationally intense, which makes the system less responsive when comparisons are implemented on mobile hardware such as microcomputers or microcontrollers.

The method we have selected for our application is the usage of a Correlation Coefficient (Pearson Similarity). To generate a value indicating the amount of similarity between the two compares spectra, the mean is subtracted from each intensity value, and the entire spectrum is scaled by the standard deviation, similar to what was done in the normalization and scaling steps of the preprocessing pipeline, allowing us to ensure the data is the best position for comparison.
Finally, the dot product is taken to generate a value, r, representative of the correlation between the two spectra. This method is optimal as it is almost entirely focused on the shape of the spectra, making it incredibly reliable when paired with a robust preprocessing pipeline. Many of the downsides of this technique, such as sensitivity to shifts in peak position, become nearly nonexistent once the data has been sufficiently prepared.

Table 38 Spectral Comparison Method Comparison

	Euclidian Distance	**Cross-Correlation**	**Pearson Similarity**
# of required spectra	2	2	2

Time complexity	O(N)	O(N log N)	O(N)
Space complexity	O(N)	O(N)	O(N)

4. Standards and Design Constraints

4.1. Industrial standards

4.1.1. IEC 60825-1

ECOspec, our Raman spectroscopy–based microplastic detection system, relies on a 785 nm laser source operating around 150 mW. While lasers are integral to achieving high-resolution Raman spectra, they also pose safety risks, especially to the eyes and skin. To address these hazards, the International Electrotechnical Commission (IEC) developed IEC 60825-1: Safety of Laser Products. This standard defines classification systems, labeling requirements, and safety measures to protect users and ensure compliance when devices are deployed in labs, industries, and potentially field environments. By aligning ECOspec with IEC 60825-1, the project not only safeguards operators but also strengthens its credibility for research and commercial adoption.

This standard uses a risk-based classification framework, this means that instead of each laser being treated equally as dangerous, the standard classifies them based on a couple of factors. These factors include output power, wavelength, exposure duration, and other potential hazards. These classes range from Class 1, which is practically safe under normal operations, to Class 4, which is extremely hazardous, capable of causing severe permanent damage to eyes and skin. ECOspec's laser would fall under Class 3B because of its output power at 150 mW and 785 nm wavelength. This category includes lasers where direct exposure or reflections from the beam could cause permanent eye damage and potentially burn skin tissue.

The classification under IEC 60825-1 does more than provide a label; it dictates how ECOspec must be designed and operated. For example, the standard requires that Class 3B lasers include engineering controls to prevent accidental exposure. In ECOspec, this translates to a fully enclosed optical path, where the laser beam is isolated from the user by protective housing. The enclosure itself will include laser safety glass, designed to block the operating wavelength while still allowing users to monitor the cuvette chamber visually. IEC 60825-1 also mandates the use of interlock systems so that the laser automatically shuts down if the protective chamber is opened. ECOspec already incorporates such interlocks into its design, ensuring that the laser cannot be activated unless the cuvette door is properly closed.

Another key component of the standard is labeling and user awareness. Devices using Class 3B lasers must carry warning labels that clearly state the wavelength, output power, and laser class. These labels provide immediate recognition of the hazard level and are an

important part of risk communication. ECOspec's design also goes a step further by integrating a key-lock mechanism and an emergency stop button, which comply with IEC recommendations for disabling high-powered lasers when not in active use.

By following IEC 60825-1, ECOspec not only protects its users but also ensures that the device is positioned for broader adoption. Research institutions, environmental monitoring agencies, and municipal facilities are unlikely to deploy a laser-based system that does not comply with international safety standards. Demonstrating adherence to IEC 60825-1 provides confidence that the device is safe, reliable, and suitable for integration into real-world applications. It also lays the groundwork for regulatory certifications such as FDA laser product compliance in the United States, which recognizes IEC 60825-1 as the baseline safety framework.

In practice, the standard enhances more than just safety. It also improves ECOspec's scalability. Because the device is being designed with Class 3B protection from the start, it will be much easier to adapt future versions for field deployment. Portable or residential systems must be inherently safe to gain public trust, and building the project around IEC 60825-1 ensures that these considerations are embedded in the engineering process.

Ultimately, IEC 60825-1 is more than a regulatory hurdle; it is a guiding principle for ECOspec's design philosophy. The laser source is the heart of Raman spectroscopy, but it is also the primary source of risk. By implementing enclosures, interlocks, labeling, and training in accordance with this international standard, ECOspec not only mitigates hazards but also demonstrates scientific and professional responsibility. Compliance with IEC 60825-1 transforms the project from a functional prototype into a credible, trustworthy system ready for use in both laboratory and environmental monitoring contexts.

4.1.2. IEC 61010-1

IEC 61010-1, "Safety Requirements for Electrical Equipment for Measurement, Control, and Laboratory Use," is one of the most significant hardware-related standards relevant to the ECOspec project. While IEC 60825-1 establishes safety requirements for the optical and laser components, IEC 61010-1 addresses the broader electrical and mechanical safety of the system. The ECOspec instrument is not a simple optical device; it integrates multiple high-power electronic subsystems within a confined enclosure. These include a 12 V, 120 W power supply, a thermoelectric cooling (TEC) system, active fans, and dual microcontroller units that coordinate laser excitation and signal collection. Compliance with IEC 61010-1 ensures that these components operate safely together and that users are protected from hazards such as electrical shock, excessive heat, and fire.

The purpose of the standard is to provide a consistent framework for designing and verifying laboratory and analytical instruments so that they can operate reliably under normal and single-fault conditions. ECOspec falls precisely within this category; it is an electrically powered measurement device intended for research and laboratory environments. The principles of IEC 61010-1 guide every part of its hardware design from component selection to grounding, insulation, and enclosure construction. The standard

ensures that if a single component were to fail, such as a voltage regulator or TEC controller, the user would still be shielded from unsafe conditions.

In the ECOspec system, electrical safety begins at the power entry point. The primary supply delivers 12 volts of DC at up to 10 amps, driving multiple downstream regulators that generate 3.3 V and 5 V rails for logic-level control. Even though these voltages are considered low, the available current is high enough to cause component overheating or fire if short circuits occur. IEC 61010-1 requires that all conductive parts accessible to the user be either fully insulated or connected to protective earth. To meet this, the internal chassis, optical mounts, and heat sinks are bonded to a grounded line that directs any fault current safely away from the user. The PCB traces carrying power to the laser driver and TEC are designed with adequate creepage and clearance distances in accordance with pollution degree 2 requirements, which apply to indoor laboratory environments. This means maintaining at least 2.5 mm spacing between high-current traces and sensitive signal paths, reducing the likelihood of arcing or unintentional coupling.

The enclosure design also reflects the intent of IEC 61010-1. The standard specifies that any metal surfaces the user can touch must remain below safe temperature limits and must be electrically isolated from hazardous potentials. In practice, this shapes both the physical and electrical layout of ECOspec. The laser compartment, TEC plate, and optical chamber are all housed within an aluminum frame, but the outer shell uses powder-coated panels that serve as an additional insulation barrier. The enclosure materials are chosen for their flame-retardant properties. Specifically, UL94-V0 rated polymers for internal brackets and cable mounts, to satisfy the standard fire protection clause. All wiring harnesses are secured with heat-resistant insulation sleeves and rated beyond their maximum expected operating temperatures.

Thermal control is a particularly important aspect of ECOspec's compliance. The spectrometer relies on the TEC to cool the CCD detector and maintain a stable temperature for accurate signal acquisition. However, this cooling system can generate significant waste heat on the hot side of the module. IEC 61010-1 requires that instruments prevent injury due to contact with high-temperature components, and that internal temperatures remain below the ignition point of any surrounding material. The ECOspec design addresses this by combining active ventilation with automatic shutdown logic in the firmware. If the internal temperature exceeds a defined threshold, power to the TEC and laser driver is immediately disabled. A hardware thermal fuse is also integrated in series with the TEC to provide a secondary fail-safe independent of software control, ensuring that even in the event of firmware failure, the system remains safe.

Beyond electrical insulation and thermal management, the standard also governs protective mechanisms such as fuses, overcurrent protection, and isolation barriers. The main power line entering the ECOspec includes a replaceable fuse accessible from the rear panel, in accordance with the standard requirement that protective devices be user-serviceable without exposing live circuits. Each power rail is individually fused or current-limited through voltage regulator protection circuitry. For communication between the low-voltage microcontrollers and higher-power circuits, optoisolators are used. This galvanic isolation prevents voltage spikes or ground loops from propagating between subsystems. Such

isolation is particularly beneficial when driving the laser module, which can experience rapid transients during startup or modulation. By incorporating these protective elements, the design achieves both functional integrity and compliance with IEC 61010-1 electrical separation requirements.

Labeling and operator awareness form another important part of the standard implementation. Every surface or terminal that could potentially exceed safe touch voltage levels must be clearly marked with the appropriate caution symbols. ECOspec's internal PCBs include silk-screened voltage ratings and fuse specifications near all power terminals, and external warning icons are printed on the rear power inlet and laser access panel. These labels are not merely cosmetic; they are a mandatory part of the standard risk communication requirements, ensuring that users are fully informed of any potential hazard before operating the device. The key-lock switch and emergency-stop button further reinforce operator safety by providing a mechanical means to isolate the system from power immediately.

From a systems engineering perspective, designing IEC 61010-1 encourages a more disciplined and testable hardware structure. Each subsystem (power, control, cooling, and optics) can be independently verified against measurable criteria. For example, the standard specifies dielectric strength tests, where circuits must withstand applied voltages significantly higher than their normal operating levels without breakdown. In ECOspec, the isolation between the primary PSU and control circuits will be verified through these tests during prototype validation. Ground continuity and insulation resistance will also be measured to confirm that no conductive path exists between user-accessible parts and high voltage nodes. These verification steps, while adding development effort, directly improve the robustness and longevity of the instrument.

The broader benefit of aligning ECOspec with IEC 61010-1 extends beyond the laboratory prototype. Future iterations of the system intended for commercial or institutional use will need formal certification to enter the market. IEC 61010-1 forms the baseline for national equivalents such as UL 61010-1 in the United States and EN 61010-1 in the European Union. Designing these standards in mind from the beginning greatly simplifies later certification and ensures compatibility with institutional safety protocols. Environmental laboratories, universities, and regulatory agencies are all accustomed to purchasing analytical instruments that bear these marks of conformity. By demonstrating adherence to the same safety principles, ECOspec becomes immediately more credible and market ready.

Perhaps the most meaningful outcome of incorporating IEC 61010-1 into ECOspec's design philosophy is that it embeds safety as an engineering parameter rather than an afterthought. The same considerations that protect the user's electrical isolation, controlled temperature, and fault containment also enhance signal quality and reliability. Stable thermal environments reduce sensor noise; robust grounding minimizes electromagnetic interference and clearly separated power domains improve measurement consistency. Compliance with IEC 61010-1, therefore, aligns perfectly with the project's scientific goals: producing accurate, repeatable, and trustworthy Raman spectra of microplastics in water samples.

In conclusion, IEC 61010-1 provides the structural framework that ensures ECOspec is not just functional but professionally engineered for safe operation in real-world environments. It complements the optical safety established by IEC 60825-1 by governing all electrical and thermal aspects of the system. Implementing this standard requires attention to detail in enclosure design, wiring layout, grounding, insulation, and labeling, but these same practices contribute directly to a higher quality, more dependable device. As ECOspec continues toward a deployable prototype, adherence to IEC 61010-1 establishes a foundation of trust and safety that will be essential for its acceptance in both academic research and environmental monitoring applications.

4.2. Design Constraints

4.2.1. Thermal Management

One of the most significant design constraints for ECOspec is thermal management. Because the system integrates multiple heat-generating components inside a small, enclosed housing, maintaining stable and safe operating temperatures is not optional but essential to the device's function. The spectrometer's accuracy, the laser's lifetime, and the CCD's signal integrity all depend on precise temperature control. This single constraint influences the electrical design, mechanical structure, and even the software logic that regulates power and cooling cycles.

The challenge begins with the basic heat balance of the device. The 785 nm laser operates up to 350 mW output power, but its total electrical draw is several times higher because of inefficiencies in conversion and thermal losses in the diode and driver circuitry. The thermoelectric cooler used for the CCD consumes additional power while pumping heat from one side of the detector to the other, creating a concentrated hot spot that must be actively removed from the system. When both the laser and the TEC are operating simultaneously, the total heat load within the enclosure can exceed 20 watts. Without proper heat dissipation, the internal temperature can rise quickly, leading to thermal drift in the Raman signal and permanent damage to temperature-sensitive components.

The CCD detector is especially sensitive to heat. Its dark current, which contributes to image noise, doubles roughly every six to seven degrees Celsius. For Raman spectroscopy, where the signal of interest is already extremely weak compared to the background, this is a serious problem. The design goal is to maintain the CCD at or below 40°C during normal operation, though the ideal range is closer to 20–25°C. This is achieved through a thermoelectric cooler mounted directly beneath the CCD sensor, which transfers heat away from the cold side toward a metal heatsink. However, TECs are inherently inefficient. For every watt of heat they move, they can generate nearly a watt of heat on their own, meaning the total thermal output on the hot side of the module can be two or three times greater than expected.

The practical implication of this is that ECOspec must be designed not only to cool the CCD but also to manage the secondary heat generated by the cooling process itself. The

TEC module sits on an aluminum heat spreader that is connected to an array of fans to circulate air through the enclosure. The fans are controlled by the main microcontroller using a pulse-width modulation signal that adjusts their speed based on real-time temperature readings from a thermocouple located near the CCD. The placement of this sensor was determined through early simulations that showed the highest thermal gradient occurs near the CCD interface rather than at the center of the board. This feedback loop allows the system to stabilize the CCD temperature within a narrow margin, even as the ambient temperature changes.

Although active cooling is necessary, it introduces additional noise and vibration into the system. Fan-induced vibrations can affect the optical alignment of the spectrometer, especially since the mirrors and diffraction grating are mounted on lightweight holders. To mitigate this, ECOspec uses rubber isolation mounts for both the fans and the TEC assembly. These dampers absorb micro-vibrations before they can be transmitted to the optical bench. The tradeoff is that vibration isolation slightly reduces heat transfer efficiency, which means the system must run the fans at a higher speed during initial cooldown or extended laser operation. This interplay between vibration control and cooling performance illustrates how thermal management is not an isolated subsystem, but an integrated constraint that touches nearly every part of the design.

In addition to component-level cooling, the overall enclosure design must support stable airflow and safe heat dissipation. The ECOspec housing is compacted by necessity; minimizing size improves portability and helps block ambient light from interfering with spectral measurements. However, a smaller volume traps more heat. The design team had to strike a balance between physical compactness and thermal headroom. Airflow simulations guided the placement of intake and exhaust vents, ensuring that hot air from the TEC and laser is expelled rather than recirculated. The vents are shielded with internal baffles to prevent stray light from leaking into the optical path, preserving measurement integrity while allowing for efficient air exchange.

Software also plays a critical role in managing this constraint. The device’s firmware continuously monitors internal temperature and can initiate staged responses as thresholds are crossed. At moderate temperatures, fan speeds are increased. At higher temperatures, the laser is throttled to a lower duty cycle to reduce heat generation, and if the limit is exceeded, the system will shut down automatically. This hierarchy of protection is necessary because thermal failures can cause more than just damage, they can distort data, reduce detector sensitivity, and invalidate calibration. Implementing a temperature-based control strategy ensures that ECOspec remains reliable during long measurement sessions or in environments with fluctuating ambient conditions.

Material selection further constrains the design. Components exposed to consistent thermal cycling must maintain structural and optical stability. The mirrors and gratings inside ECOspec are mounted to aluminum and stainless-steel frames, which have high thermal conductivity and stable coefficients of expansion. Using dissimilar materials could lead to misalignment as temperatures rise and fall, so all mounts are selected to have matched expansion properties wherever possible. Even the adhesive compounds used to secure optical elements are chosen based on their rated performance over the expected

temperature range. These small details prevent the optical train from drifting out of alignment, a subtle but critical consequence of thermal stress.

From a safety standpoint, managing heat is also about protecting the user. If surface temperatures of the enclosure or laser housing exceed safe touch limits, there is a risk of burns or material degradation. IEC 61010-1, which governs electrical and mechanical safety for lab equipment, specifies maximum surface temperatures under both normal and faulty conditions. To remain compliant, the external surfaces of ECOspec must not exceed 60°C during operation. This requirement led to the inclusion of a temperature sensor near the outer panel, ensuring that if airflow is obstructed or fans fail, the device can detect the abnormal condition and shut down safely before reaching hazardous levels.

The power budget directly ties into thermal constraints as well. Because heat generation scales with power consumption, each subsystem must operate within strict limits. The laser driver, cooling system, and microcontrollers all draw from the same 12 V supply, which is capped at 120 W. Allocating too much current to the TEC reduces the available headroom for the laser, while underpowering the TEC risks overheating the CCD. Careful distribution of current is therefore essential, and each rail includes inline current sensing to track power drawn during operation. Data from these sensors can also be logged for diagnostics, providing insight into how the thermal behavior of the system evolves.

In the long term, this constraint shapes how ECOspec can scale beyond the laboratory prototype. A field-deployable version of the system, for instance, would need to operate in outdoor environments where ambient temperatures can vary from near freezing to over 40°C. The internal cooling system would need to be both more efficient and more rugged, possibly replacing active air cooling with liquid heat exchange or improved passive heat sinking. Power-efficient components would become a necessity rather than an advantage. In this way, thermal management defines not just the current design but also the path forward for future iterations.

Overall, thermal management is not simply a background engineering consideration but a defining design constraint for ECOspec. It dictates the architecture of electronics, the choice of materials, and the internal geometry of the housing. It even extends to the software logic that governs operation and safety. Maintaining precise temperature stability is the foundation upon which accurate Raman detection depends. Without it, the system could produce unreliable spectra or suffer irreversible damage to its components. Balancing performance, safety, and compactness within these thermal limits has required careful trade-offs and iterative testing; however, these trade-offs are what transform ECOspec from a conceptual design into a practical, working instrument.

4.2.2. Optical Alignment

Another critical design constraint for ECOspec is mechanical stability, particularly as it affects optical alignment. Raman spectroscopy depends on maintaining a precise and consistent optical geometry between the excitation laser, the sample, and the collection of optics. Even minor misalignments can alter the position or intensity of Raman peaks, leading to measurement errors or a complete loss of signal. Because the ECOspec system

integrates multiple optical elements in a compact enclosure, structural rigidity and vibration control are key to preserving measurement accuracy and reproducibility.

The optical subsystem of ECOspec relies on a Czerny–Turner spectrometer configuration, where the slit, collimating mirror, diffraction grating, focusing mirror, and detector must remain fixed within strict mechanical tolerances. The alignment between these components directly determines the instrument's spectral resolution. Any angular shift or positional drift can distort the light path and reduce the precision of wavelength calibration. To minimize this risk, all optical components are mounted to a rigid aluminum baseplate that serves as a mechanical reference frame for the spectrometer. Aluminum was chosen for its strength-to-weight ratio and machining ease, but its relatively high thermal expansion coefficient presents a challenge. To offset this, the team selected optical mounts that use materials with similar coefficients of expansion and designed flexible joints that allow slight movement without stressing the optics. Once aligned, each adjustable mount is locked in place with low-outgassing epoxy and thread-locking compounds to resist vibration and long-term mechanical creep.

Vibration is another major source of optical instability. The Raman signals that ECOspec measures are extremely weak, so even small mechanical oscillations can shift the alignment of mirrors or gratings enough to change the detected intensity. The primary sources of vibration within the device are the cooling fans, the thermoelectric cooler attached to the CCD, and the general handling of the instrument. To mitigate these effects, the optical subassembly is isolated from the power and cooling sections using elastomer dampers that absorb low-frequency vibration. The baseplate is suspended on vibration-dampening standoffs that separate it from the chassis and reduce coupling between moving parts. This arrangement ensures that heat-producing and mechanically active components do not interfere with optical precision.

Environmental factors further influence mechanical stability. Temperature fluctuations cause expansion and contraction in the optical mounts, which can slightly change the optical path length. Because Raman peak positions are measured in nanometers, even small dimensional shifts can have measurable effects on results. The internal layout of ECOspec addresses this by physically separating heat-generating elements, such as the laser driver and thermoelectric cooler, from the optical path. Passive thermal insulation around the optical chamber ensures that temperature changes occur gradually and uniformly, limiting the effects of differential expansion. The interior environment is kept dry with desiccant packs to prevent condensation or corrosion, which could affect optical surfaces and alignment over time.

Mechanical stability is also tied to user safety. Misalignment could redirect the laser beam toward unintended surfaces or small openings, increasing the risk of stray reflections. The enclosure design prevents this by surrounding the optical path with light-absorbing matte coatings and ensuring that no direct or reflected beam can exit the housing under normal operation. The optical window is made of laser safety glass matched to the 785 nm wavelength, providing an additional layer of protection while allowing visual inspection of the cuvette during measurement.

To maintain alignment over the lifetime of the instrument, ECOspec incorporates a calibration and verification routine in its control software. The system periodically checks its alignment by comparing the measured spectrum of a known reference material with its baseline data. Any significant deviation indicates that the optical path may have shifted. In such cases, the system alerts the user to perform recalibration or mechanical inspection. This automated check ensures consistent performance and minimizes the need for manual adjustments. For research or field deployments, this feature also provides a record of mechanical stability over time, allowing the team to assess long-term durability.

Overall, mechanical stability and optical alignment represent a fundamental design constraint that influences nearly every engineering decision in ECOspec. The system's ability to deliver accurate, repeatable Raman spectra depends on maintaining a precise and stable optical configuration in the presence of vibration, heat, and physical handling. Designing rigidity, isolating sources of disturbance, and integrating automated verification routines all contribute to ensuring that ECOspec remains reliable both in laboratory environments and in future portable or field-deployable versions.

4.2.3. Low Intensity and Scattering

Raman scattering is a phenomenon which occurs roughly every 1 out of 100,000,000 photon interactions. This inherently makes a Raman signal 8 orders of magnitude weaker than the exciting source. The signal strength of detected Raman scattering is often in the nano or picowatt regime. Furthermore, the broadband fluorescence spectrum often generated by short wavelength interactions tends to overpower the Raman signal. The optical design in the filtering components of the collection system must be chosen with great care in order to obtain a useful Raman spectra.

Maximizing collection of Raman signal is a difficult task. The Raman scattering profile is nondirectional. It follows a scattering profile similar to Rayleigh scattering, with possible reflection directions in almost every angle. For example, the sky being blue is responsible due to the Rayleigh scattering of blue light being incident with molecules in the atmosphere. Shorter wavelengths, like blue light, scatter more strongly than longer wavelengths, like red light. The scattered blue light appears to go in every direction, and other colors are not visible.

A majority of Raman systems perform the collection of the Raman signal very close to the point of laser incidence. Bringing the collection optics closer to origin point of the scattering allows for a larger steradian collection angle, allowing for more light to be focused onto the detector. That is why confocal Raman microscopy is a very popular method, and why many Raman collection systems closely follow a confocal microscopy structure. Fiber probes are also very popular tools for Raman spectroscopy. They allow for a small area of a sample to be illuminated with a high intensity, while also allowing the collecting fiber to reach proximities to area closer than traditional microscope objective based systems.

4.2.4. Safety Control Circuit

With the use of an enclosed class 3B laser, safety interlocks must be used to ensure safe operation of the device. As per regulation, safety interlocks must be engaged before any laser emission may occur. The circuit controlling the safety interlocks will ideally operate independently of the main processing unit. This is done to minimize failure points in the safety subsystem of ECOSPEC. A dedicated MCU will operate the safety interlocks, power output of the laser, and monitor status of the system at all times in the background.

The laser will have two conditions that must be met prior to emission: the doors of the enclosure must be closed, and the safety interlocks must be engaged. If the doors are closed, but the locks are not engaged, the laser shall not begin emission. If the locks are engaged, but the doors are open, the laser shall also not begin emission. If the safety interlocks do not come with sensors to monitor the status of door closure, additional sensors will need to be implemented. It is crucial that an enclosed class 3B laser system utilizes safety interlocks during operation.

4.2.5. Detector Cooling

Raman spectroscopic measurements are very sensitive to thermal fluctuations. A certain operating temperature is required to obtain a high enough signal-to-noise ratio (SNR) from any detector. Ideally, the detector will operate at temperatures of sub 20 °C, but it appears that practical applications involve temperatures as low as -20 °C.

Creating a control system to maintain the detector's temperature level is not easy. Typically, a thermoelectric cooler (TEC) is used for sensor temperature control. They often come in 1-stage or 2-stage configurations, with the latter achieving temperatures as low as – 25 C. In many scenarios, including Raman spectroscopy, 1-stage TECs provide sufficient thermal management to obtain clear Raman spectra. If the detector is not cooled, it is typically very difficult for the Raman signal to overcome the noise level within the sensors itself. This is especially true with IR excitation wavelengths. As the wavelength shortens, the quantum efficiency for most sensors begins to quickly drop off. This means that IR detection schemes, like ECOspec, require direct cooling of the sensor to obtain useful Raman data.

4.2.6. Signal amplification circuit and noise

An amplification circuit for Raman signal detection will require much consideration in isolation, noise reduction, signal integrity, and component placement. Due to the nature of the weak Raman signal, and a low quantum efficiency of the detected wavelengths of light, nano or picoamp signals will be output from any detector used for this application. The complexity required to design this circuit with the limited time and budget for the project is not feasible. A premade detector module will be required for the success of this project.

4.2.7. Expense

Financial limitations have a significant influence on the design and implementation of the ECOspec system. The available budget restricts the selection of components, materials, and manufacturing methods, requiring a careful balance between performance and affordability. High-precision optical sensors and spectrometer modules often exceed cost targets, so components are chosen based on acceptable performance-to-price ratios rather than maximum specifications. To manage expenses, open-source software and university resources, such as 3D printing and in-house machining, are utilized whenever possible, thereby reducing reliance on commercial services. Effective cost planning ensures that the system remains both functional and financially feasible, allowing design goals to be achieved within the project's limited funding.

4.2.8. Time

Time represents a significant limitation in the ECOspec project, affecting every stage, from design to testing. The Senior Design schedule provides fixed deadlines for major deliverables, requiring the team to complete research, prototyping, and documentation within a restricted period. Because each subsystem depends on the timely completion of others, tasks must be carefully sequenced and monitored to avoid delays. Limited time also restricts opportunities for redesign and optimization, encouraging the selection of proven components and practical solutions over experimental alternatives. Efficient time management, regular progress evaluations, and clear task distribution are essential to ensure that all project objectives are met within the timeframe.

4.3. Other Constraints

4.3.1. Sustainability

Sustainability considerations are essential to ECOspec's design philosophy, particularly given that the device is intended to address environmental pollution caused by microplastics. The irony of creating an environmentally harmful device to detect environmental contaminants would undermine the project's core mission. Several sustainability principles guide design choices throughout the system.

Electronic component selection also reflects sustainability goals. The modular architecture allows individual subsystems to be upgraded or repaired without discarding the entire device. For example, if a more efficient detector becomes available, the CCD module can be swapped without redesigning the optical or control systems. PCB manufacturing follows RoHS (Restriction of Hazardous Substances) compliance, eliminating lead and other toxic materials from solder and components. The power supply is selected for high efficiency, reducing energy consumption during operation, and minimizing heat waste that would otherwise require additional cooling.

The long-term environmental impact of ECOspec extends beyond its physical construction. By enabling widespread detection and monitoring of microplastic pollution, the device contributes to data collection efforts that can inform policy decisions and remediation strategies. A sustainable design ensures that ECOspec can remain operational for many

years, providing consistent measurements that contribute to longitudinal environmental studies. Furthermore, designing the software to be open source in future iterations could enable broader adoption without requiring duplicate research and development efforts, maximizing the environmental benefit per unit of resources invested.

4.3.2. Political

Political considerations influence both the development and deployment of ECOspec, particularly regarding regulatory compliance, data transparency, and the potential for policy impact. Microplastic pollution has become an increasingly prominent political issue, with municipalities, state governments, and federal agencies beginning to establish monitoring requirements and contamination thresholds. ECOspec must be designed to produce data that meets the evidentiary standards required for regulatory enforcement and policy development.

One political constraint involves the standardization of measurement protocols. Different regulatory bodies may require specific sampling procedures, detection limits, or reporting formats. ECOspec's software architecture accommodates this by allowing customizable output formats. The device's calibration and validation procedures must be transparent and reproducible, enabling independent verification of results, a critical requirement when data may be used in legal or regulatory contexts.

Data ownership and access represent another political dimension. Environmental monitoring data collected by ECOspec could have significant implications for water quality regulations, industrial compliance, and public health advisories. The system design must address questions of who owns the collected data, how it can be shared, and what protections exist against tampering or misrepresentation. Implementing secure data logging with timestamp verification and user authentication ensures that measurements can be traced back to specific instruments and operators.

4.3.3. Ethical

Ethical considerations permeate the ECOspec project, from research integrity to equitable access and responsible innovation. The fundamental ethical motivation for the project is the protection of human and environmental health from the largely invisible threat of microplastic contamination. This mission carries with it responsibilities to ensure that the technology is accurate, reliable, and accessible to those who need it most.

Research ethics require that all claims about ECOspec's capabilities be supported by rigorous testing and validation. Overstating the device's sensitivity or accuracy could lead to false confidence in water safety or missed contamination events. All testing protocols and calibration procedures are documented transparently, allowing peer review and replication by other researchers.

Equitable access represents a significant ethical constraint. Microplastic pollution disproportionately affects vulnerable communities that lack resources for advanced environmental monitoring. Designing ECOspec to eventually be affordable, user-friendly,

and maintainable helps ensure that the technology can reach underserved populations. The decision to use open-source software components and publish design documentation reflects a commitment to democratizing access to environmental testing capabilities. Future iterations may explore low-cost versions specifically designed for community-based monitoring programs in developing regions where microplastic contamination may be highest, but detection resources are most limited.

The ethical implications of detection without remediation must also be acknowledged. ECOspec can identify microplastic contamination, but it cannot remove it from water samples or ecosystems. The team recognizes that deploying detection technology without corresponding cleanup capabilities may create awareness of problems that cannot be immediately solved, potentially causing distress without providing immediate relief. This ethical tension is addressed by designing the system not as an endpoint but as a tool for informing remediation strategies, tracking pollution sources, and evaluating the effectiveness of intervention measures.

4.3.4. Health and Safety

Health and safety constraints extend beyond laser and electrical hazards to encompass the full spectrum of risks associated with operating and maintaining ECOspec. These considerations protect not only the immediate users of the device but also technicians, researchers, and potentially the public in field-deployment scenarios.

Chemical and biological safety are paramount when working with environmental water samples. Microplastic contamination often co-occurs pathogenic bacteria, toxic chemicals, and other hazardous substances. The handling system is designed to minimize user contact with samples through enclosed loading mechanisms and sealed chambers during measurement. Proper disposal protocols for contaminated samples are included in the operating procedures, and the device housing includes surfaces that can be easily decontaminated with standard laboratory disinfectants. Users are advised to treat all environmental samples as potentially hazardous and to employ appropriate personal protective equipment during sample preparation and handling.

Long-term operator health is also a consideration, particularly in relation to repetitive strain and ergonomic issues. The device is positioned at a comfortable working height, with controls located to minimize awkward reaching or bending. The user interface is designed to be operated from a safe distance, with the emergency stop button large and easily accessible. Visual displays use appropriate contrast and font sizes to reduce eye strain during extended operation sessions. These seemingly minor design choices collectively reduce the risk of cumulative injuries and operator fatigue, which can compromise both safety and measurement of quality.

Maintenance safety is addressed through clear documentation and designed-in serviceability. High-voltage components are enclosed behind labeled panels that require tools to access, preventing accidental contact. Capacitors include discharge resistors to eliminate stored charge hazards. Thermal components such as the TEC and heat sinks are marked with temperature warning labels and positioned to minimize burn risk during

routine maintenance. The modular design enables technicians to service one subsystem without exposing themselves to hazards from other subsystems. By treating maintenance as a normal operational mode rather than an exceptional circumstance, ECOspec's design reduces the risk of improvised repairs that could compromise safety.

4.3.5. Scalability

Scalability is a long-term design constraint for ECOspec because the prototype is intended to demonstrate a technology that could later be adopted in large-scale environmental monitoring programs. The current system is optimized for laboratory use, but future versions may need to operate in automated field installations such as water treatment facilities or coastal measurement stations. Designing the hardware and software to be modular supports this transition. For example, the optical system can be upgraded to higher power lasers or cooled scientific detectors if lower detection limits become necessary. Control electronics can be expanded to support remote monitoring, battery operation, and wireless communication.

Scalability also depends on manufacturing considerations. The prototype uses high performance optical components expected in scientific instruments. However, to support large deployments, lower cost alternatives may be required while still maintaining acceptable levels of accuracy. Component availability and supply chain reliability must be evaluated early to prevent later redesigns. The system enclosure and mechanical parts may need ruggedization for outdoor deployment where humidity, vibration, and temperature extremes are present.

Software scalability is another key factor. The Raman reference library will expand as additional plastic types, and environmental samples will be tested. To support a wide user base, the software interface must allow cloud storage of results, database integration, and efficient spectral comparison for possibly thousands of samples. Data collected from many devices could contribute to real-time pollution mapping, which would greatly increase the environmental value of the system. By planning scalability from the beginning, ECOspec can evolve beyond a single research prototype and become a practical tool for addressing global pollution challenges.

5. Application of ChatGPT and Other Similar Platforms

The emergence of large language model-based platforms such as ChatGPT, Google Gemini, Anthropic Claude, and Microsoft Copilot has changed the way students and professionals interact with information. These systems can interpret complex written inquiries and produce coherent, structured responses that can summarize, explain, or expand technical subjects. Their rapid adoption across academia and industry highlights their potential as tools for assisting with engineering research, documentation, and design. In the context of a senior design project such as ECOspec, where multiple engineering disciplines converge, the integration of these platforms could support a wide range of tasks

from research planning and report development to algorithm exploration and communication management.

ChatGPT represents one of the most comprehensive and widely applied tools. It can generate organized text, produce simplified explanations of technical topics, and structure complex ideas into logical sequences. When applied to an engineering design environment, ChatGPT could assist students in outlining system architectures, explaining optical or electrical principles, or generating initial drafts of documentation. Its ability to maintain context across multiple exchanges allows for in-depth discussion and refinement of ideas. However, its reliance on statistical language prediction rather than verified data presents limitations when technical accuracy is required. The system does not inherently reference experimental data or authoritative standards, meaning that while it can articulate concepts effectively, it cannot confirm the validity of its own statements. This distinction makes it valuable for preliminary exploration but unsuitable as a definitive source of technical information.

Google Gemini differs from ChatGPT primarily through its integration with current online data. Its connection to live web content allows it to reference more recent developments, specifications, and market information than models trained exclusively on static datasets. This can be advantageous in situations that require up-to-date product comparisons or references to current standards. In an engineering design project, such a capability could assist in identifying recently released sensors, lasers, or materials. However, this advantage comes with notable tradeoffs. Because Gemini draws from dynamic web sources, its responses can vary significantly between sessions, and the quality of its information depends on the reliability of the sources it accesses. It also tends to emphasize width over depth, providing general summaries rather than detailed technical discussion. As a result, while Gemini can be an effective tool for rapid contextual research, it cannot replace the detailed evaluation that accompanies formal design documentation.

Anthropic Claude occupies an intermediate role between ChatGPT and Gemini. It is designed to produce coherent and logically structured responses that emphasize interpretability and caution. Its language style is particularly suited for formal writing, ethical discussions, and reflective analysis. Within the scope of engineering projects, Claude could be used to develop sections related to sustainability, social responsibility, or health and safety, where clear reasoning and careful tone are essential. While its attention to logical consistency makes it well-suited for academic writing, its capacity for technical specificity is limited. Claude's conservative approach to language generation results in fewer factual inaccuracies, but also less detailed or quantitative explanations. In this sense, it serves as a stable editorial assistant and planning tool, though it lacks the precision required for component-level engineering design.

Microsoft Copilot differs substantially from the other platforms. It is specialized for programming support, integrating directly into development environments such as VS Code to provide real-time code suggestions. For software-heavy senior design projects, Copilot can accelerate implementation by suggesting syntax structures, variable names, and algorithmic patterns. It can also assist in learning unfamiliar programming languages by producing contextual examples. However, its outputs are limited to code completion

and cannot guarantee logical accuracy or adherence to system requirements. In cases involving safety interlocks, real-time data processing, or hardware control, reliance on automatically generated code would pose a significant risk. Thus, while Copilot can improve productivity for repetitive programming tasks, it still requires human oversight for algorithm design and system integration.

Although these platforms differ in their design and application, they share several overarching strengths that explain their growing presence in engineering education. One of their most prominent advantages is the ability to translate complex technical language into accessible explanations. Engineering design frequently involves the integration of multiple domains, and teams often include members with varying levels of expertise. By providing simplified explanations of topics such as optical alignment, noise filtering, or signal amplification, these platforms can help teams establish a shared understanding that facilitates collaboration. They can also improve writing quality, particularly in large collaborative reports where maintaining consistency of tone, structure, and clarity is challenging. AI-assisted drafting allows students to focus on the conceptual and analytical aspects of the work, rather than the mechanical task of sentence construction. This can result in clearer reports and a more professional presentation of technical material.

Another strength lies in the speed with which these systems can organize and summarize information. Engineering design requires the rapid assimilation of large volumes of data from diverse sources, including academic papers, manufacturer datasheets, and design manuals. AI tools can synthesize this information into concise outlines that serve as starting points for detailed human analysis. In the early planning phases of a project like ECOspec, where optical, electrical, and software subsystems must be coordinated, such an organization can help define subsystem boundaries and identify interdependencies. By accelerating this process, language models can increase overall efficiency and allow teams to dedicate more time to experimentation, testing, and validation.

Despite these benefits, the limitations of language-model platforms are equally significant and must be addressed carefully in academic and engineering contexts. The most fundamental limitation is the issue of accuracy. Because these systems are not connected to verified experimental databases, they often produce information that appears reasonable but is technically incorrect. This can include incorrect equations, unrealistic numerical values, or misinterpretation of physical principles. Without expert verification, such errors can propagate into design documents or experimental procedures. In an educational setting, this risk is especially relevant, as students may overestimate the authority of AI-generated text. Recognizing that these platforms operate on linguistic probability rather than reasoning is crucial to maintaining scientific rigor.

A related concern is the lack of transparency in information sources. Most platforms do not disclose where their training data originated, or which references influenced specific responses. This poses difficulties in academic writing, where citation of sources is a core requirement. In the absence of traceable references, any information derived from these tools must be treated as unverified background material rather than citable evidence. Gemini's partial use of live web results addresses this issue only marginally, as it may still

rely on secondary or non-peer-reviewed sources. Users must approach AI-generated information with the same skepticism reserved for anonymous or unverified references.

There are also challenges related to continuity and contextual retention. While models like ChatGPT can maintain conversation context across short exchanges, they do not retain memory between independent sessions, and long technical discussions can exceed their effective context window. This limitation makes it difficult to use them for large, ongoing projects that evolve over several months, such as senior design courses. Maintaining version control and ensuring consistency across multiple outputs can become time-consuming, particularly if different team members use the platform separately.

Beyond the technical and procedural aspects, the use of artificial intelligence in education introduces important ethical considerations. The goal of senior design is not only to produce a working prototype or system, but also to develop the analytical, communication, and problem-solving skills required by professional engineers. Overreliance on AI-generated explanations or writing can undermine these objectives by substituting genuine comprehension with automated synthesis. The proper educational role of these tools is therefore supplementary. When used responsibly, they can promote deeper understanding by clarifying complex topics and offering alternate perspectives. When used carelessly, they can erode individual accountability and reduce the educational value of the design process.

It is also important to consider the implications of intellectual ownership. Work produced by AI models does not originate from human authors and may incorporate fragments of existing text or code. In academic settings, unacknowledged AI use could blur the boundary between original authorship and automated assistance. To preserve transparency, students and researchers are encouraged to document the extent of AI involvement in their work, specifying when it was used for editing, summarization, or idea generation. Maintaining such disclosure aligns with the principles of academic integrity and ensures that human contributions remain identifiable.

When comparing the overall performance of the major platforms, several distinctions become apparent. ChatGPT remains the most versatile general-purpose system, providing detailed, well-structured explanations suitable for technical writing and report development. Gemini excels in speed and access to current data but lacks depth of technical reasoning. Claude provides consistently logical and organized prose, making it ideal for reflective or ethical analyses, though it does not match the analytical power of ChatGPT. Copilot stands apart as a programming assistant with specialized but narrow functionality. Each platform exhibits strengths that make it suitable for certain stages of project development, yet none can function as a replacement for verified engineering analysis or experimental validation.

In conclusion, artificial intelligence platforms such as ChatGPT, Gemini, Claude, and Copilot represent valuable auxiliary tools for modern engineering design and education. They are capable of improving clarity, organization, and efficiency in project documentation, while also supporting conceptual understanding across disciplines. However, their role remains secondary to human expertise and empirical reasoning. The

outputs they generate should be treated as provisional, useful for structuring ideas and guiding discussion, but always subject to independent verification and correction. The continued integration of such tools into academic environments will likely shape future design methodologies, but responsible use must remain grounded in transparency, critical evaluation, and adherence to professional standards. All projects employing artificial intelligence systems should document their involvement clearly, ensuring that the educational process maintains its emphasis on independent analysis and technical accuracy.

6. Hardware Design

6.1. Optical Hardware Design

6.1.1. Probe Optics

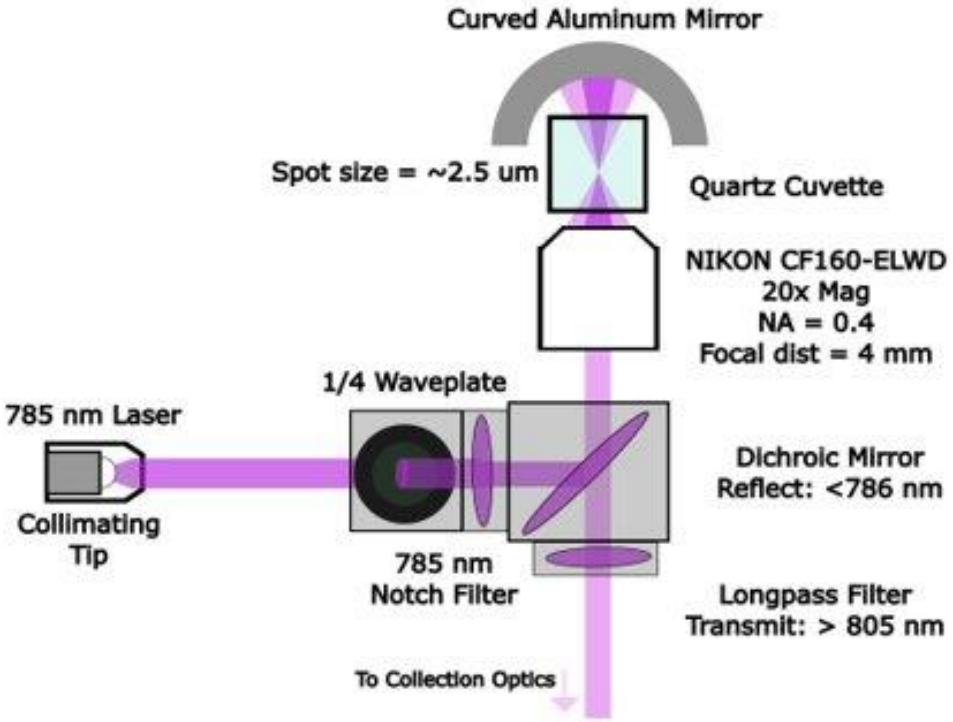

Figure 22 Probe Optics Diagram

Table 39 Probe Optics Part List

	Application
Laser	Ocean Optics LASER-785-ADJ-S
Fiber	Ocean Optics SMA-coupled Single-mode Fiber
Collimating Tip	Ocean Optics

Mirrors	Thorlabs BB-EO3
ND Filter	Thorlabs NE05 ND Filter
Iris	Newport
Lenses	Thorlabs AC050-008-B and AC254-045-B
Dichroic Mirror	Thorlabs DMLP805
Microscope Objective	Nikon CF160 TU Plan Epi ELWD
Quartz Cuvette (Sample)	Ocean Optics

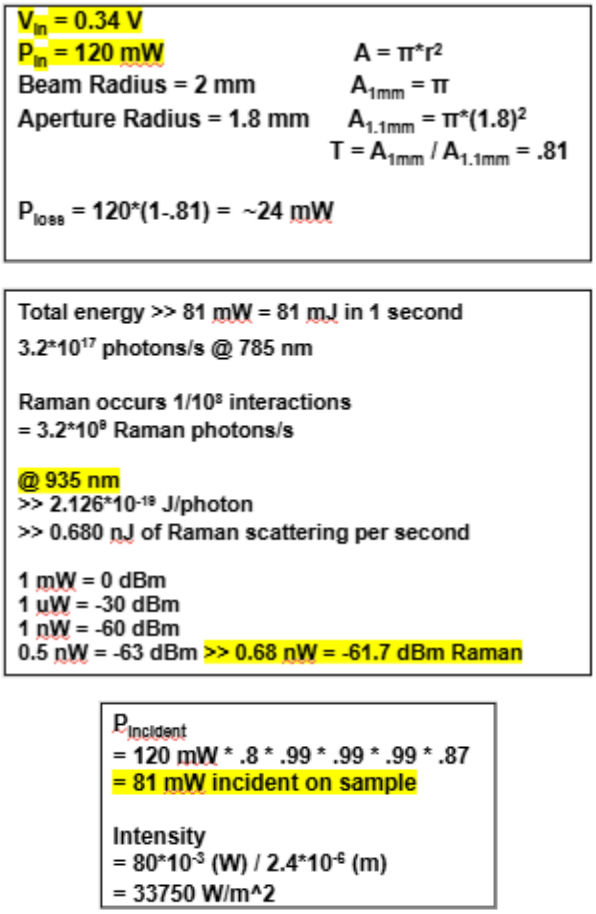

Figure 23 Optical Power Attenuation Calculations

The excitation laser is adjustable up to 350 mW. It is unlikely the maximum power output will be necessary to generate Raman scattering, however it must be powerful enough to transmit through all the clean-up and filtering optics. A 2 mm iris will produce a cleaner spot to illuminate the sample, but will cause a noticeable drop in power due to the decrease in transmit beam area. The beam expander and microscope objective system innately has some losses due to absorption and Fresnel reflections.

- **Assuming 2.5 mm diameter collimated spot out of fiber**
- **14 mm clear aperture on back of microscope objective, infinity corrected**
- **Don't want to overfill**
  - Expand to 12 mm collimated input
- **Adjustable aperture**
- **6x Mag needed**

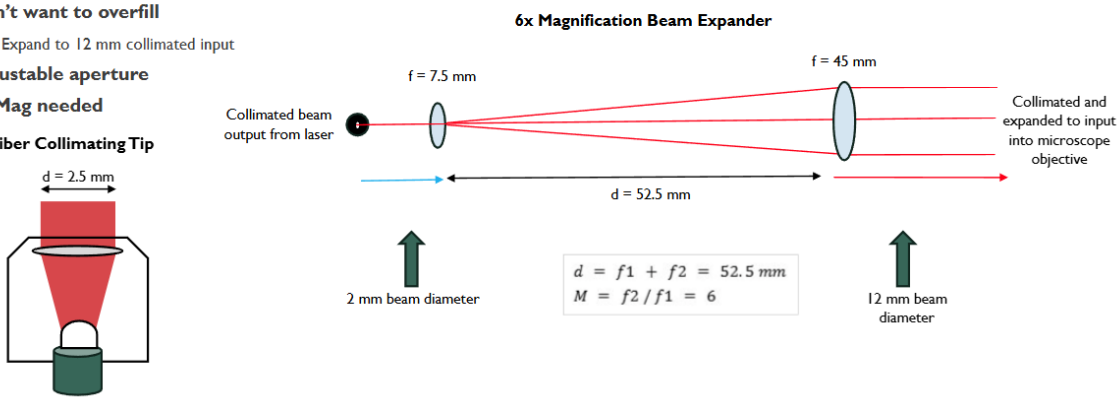

Figure 24 Beam Expander Calculations

The beam expander is a necessary subsystem to maximize the implementation of the microscope objective. To generate the minimum spot size, the input beam should be expanded to ~80% of the diameter of the rear aperture. Any larger of an input would lead to chromatic aberration, increasing the experimental minimum spot size and complicating the collection optics. The chosen lenses are Thorlabs' AB coated to minimize reflections at 785 nm.

- **Rear conjugate of microscope objective is infinite**
- **Collimated image out of rear aperture is collimated**
- Transmittance @ 785 nm is 87%
- NA = 0.4
- @ 785 > 2.4 micron diameter spot

- **Raman scattering profile is similar to Rayleigh scattering profile.**
- **Care must be taken when using a mirror to refocus light back into the objective. May lead to aberrations in the spectrometer.**

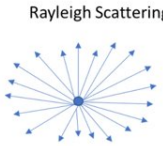

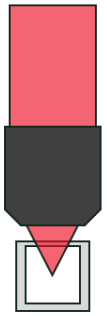

$$r_{airy} = 0.61 * \frac{\lambda}{NA} = 1.2\ micron$$

Figure 25 Spot Size and Sample Illumination Calculations

The microscope objective generates the point of highest intensity. The smaller the spot size that is obtained, the higher the intensity, leading to a stronger Raman signal generated from a smaller sample size. This gives us stronger confidence that a certain plastic's spectra has been identified in the sample under test.

6.1.2. Collection Optics

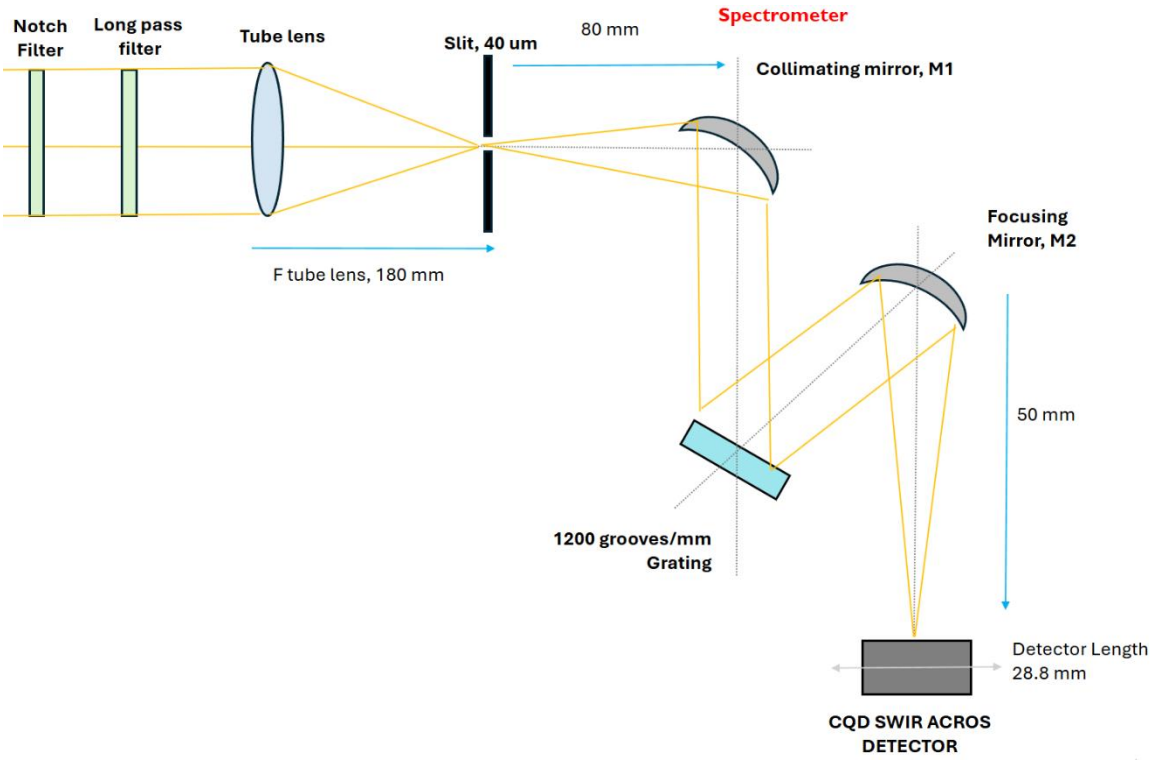

Figure 26 Collection Optics Diagram

Table 40 Collection Optics Part List

	Application
Notch Filter	Semrock, LPD02-785RU-25 785 nm RazorEdge Dichroic
Long Pass Filter	Thorlabs, FELH080
Achromatic doublet	Thorlabs, F 30 mm, AC254-030-B-ML
Slit	Thorlabs, S40K
Collimating Mirror	Torrent, F 101.6 mm
Diffraction Grating	Optometrics, 800 nm blaze, 830 g/mm
Focusing Mirror	Thorlabs F 101.6 mm

6.1.2.1. Spectrometer Design

This section will be a discussion on the optical hardware components and design that was implemented into the spectrometer portion of ECOSpec. A Czerny-turner spectrometer configuration was selected, consisting of a slit, a collimating spherical concave mirror with a 101.6 mm focal length, a planar reflective-ruled diffraction grating with a groove density of 800 grooves/mm, and a focusing spherical concave mirror with a 101.6 mm focal length. After careful selection of the optical components and specific design constraints, our chosen optical components enable the spectral range required with the highest resolution

possible, even after aberrations. After filtering, the Raman signal is focused into a pinhole aperture, and then onto a rectangular entrance slit with an achromatic NIR doublet, which enables high coupling efficiently into the spectrometer. For initial spectrometer alignment, a variable slit was used that could change width with rotations of the handle. This choice was made because during alignment, it is important to maximize the signal through the unit during initial alignment before lowering the power incident on the detector by decreasing the slit width or increasing the resolution. The advantage of the variable slit is that both a smaller and larger slit size is possible with minimal hardware or re-alignment needed when adjusting the size. The circular aperture before the slit is in place to improve light throughput and reduce polarization artifacts and reduce the height of the slit being illuminated qw22`if need be.

6.1.2.2. Spectral Range

One of the most critical designs parameters is the wavelength range your spectrometer supports, because it defines what portion of the spectrum you can observe, and how well you can interpret your Raman data. Because we are interested in Raman shift, and not absolute wavelength, we must calculate what wavelength range the desired shift translates to. With a set goal of Raman shift detection from 0 to 3000 wavenumbers, we need a wavelength range of approximately 785 to 1050 nanometers, a wavelength width of about 270 nm, with a central wavelength of 910 nm. This set range of 0 to approximately 3000 wavenumbers is a result of the Raman spectra databases of polystyrene, nylon, and polyethylene terephthalate, and where their fingerprint peaks typically occur for detection and identification purposes. Our group plans to detect up to 3000 wavenumbers to not miss parts of the Raman spectrum that could be highly useful for detection and identification of microplastics, such as O-N and C-H stretches that can be found around 2800 nm. There is a known tradeoff between resolution and range of the spectrometry, as a wide spectral range can reduce your spectral resolution since the detector size does not change, so the design has to be carefully done to balance these two parameters.

Spectral Range

$$3200\ cm^{-1} = \left(\frac{1}{785\ nm} - \frac{1}{\lambda_{scattered}}\right) \cdot 10^{-7} \tag{6.1}$$

Equation 6.1_ was utilized to convert the total 3200 wavenumbers dispersion to a wavelength range, spanning approximately 785 to 1050 nm.

6.1.2.3. Infinity-corrected Microscope Objective System

Due to the illumination setup containing a microscope objective to allow for small particle detection, the type of magnification system needs to be taken into consideration. Typical magnification systems containing an objective typically come in 2 variations, finite and infinite. The finite-conjugate was developed first, and contains just an objective, and the intermediate image plane occurs at the focus of the objective, and the image at the

intermediate plane is real. The major drawback is the limited space for intermediate optics and the chromatic and spherical aberrations that degrade the image quality when additional elements, such as filters, are added. After the sample is illuminated, the laser light needs to be filtered out, but aberrations would decrease the quality and resolution of the final signal. That is why our group decided on an infinite-conjugate microscope system, which includes a microscope objective and a tube lens. The objective lens outputs collimated light that is focused at infinity, and a separate tube lens refocuses the collimated beam to form the intermediate image. This collimated space between the objective and tube lens gives modularity to the system that the traditional finite-conjugate system does not, and the filters and dichroic mirror can now be added without affecting the focus and provides consistent magnification. Although it is more complex and can be more expensive, the inclusion of the filters without the additional aberrations is worth the complexity of working with an infinity-corrected system.

The fundamental diffraction limit of a microscope can be described by Equation 6.2, which is a physical boundary on its resolution, which is determined by the wave nature of light. 2 points cannot be resolved if they are closer than approximately half the wavelength of the imaging light, divided by the numerical aperture of the lens, which is described below. When light passes through the microscope's aperture, it diffracts and spreads out, which causes the single point source to be imaged as a diffraction pattern- a central bright spot called the Airy disk surrounded by fainter rings. Two points can only be distinguished if their Airy disks are significantly separated. If the distance between the two points is smaller than the limit, then their Airy disks overlap, and the two objects appear as a single blur. λ represents the excitation light source, 785 nm, and NA describes the numerical aperture of the lens. With our microscope objective of choice, a NA of 0.4 is used, so our diffraction limit and minimum spot size possible for focusing the 785 nm excitation beam onto the sample plastic is 2 μ m- demonstrating our ability to reach our goal of detecting plastic sized smaller than a 5 mm square.

Diffraction limit of Microscope image

$$D_{airy} = \frac{1.22\lambda}{NA} \tag{6.2}$$

To maintain a high resolution through our system, we need to take the diffraction limit of our microscope objective into consideration. Additionally, this image size also provides insight into the size of the slit.

6.1.2.4. Spectrometer Design – Slit Size

For choosing the slit size of your spectrometer, you want to optimize the signal into the spectrometer, so matching the image size at the intermediate plane with your slit size or slightly smaller is ideal. The slit can be reduced in size to increase the resolution, but the tradeoff of lower signal exists, and has to be mitigated carefully, as Raman signal is already

low. I am starting with a slit width that matches or is slightly larger than expected image size at the slit to maximize signal collection, and plan to reduce it to increase the resolution later on in the design process. Referring to Equation 6.3, using a 20x microscope objective with a D_{airy} = 2 m, our expected image size, assuming perfect conditions since this is just to get an idea of what the slit size should be, is approximately 40 μm , which describes why a slit size of 30 – 50 μm would be efficent for our spectrometer design.

Image Size at Intermediate Plane $$Image\ size\ =\ M\ \cdot D_{airy}$$ 6.3)

Due to our system being free space, the coupling efficiency into our spectrometer can be calculated using the slit width, height, and spectrometer's numerical aperture, equation 6.3, which can be calculated using theta, the input angle of light into the spectrometer's entrance slit. With our design, the focal length of the tube lens is expected to be 180 mm, so a theta input angle of 26.7 degrees is found, directly relating to a numerical aperture of 0.45.

Spectrometer's Numerical Aperture $$NA\ =\ n \cdot \sin(\theta)$$ 6.3)

6.1.2.5. Spectrometer Design – Optical Power

A high NA enables a high sensitivity, meaning the instrument can collect more light, but it also introduces optical aberrations. A low NA increases the resolution, resulting in less aberration, but then less power is captured by the spectrometer, as seen by equation 6.4. The amount of optical power reaching the detector is fundamental for understanding how your system works, and what range of signals you will be able to detect. Parameters such as signal-to-noise ratio (SNR), dynamic range, usable spectral resolution, and measurement speed of the spectrometer are all dependent on the amount of optical power reaching the detector. SNR is so important to consider because even a highly optimized spectrometer with high-quality mirrors, large grating, and high dispersion cannot deliver high-resolution spectra if the signal is buried in shot noise. Particularly concerning our application of Raman spectroscopy, we have to take into consideration that low power directly increases the minimum detectable signal and raises the noise floor. Dynamic range describes how the detector must be able to distinguish strong features from weak features. If the power is too low, weak peaks become hidden in the noise, and if the power is too high, strong peaks are lost to saturation, and the usable dynamic range collapses. Our spectrometer design must be done so that the power per pixel stays within the well depth, and that the brightest part of the spectrum does not saturate, and that the weakest signals remain above the read-noise floor. The resolution of our system also depends on power. High resolution requires a high signal-to-noise ratio. When the system resolves finer spectral features, the energy is spread over more detector pixels. Higher dispersion leads to narrow linewidth per pixel; longer focal length results in a larger image size, and smaller slit widths result in less collected light. High resolution is fundamentally power-limited, and without sufficient optical power, the lines appear broad, thermal drift can occur, so peak positions can shift, spectral fitting is unstable, and integration times must increase to compensate.

Spectrometer Captured Power $P = h \cdot w \cdot (NA)^2$ 6.4)

With our design, a best-case scenario captured power would be approximately 32.4 μW .

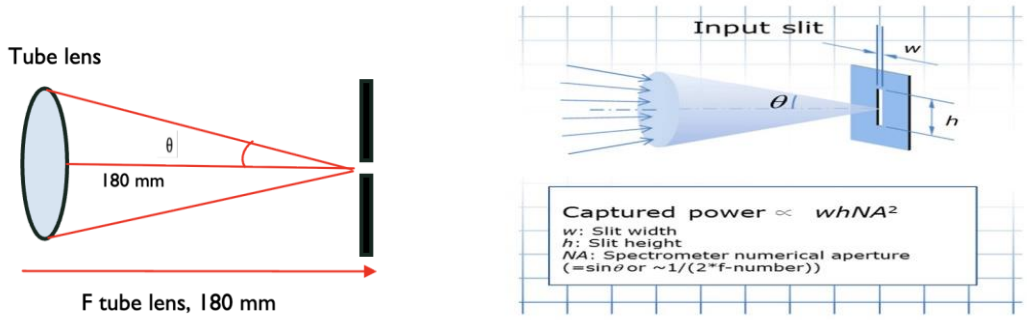

Figure 27 Dimensions for optical power calculation.

left describes our design. Figure taken from Isben Photonics, Coupling into your Spectrometer. https://ibsen.com/wp-content/uploads/ebook/spectrometer-resources/Coupling-into-your-spectrometer-1-B.pdf

Minimum wavelength: λ_1: 780 nm

Maximum wavelength: λ_2: 1050 nm

Range: $\lambda_1 - \lambda_2$: 270 nm

Center wavelength λ_c: 915 nm

Goal Resolution $\Delta\lambda$: < 2 nm

Total deflection Φ : 30 degrees

- (typical for czerny turner)

Grating groove density G: 1200 g/mm

Detector width L_D: 28.8 mm

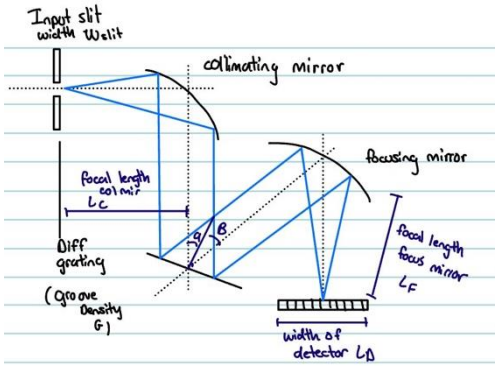

Figure 28 Czerny-Turner spectrometer input constraints.

6.1.2.6. Spectrometer Design – Angle of Incidence and Diffraction

Designing a Czerny-Turner spectrometer begins with establishing the geometric relationship between the input wavelength range, the diffraction grating, and the required mirror focal lengths. A small number of key input parameters, such as the grating groove density, the center wavelength, the detector width, the target spectral coverage allows us to determine the angle of incidence onto the diffraction grating, the corresponding diffraction angle, and the necessary optical geometry for both the collimating and focusing mirrors.

For our design, the minimum and maximum detectable wavelengths were defined earlier. We know that our minimum detected wavelength is 780 nm, and our max is 1050 nm, based on the spectral range calculation illustrated earlier in chapter 6. This would result in a range of 270 nm, with a center wavelength at 915 nm. Our goal resolution is approximately 2 nm, with a grating groove density of 1200 g/mm. This has since been updated to 800 g/mm with budget constraints being taken into consideration. Typical Czerny-turner spectrometer design starts with a deflection angle of approximately 30 degrees, and our detector width is 28.8 mm.

Angle of Incidence on Diffraction Grating

$$\alpha = \sin^{-1}\left(\frac{\lambda_c \cdot G}{2 \cdot \cos\left(\frac{\theta}{2}\right)} - \frac{\phi}{2}\right) \quad 6.5)$$

The angle of incidence is calculated directly from the grating equation under symmetric Czerny-turner mounting conditions, where the diffraction angle and incidence angle share a defined relationship set by the deflection angle. Using our center wavelength, updated groove density, and system geometry, our angle of incidence is calculated to be approximately 27.14 degrees. This angle defines how strongly the incoming beam interacts with the grating, and in turn, determines the dispersion profile across the detector.

Angle of Diffraction off Diffraction Grating

$$\beta = \phi + \alpha \quad 6.6)$$

Once the incidence angle is determined, the diffraction angle follows directly by adding the system deflection angle with the angle of incidence. For our geometry, this results in a diffraction angle of 57.14 degrees. This diffraction angle establishes the direction in which the central wavelength exits the grating and sets the orientation of the focusing mirror relative to the grating plane. The relative separation between the angle of incidence and the diffraction angle ultimately dictates the linear dispersion across the detector.

Focal Length of Focusing Mirror

$$L_F = \frac{L_D \cdot \cos(\beta)}{G(\lambda_2 - \lambda_1)} \quad 6.7)$$

The focal length of the focusing mirror is derived from the required projection of the full spectral range onto the detector with a width of L_D. Because the dispersion is controlled almost entirely by the grating geometry, the mirror must focus on the angularly separated wavelengths so that the longest and shortest wavelengths map precisely onto the edges of the detector. After entering our known detector width, groove density, and wavelength range, we find a focal length of 48.2 mm for our focusing mirror.

This is a relatively short focal length, but it is typical for a Czerny-Turner spectrometer. Czerny-Turner spectrometers are compact, and it contributes to the system's high throughput.

Focal length of Collimating Mirror

$$L_c = L_F \cdot \frac{\cos(\alpha)}{M \cdot \cos(\beta)} \quad 6.8)$$

The collimating mirror focal length is found by scaling the experimentally calculated focusing mirror's focal length by the incidence angle and diffraction angle, and by the systems magnification, M. The collimating mirror must transform the diverging beam from the entrance slit into a well-collimated beam at the grating, to ensure that each individual separate wavelength interactions with the grating under uniform conditions. Using our previously calculated angle of incidence and angle of diffraction, a focal length for the collimating mirror of 79.05 mm is found.

Table 41 Calculation Result of Mirror Focal Lengths

	Collimating Mirror	Focusing Mirror
Focal Length Calculation	79.05 mm	48.2 mm
Focal Length Choice	80 mm	50 mm

It is important to note that in an ideal spectrometer design workflow, the angles of incidence, diffraction geometry, and detector size are first used to calculate the required focal lengths for the collimating and focusing mirrors. However, due to budget limitations and the need to utilize existing optical components we already have access to, our design process must proceed in the reverse direction, as the available mirrors used for this spectrometer both have fixed focal lengths of 101.6 mm. This constraint forces the optical geometry, including the grating placement, angle of incidence, diffraction angle, and slit-to-mirror distances to be derived from the fixed focal length, rather than optimized independently. Our spectrometer design is now constraint driven, by optimization, in order to use the mirrors, we have on hand, while also still achieving our required spectral range and resolution.

6.1.2.7.

Particularly in Czerny-turner, Echelle, and imaging spectrometers, the chance of optical aberrations getting in the way of the goal resolution and line quality is high. Aberrations distort the position mapping and reduce throughput to the detector. Typical aberrations include spherical, coma, astigmatism, and chromatic aberration. Spherical aberrations are caused by the fact that spherical surfaces focus marginal and paraxial rays to different axial positions. Some design fixes include using aspheric or paraboloidal mirrors for collimating and focusing. Increasing the focal length reduces marginal ray angles and spherical contribution, which decreases the chance of spherical aberrations. Some tradeoffs to those fixes include that aspheric shapes are more expensive, and aligment sensitive. Additionally, longer focal lengths increase the instrument size, and is not always applicable. Another aberration type is coma. Off-axis imaging by curved mirrors creates asymmetrical tails in spot profiles, which is seen often in Czerny-Turner geometry. This can be helped by minimizing of-axis angles as much as possible, which means reducing the angle between the optical axis of the mirror and the chief ray. Even small reductions tend to make a large difference when it comes to coma. Additionally, symmetric designs are possible. To explain, the collimating mirror and focusing mirror can be made symmetric as possible around the grating to further prevent coma. Astigmatism is another aberration caused by

off-axis systems. Off-axis systems produce different focal planes for sagittal and tangential rays. A smaller slit height can help to limit astigmatism, and for most Raman systems, a shorter slit is used. Longer focal lengths also help in this case, particularly with the camera, as a longer focal length reduces angular spread at the detector, which reduces the astigmatic blur. A notable tradeoff in reducing the slit height is decreasing the signal that reaches the detector.

6.2. Electrical Hardware Design

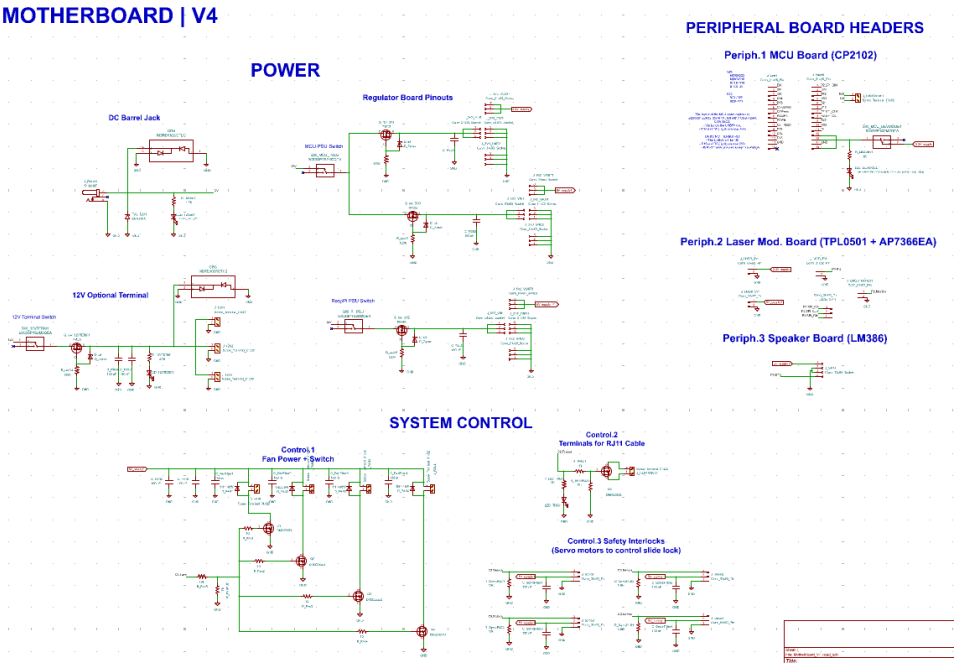

Figure 29 Motherboard Schematic

Table 42 Electrical Subsystems List

Electrical Subsystems
Data Acquisition and Processing
Safety and Status
Power

6.2.1. Data Acquisition and Processing System

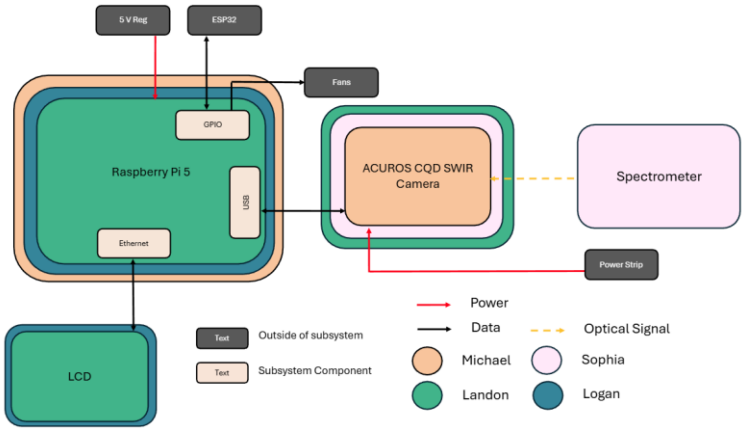

Figure 30 Data Acquisition and Processing Block Diagram

Table 43 Data Acquisition Parts List

	Application
Raspberry Pi 5	Data processing and interfacing with the camera.
ACUROS CQD SWIR	Obtains spectral data from the spectrometer system.
LCD for Display	The LCD allows ECOSPEC to operate as a standalone device.

6.2.2. Safety and Status Subsystem

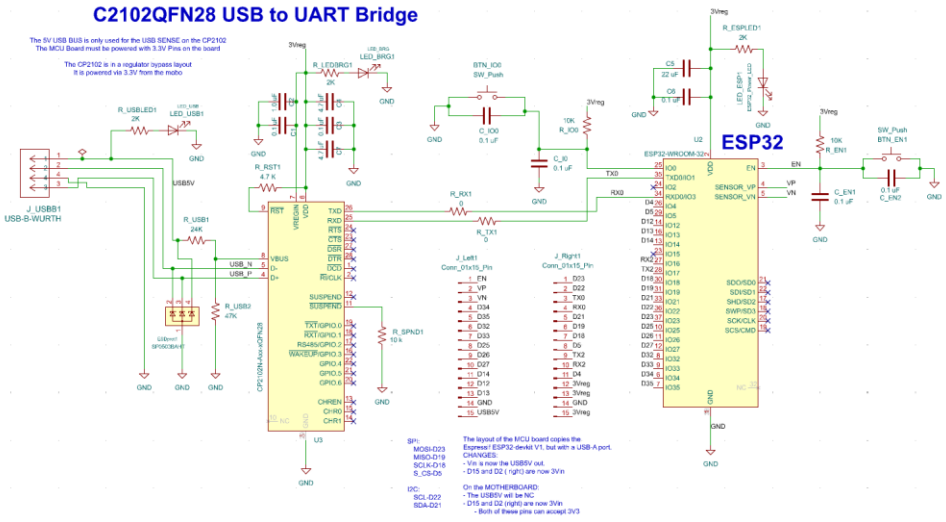

Figure 31 MCU Board Schematic

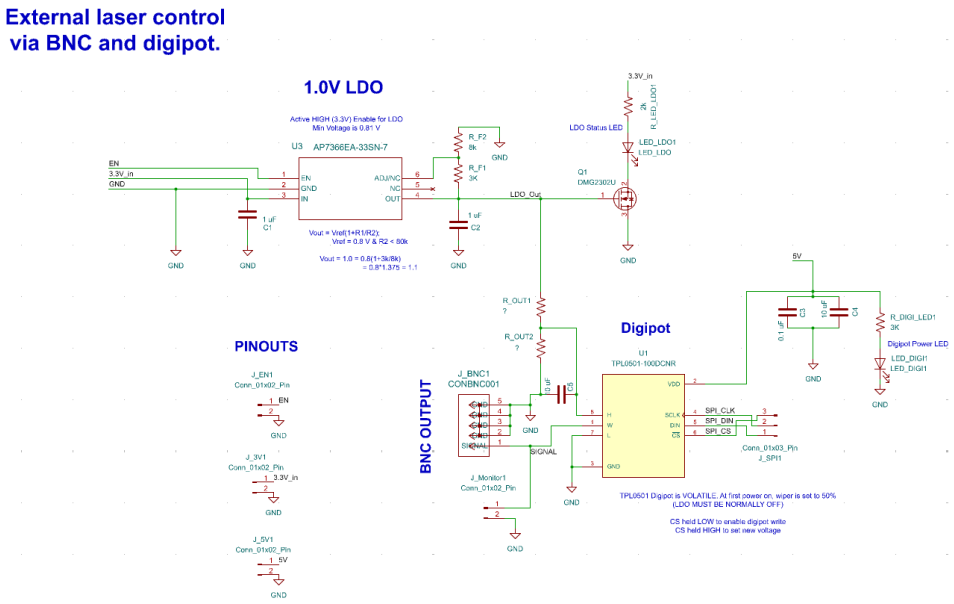

Figure 32 Laser Modulation Board Schematic

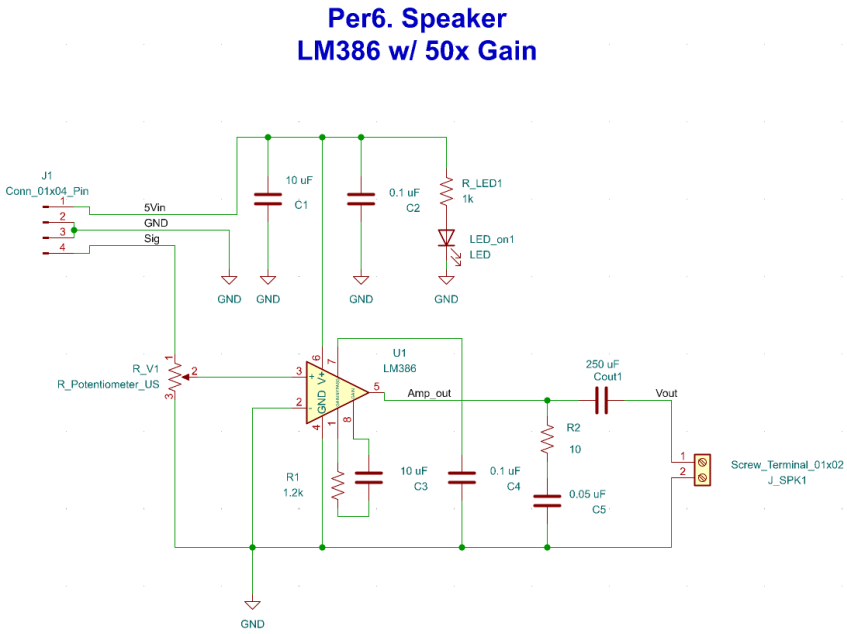

Figure 33 Speaker Board Schematic

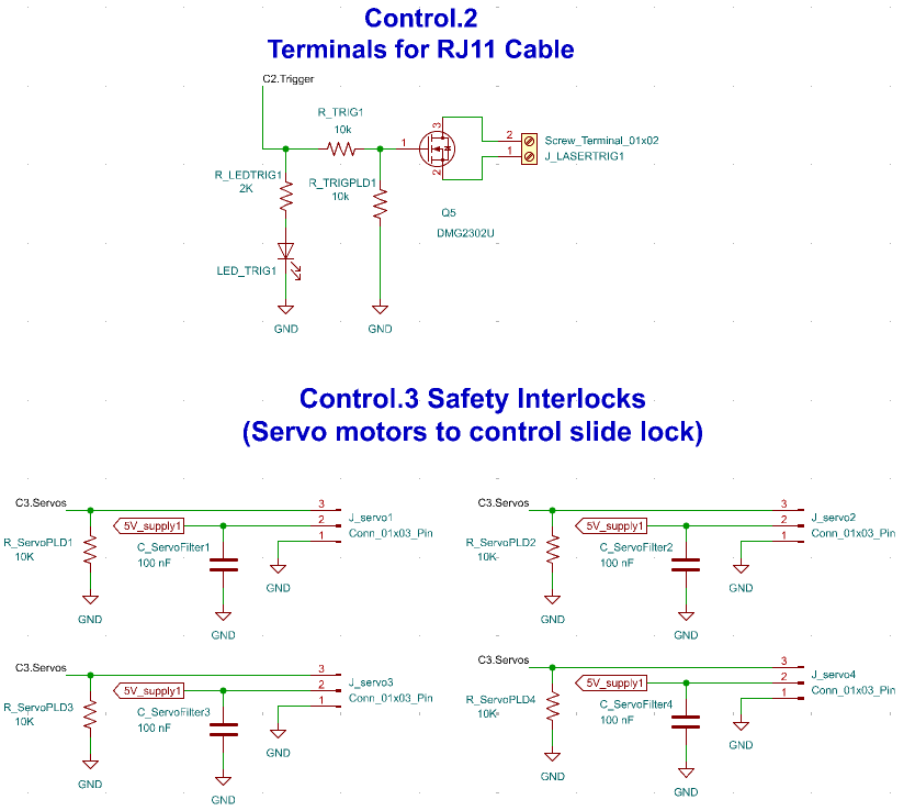

Figure 34 Laser and Servo Pinout Schematic

Table 44 Safety and Status Parts List

Part	Part ID	Application
MCU	**ESP32**	Controls interlocks, laser power, and monitors status.
Safety Interlocks	**Servo**	Locks the enclosure during laser operation.
Digital Potentiometer	**TPL0501**	Allows the MCU to create different voltage levels to control laser power through the rear panel BNC input.
LCD	**GeeekPi 10”**	Indicate ECOspec device subsystem statuses.
Speaker	**N/A**	Acts as an indicator for the user when LEDs are not visible
Fans	**N/A**	Ventilate the internals of the system.

6.2.3. Power Subsystem

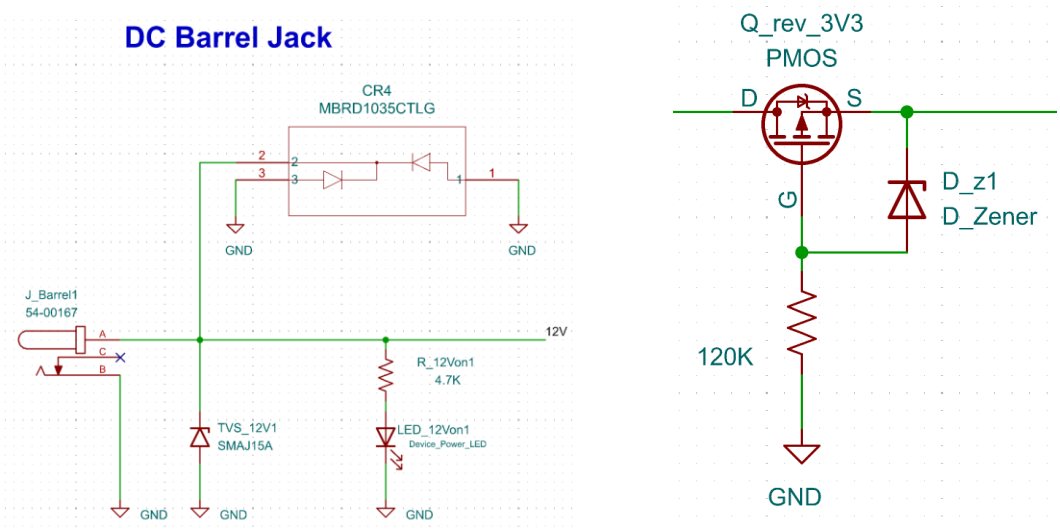

Figure 35 Reverse Voltage Protection Circuitry on Motherboard

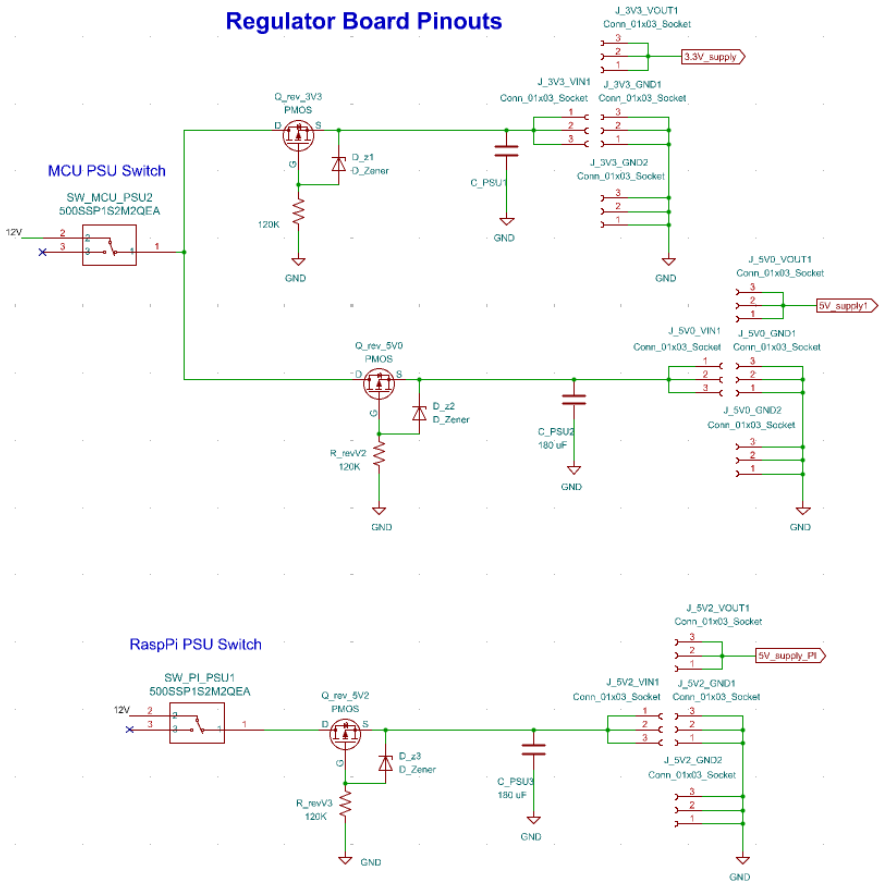

Figure 36 Power Subsystem Circuitry on Motherboard

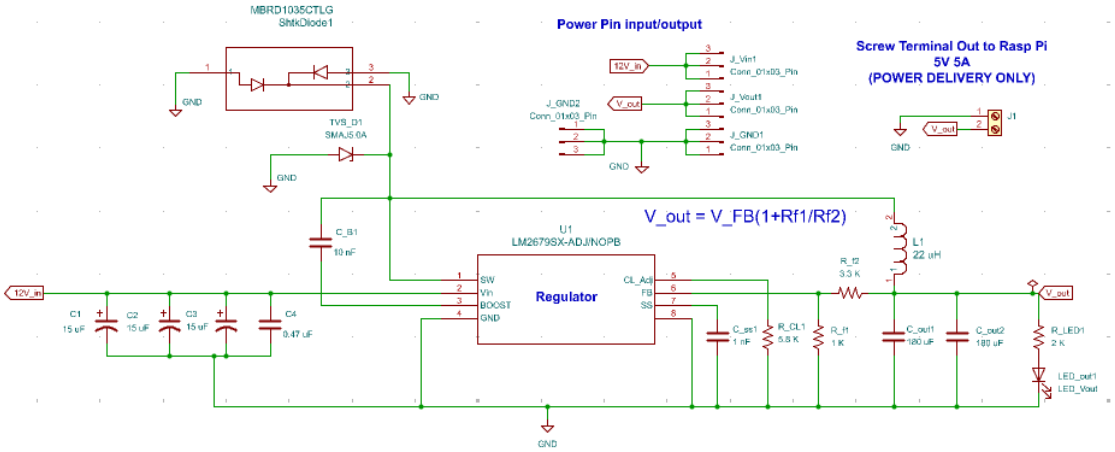

Figure 37 Regulator Board Schematic

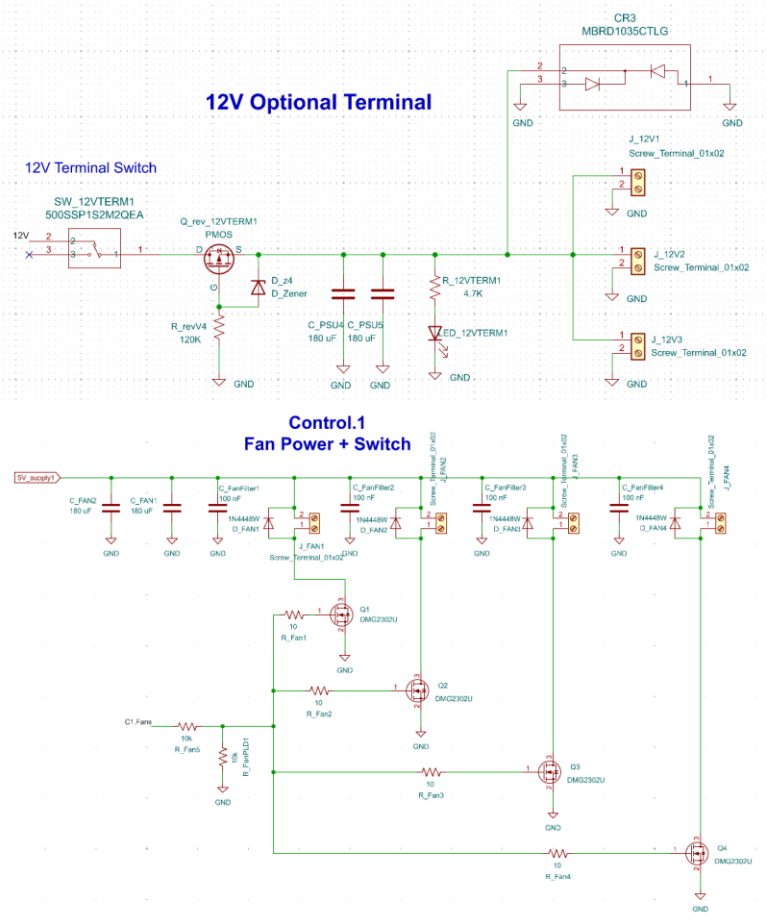

Figure 38 5V and 12V Output Port Circuitry

Table 46 Power System Part List

Part	Part ID	Application
3.3 Voltage Regulator	LM2679	Supplies a stable 3.3 V for the ESP32 and digital pot.
5 Voltage Regulator	LM2679	Supplies a stable 5 V for the Raspberry Pi and fans
12 V Power Supply	Alitove 12V 15A 180W DC Barrel	Supplies a stable 12 V for the voltage regulators.
Power Strip Extender	N/A	Main source of power for the system. Supplies power to the laser, detector, and main power supply.
PMOS Fets	AOI21357	PMOS Fets employed for reverse voltage protection

6.3. Mechanical Hardware Design

A rigid mechanical design is crucial in any stable optical system. The mechanical portion of our system involves ease of alignment, minimizing vibration, minimizing alignment deviation, total enclosure of our spectroscopic system, and ensuring a stable operating temperature.

Our ability to dampen vibration is limited. Damping components are very expensive compared to traditional optomechanics. However, the most important part of our system is that vibration does not cause misalignment of aligned optics. To accomplish this, high precision and quality checked components from ThorLabs, Newport, Edmund Optics, or another reputable optics component supplier will be used for all major optical alignment systems. The most sensitive system to misalignment is the spectrometer. Any small deviation of the entrance angle of slight, collimating mirrors, grating, or focusing lens for the detector

Access to the subsystems must also be taken into account. Loading cuvette samples into ECOspec should be simple and easily accessible. The loaded position of the cuvette must have little room for deviation while not being too difficult to set in place. The front panel of the laser module should be accessible at all times for its Estop button. The airflow for ventilation fans must be taken into consideration to prevent thermal fluctuation or a nonuniform temperature distribution.

6.3.1. Cage Mounts

Cage mounts are precision opto-mechanical building blocks that provide rigid, self-aligning framework for constructing optical systems. They typically are made of a set of parallel rods- 4 in a square, where optical mounts, folder holders, and translation stages can be attached. It provides high stiffness and ensures that all components remain coaxial along a defined axis. For our optical setup, employing a cage mount system could be crucial in maintaining our spectral resolution. This modular system enables rapid prototyping and

wastes less time with the optical setup, with components sliding along the rods simply locking at the wanted position. They are also already set up to be compatible with lens tubes, enabling quick integration of fibers, slits, apertures, and objectives in this compact, safe form. They are highly stable and tend to maintain alignment and minimize thermal drift and mechanical creep. Our entire optical system, the illumination and collection optics will hopefully be set in their final aligment using a cage mount and rail system, hosting the beam expander optics, the fiber collimator, microscope objective, Raman filters, slit mount, mirrors, and grating.

6.3.2. Cuvette Holder

Cuvette holders are the mechanical interface that positions a liquid or solid, in our case plastic samples, in a cuvette in the correct optical path for spectroscopic measures, including absorption, fluorescence, and Raman spectroscopy. Its design is critical for signal collection, optical throughput, scattering behavior, and repeatability. This cuvette holder maintains the path length, vertical, and angular alignment. The alignment prevents beam clipping and ensures that the same physical volume is interacting with the collection and excitation of optics. The design of the cuvette holder is also necessary for the repeatability of measurements using our Raman spectrometer. High quality holders provide kinematic seating or spring-loaded pressure pads to ensure that replacing a cuvette does not change or harm the optical geometry. The material also should be taken into consideration. Black anodized aluminum would be the material of choice to minimize stray reflections that would otherwise increase background noise and to protect the user from unintended laser scattering. Poor-quality cuvette holders can introduce scattering and reflections in the cuvette, which increase the spectral baseline or generate artifacts, peaks that are not our peaks of interest.

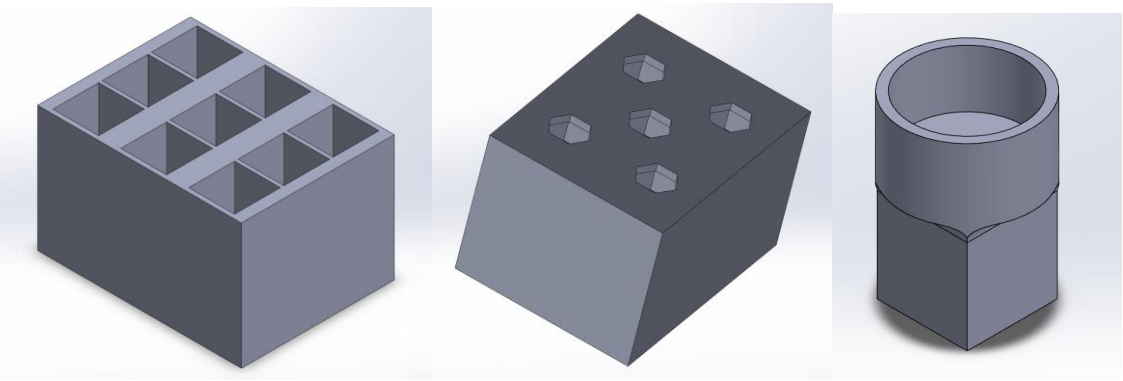

Figure 39 3D Models of Cuvette Holder and Adapter

For our final design, we used a 3D printed cuvette holder. Multiple positions for the cuvette, as well as multiple different standoff positions for the holder itself, were included in the design to allow for finer positional adjustment. Some materials used for testing came in

variety of shaped containers, thus adapters were required to be printed for the primary mount.

6.3.3. 3D Printed Optomechanics

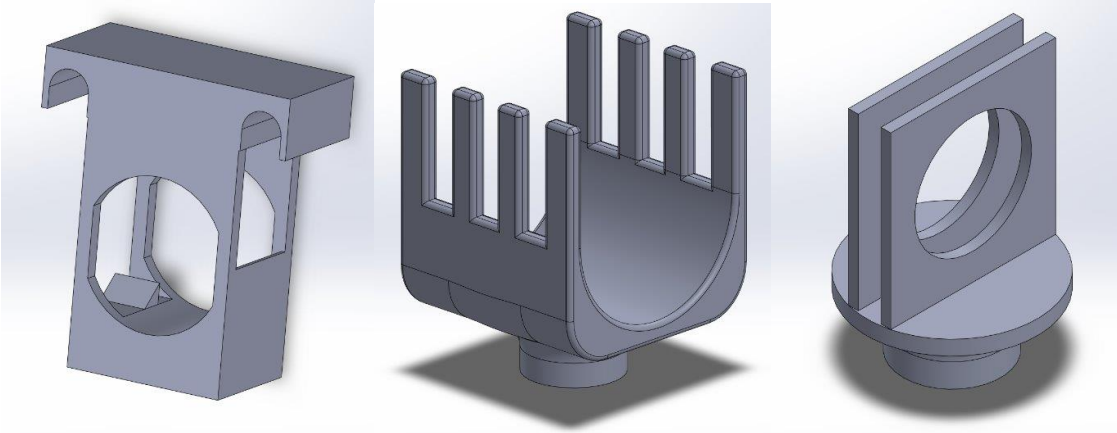

Figure 40 3D Models of Optomechanics

The custom mechanical hardware in ECOspec consolidates the printed components that locate every optic between the laser fiber output and the detector plane onto a shared cage-and-baseplate framework. All custom parts in this subsystem are FDM-printed in PLA, selected based on filament available on hand at print time. Print parameters and part placement deliberately keep these components away from sustained heat sources, because the approximately 60 °C glass transition of PLA would otherwise create dimensional drift in any holder positioned near the laser module, the regulator boards, or the camera TEC heatsink. Mounting interfaces that attach printed parts to the aluminum baseplate use print-in-place captive 1/4"-20 nuts. The print is paused at the appropriate layer, the nut is dropped into a cavity sized to its outer profile, and the print resumes around it to lock the nut in permanently.

The cage-compatible slit holder lets us swap slit widths during integration without buying multiple dedicated Thorlabs holders. The holder uses the standard 30 mm cage interface, with through-bores at the four cage-rod positions and the optical axis maintained at the standard cage-center height to preserve the common reference frame shared by every other component on the rail. A side-loading slot oriented normal to the optical axis accepts a thin slit card without disassembling the cage, which significantly reduces the alignment recovery effort after a slit change.

A thread-mismatch on the illumination side drives the microscope objective mount. The Nikon CF160 TU Plan Epi ELWD uses an M25x0.75 thread and a 60 mm parfocal length, neither of which match the RMS or SM1 adapters that Thorlabs stocks for compact cage assemblies, leaving the objective without a commercial mounting path into the cage system. The printed mount holds the objective from below, using compression to secure the optic in place. The microscope objective was designed not to be integrated with the

cage system. It was found experimentally that the objective needed to be slightly angled to produce a perfectly focused spot. This angle was incompatible with the cage system structure.

A family of smaller utility prints handles the rest of the optical bench. These include cage-compatible iris and beam-dump holders, lens-tube adapters that bridge to the non-standard mirror diameters in the spectrometer arm, and fluorescent alignment-card frames for walking the 785 nm beam through the system without exposing the SWIR detector to direct scatter. Each of these prints uses the same conventions as the larger mounts: 30 mm cage rod spacing, captive 1/4"-20 nuts at any baseplate interface, and a fixed optical-axis height referenced from the printed baseplate. The result is that any holder can be dropped into any position along the rail system without re-deriving the mounting geometry, which has been a meaningful time savings during the iterative alignment phase of integration.

6.3.4. 3D Printed Electrical Housing

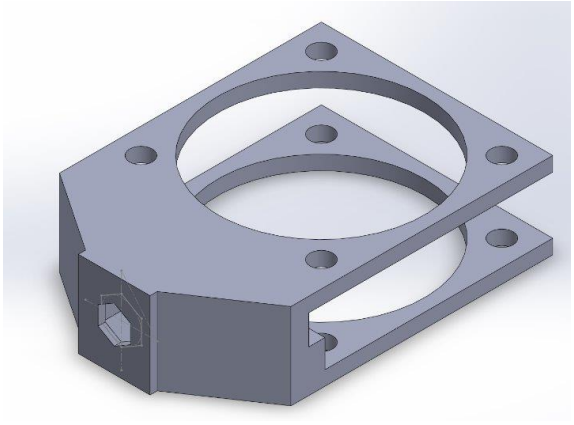

Figure 41 3D Model of Fan Mount

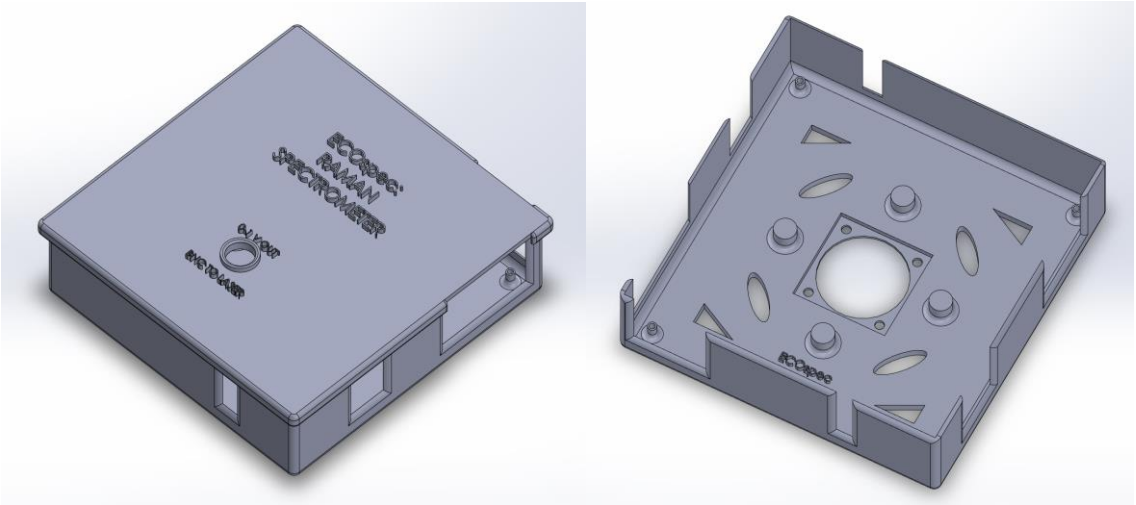

Figure 42 3D Model of PCB Housing

7. Software Design

This section provides a high-level overview of the software design components and structure of ECOSpec. This includes implementation of control systems, data processing, and user experience. The complete and comprehensive diagrams for the software systems can be found in section 2.5.

7.1. Device Control Systems

As is the goal of any system, a robust control scheme is required. This is especially true for our ECOSpec, which utilizes optical components that can prove to be hazardous to the user if not properly managed. Since our application contains numerous subsystems, each of these has specific software requirements.

For our control systems, such as safety interlocks, power management, cooling, and normal operation, we implemented a set of basic state machines, using integrated C and FreeRTOS. This simple and lightweight suite allows us to directly manage the state of our device and therefore ensures that at no point will the system operate in a way it is not designed for or execute a function without meeting the required prerequisites. FreeRTOS allows us to split many of the different methods used into tasks that can be managed directly by the operating system, allowing efficient usage of hardware resources while maintaining responsiveness and safety. Much of the software control is issued through GPIO pins on the various controllers and ICs used.

Additionally, some of the software control for specific devices within our system is handled by device specific software development kits (SDKs). In our design, we utilize the Acuros CQD camera to handle the detection aspect of our acquisition process. The camera control is handled on the Rasberry Pi within our system and is interfaced using the harvesters python library.

The Acuros camera comes with software for control and data acquisition, however, as this software is incompatible with linux systems, it is therefore incompatible with our Raspberry Pi meant for acquisition and processing. To remedy this, we can utilize the SDK mentioned previously, allowing us full control of the camera from our own codebase. Additionally, accessing these SDK API functions gives us the ability to utilize our own GUI, as well as extend functionality of the camera as we see fit, providing us the tools to create usable spectral readings for comparison, as well as custom GUI applications for device usage.

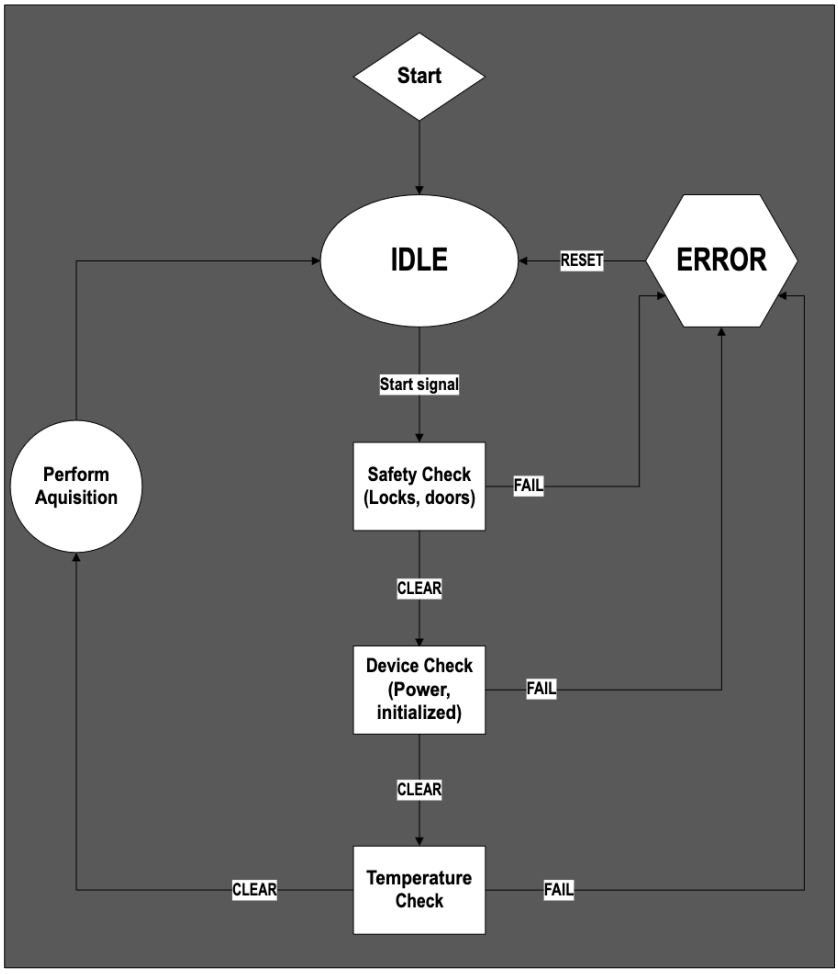

Figure 43 Control System State Diagram

7.2. Data Processing

ECOSpec's use-case brings with it a large data-cost in the form of sizable raw data acquisitions that are unsuitable for comparison and identification initially. To remedy this, all raw data is put through a thorough pipeline to remove impurities and ensure the data is put in a usable condition before any conclusion is drawn by the system.

The processing begins with noise removal, performed using a median filter, which effectively suppresses high-frequency noise while preserving the sharp spectral peaks characteristic of Raman signatures. Following denoising, we apply a fluorescence correction stage using a 7th-order polynomial baseline removal. Fluorescence backgrounds can dominate Raman spectra and distort peak intensities; the polynomial baseline method subtracts these broad trends while retaining the structure of the true Raman peaks. These

two stages ensure that the fundamental shape and vibrational features of the spectrum remain intact before normalization.

Once the spectrum has been cleaned, the next stage involves standardizing the intensity distribution. ECOSpec applies standard normal variate (SNV) normalization, which rescales each spectrum to have zero mean and unit variance. SNV corrects multiplicative and additive effects such as varying laser intensities, fiber coupling differences, or changes in detector sensitivity. After SNV, we apply a final min-max scaling step, mapping the processed intensities to a fixed range of 0 to 1. This ensures that all spectra, whether from the field, calibration samples, or the reference libraries exist with a consistent set of comparable axes.

Importantly, this exact pipeline is applied not only to real-time sample data but also to all spectra stored within ECOSpec's reference library. Maintaining absolute consistency in preprocessing is essential; even small discrepancies in filtering, baseline correction, or normalization can lead to significant deviations in similarity measurements. By enforcing a standardized transformation on every dataset, ECOSpec ensures that all spectral comparisons are fair, reproducible, and scientifically grounded.

The goal of a comprehensive processing pipeline is to allow us to make confident assumptions regarding the material being tested. The results of this process will be used in our final identification step. This step uses a Pearson similarity coefficient to determine the most similar spectra within the established library, when compared to the tested sample. Once a confident match is found, the final aspect of our data handling will be the transmission of all found information to the user through our graphical interface.

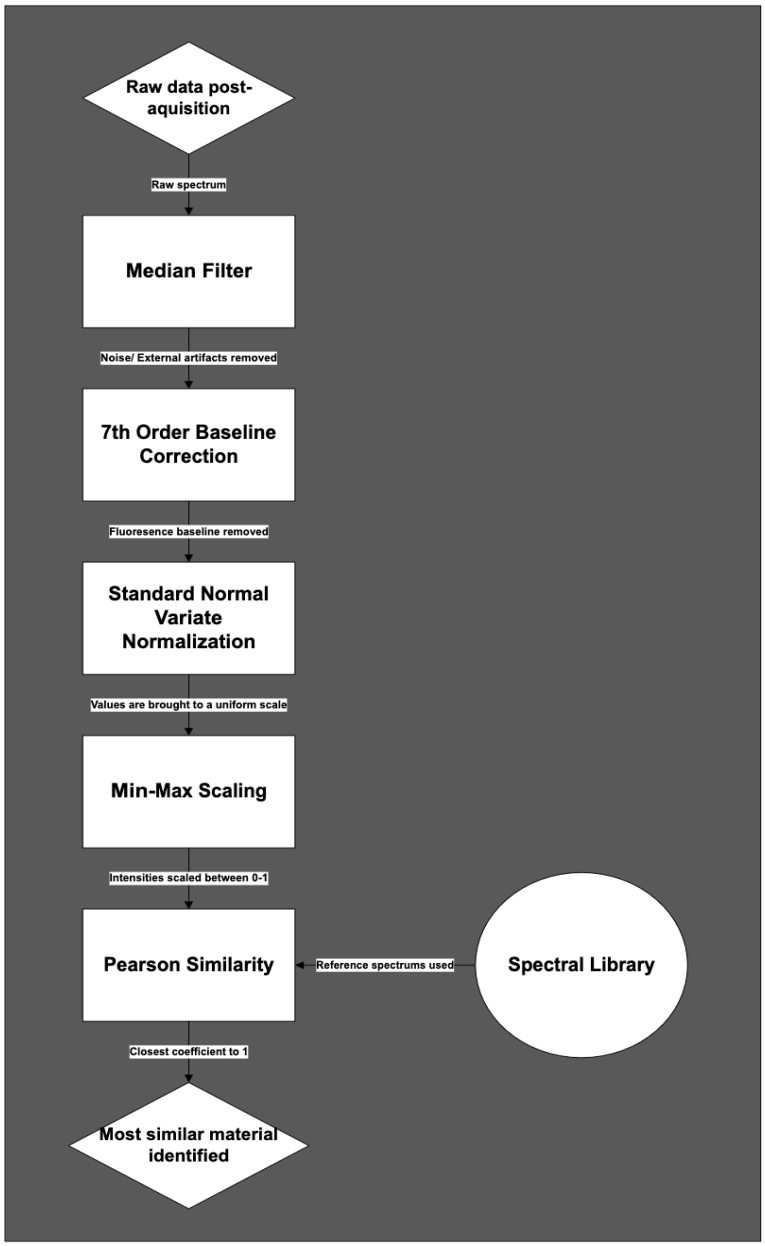

Figure 44 Data Processing Flow

7.3. User Experience

The user experience subsystem of ECOSpec provides a simple and powerful graphical interface hosted directly on the Raspberry Pi 5, consolidating user control and result display into a single touchscreen application. The interface is rendered as a native application on a 1024 by 600 display, built with HTML5 and JavaScript and presented through PyWebView so that no external browser is required at runtime. This architecture keeps the application self-contained on the Raspberry Pi, eliminates the dependency overhead of a full browser stack, and gives the system the look and responsiveness of a dedicated instrument rather than a general-purpose computer running web software.

User control is exposed through configurable acquisition parameters, including integration time and laser power, both of which are adjustable through sliders before a scan is initiated. A dedicated scan button and an emergency stop are prominently placed and always visible at the top level of the interface, ensuring that the most safety-critical and most frequently used controls are never more than a single touch away. The scan button remains locked until both the ESP32 microcontroller and the ACUROS CQD camera are confirmed connected, preventing accidental triggering when hardware is not present and providing a clear failure mode to the operator rather than a silent error during acquisition. Direct hardware commands, including servo positioning, laser modulation, fan control, and audio output, can also be issued to the ESP32 through a built-in control panel accessible from the interface, supporting both routine operation and lower-level diagnostics from the same screen.

Result display is handled on a single unified view that presents the most important measurement outputs simultaneously, avoiding the navigation overhead of switching between screens during a scan. The live Raman spectrum is rendered in real time on an HTML5 canvas across the full 3200 cm^{-1} range defined by the spectrometer's built-in optical limits. Identification results display the top material match, the Pearson similarity score, and the three closest library candidates ranked by correlation, giving the operator both a primary classification and the supporting evidence needed to assess the confidence of that classification. A real-time system log records all hardware events, processing steps, and errors with timestamps, and a system status panel shows the live connection state of each hardware component, providing a continuous view of system health alongside the active measurement. After a scan completes, results can be exported as a timestamped CSV file containing the calibrated wavenumber axis, normalized intensity values, and match result, supporting downstream analysis and record-keeping outside the instrument.

8. System Fabrication

8.1. PCBs

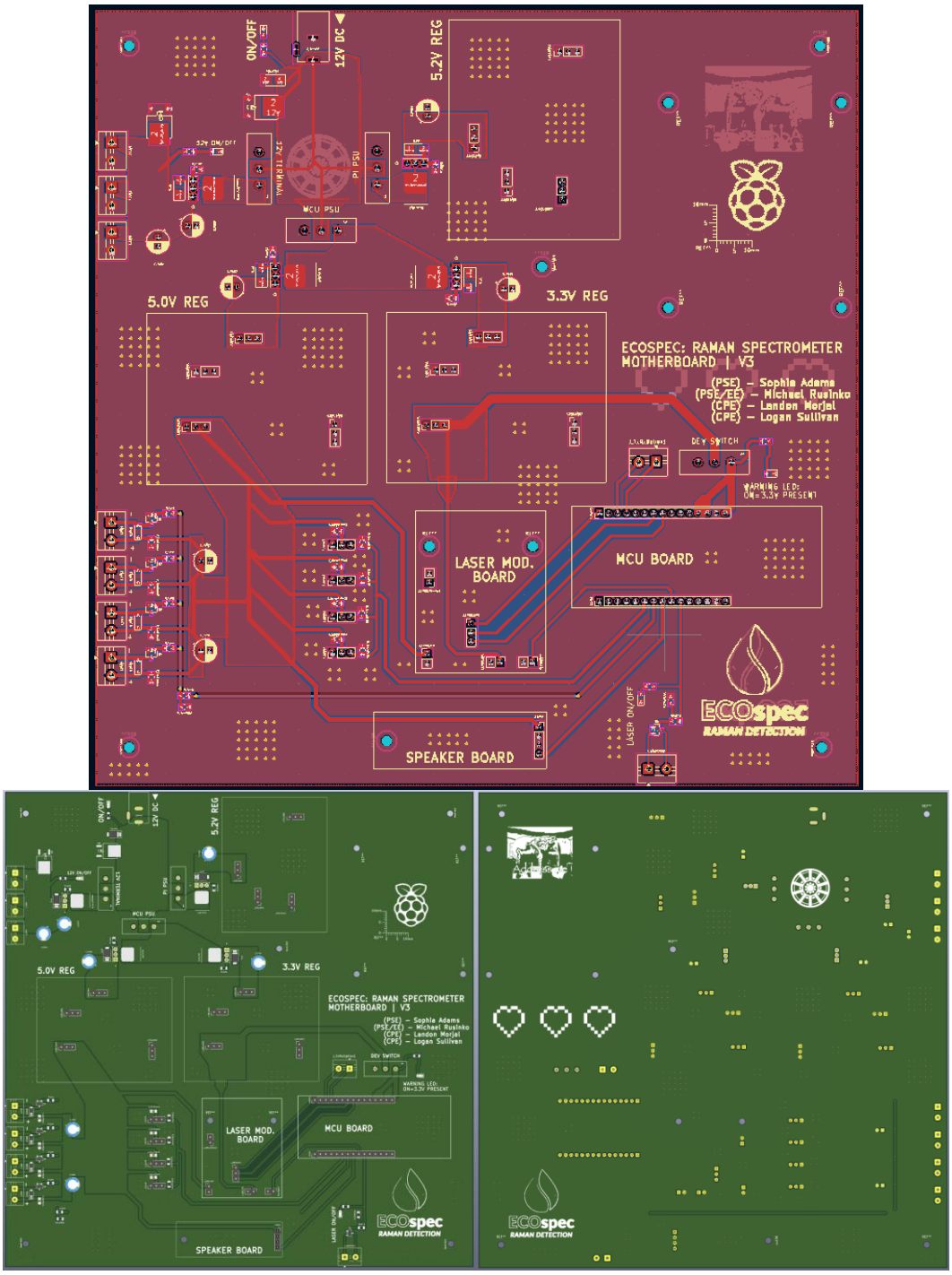

Figure 45 Motherboard Layout

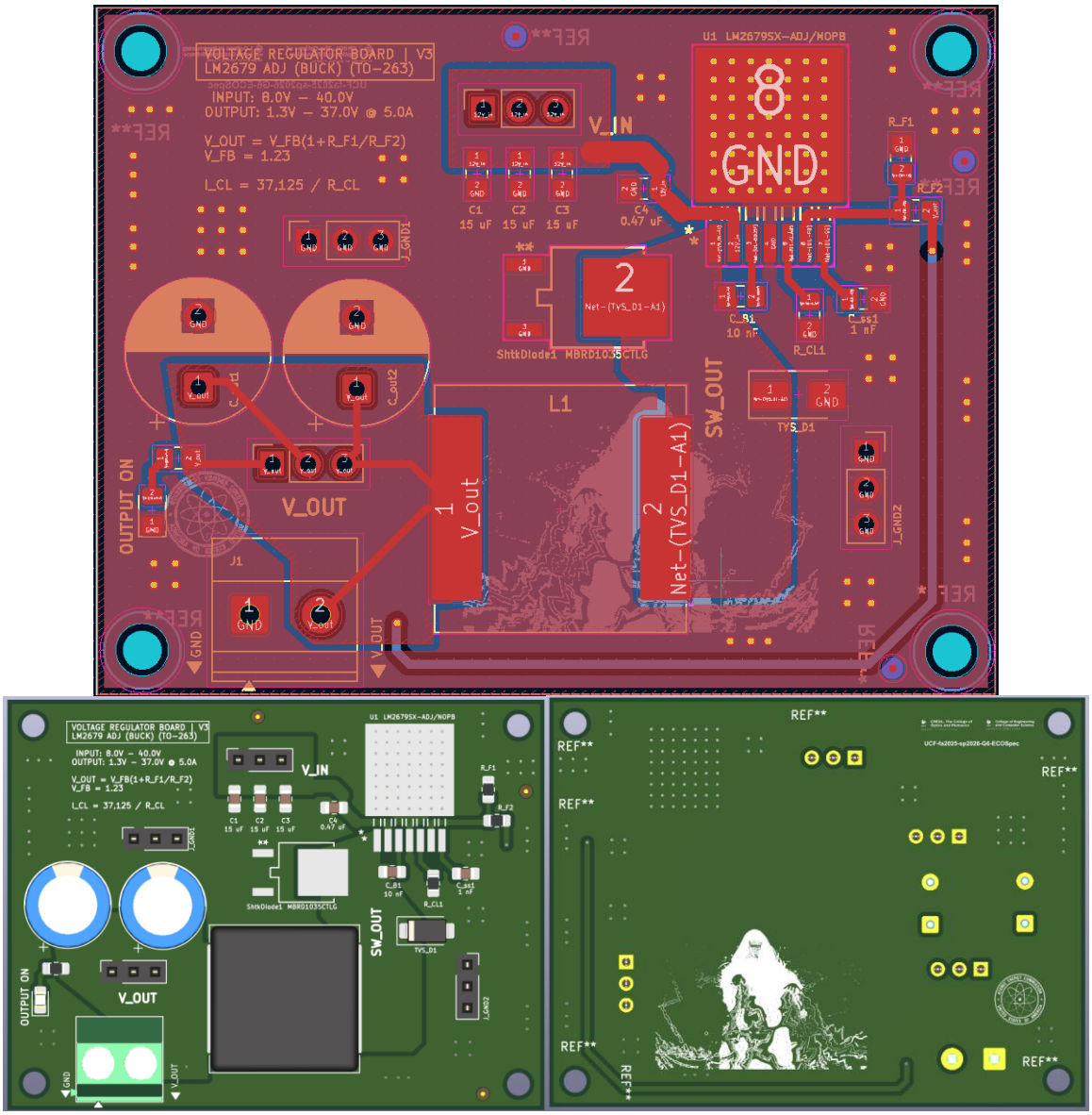

Figure 46 Regulator Board Layout

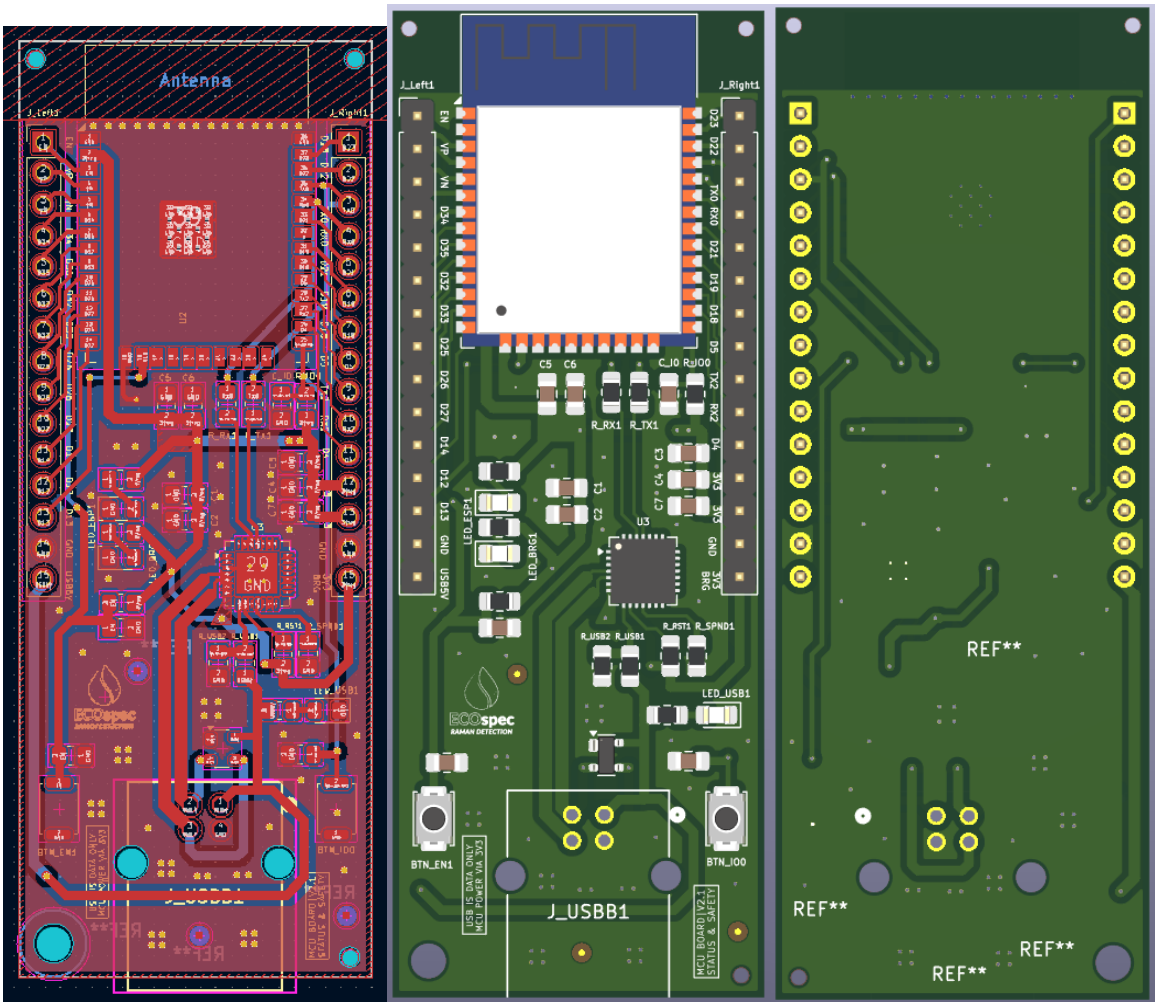

Figure 47 MCU Board Layout

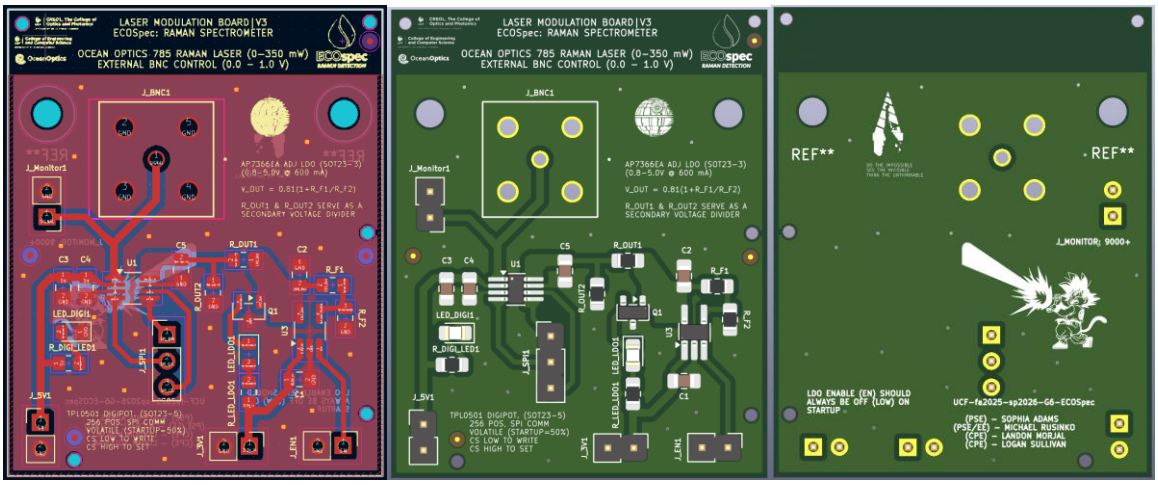

Figure 48 Laser Modulation Board Layout

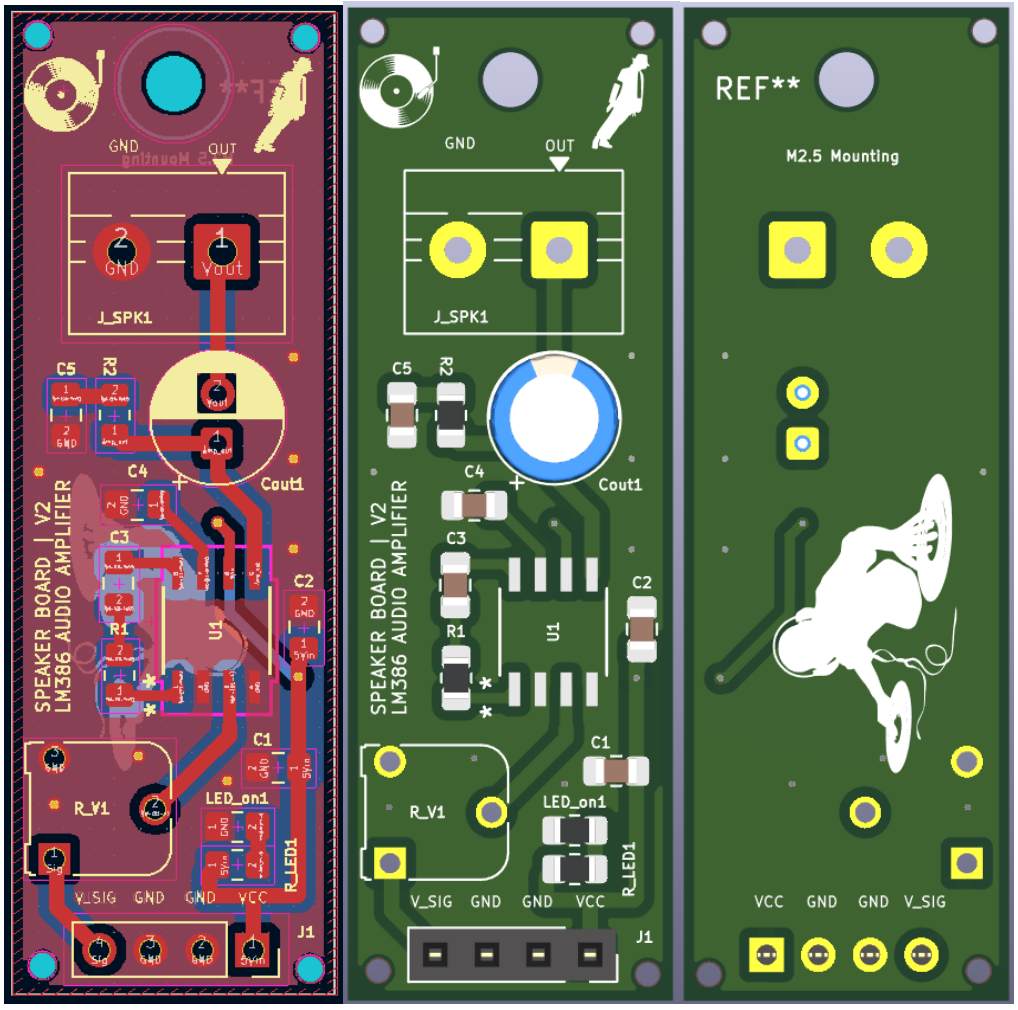

Figure 49 Speaker Board Layout

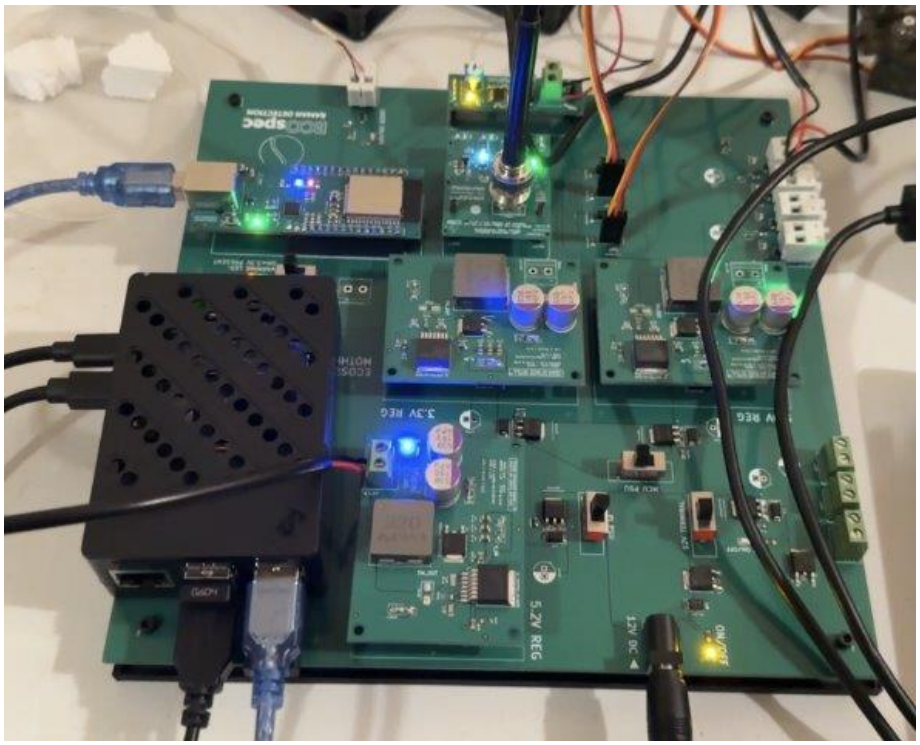

Figure 50 Fabricated and Powered PCBs

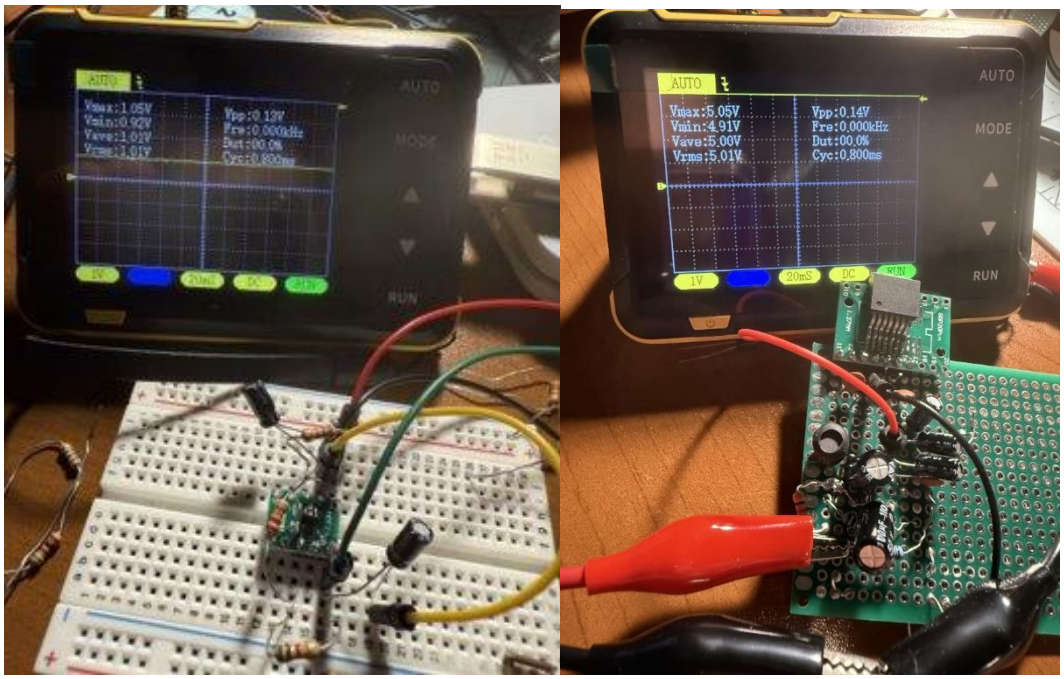

Figure 51 Voltage Regulator Testing

8.2. Probe Optics

The probe optics subsystem delivers the 785 nm excitation beam to the sample and routes the Raman-shifted return light into the collection path. The entire assembly is built on a Thorlabs 30 mm cage system, which replaced the earlier breadboard layout to provide a rigid, self-aligning mechanical reference for every component between the fiber input and the spectrometer entrance fiber. The cage architecture preserves a common optical axis across the excitation and collection legs, eliminates the per-component alignment drift that the earlier breadboard layout exhibited, and accommodates standardized SMA fiber mounts, filter holders, and lens tubes without custom machining.

Figure 52 785 nm Light Visible in Lossy Fiber

Excitation is sourced from the Ocean Optics LASER-785-LAB-ADJ-S, a multimode 785 nm diode laser with a narrow 0.2 nm linewidth, dedicated current and temperature control, and an SMA-coupled single-mode fiber output. The fiber terminates in an Ocean Optics collimating tip whose internal lens matches the numerical aperture of the fiber, producing a collimated free-space beam at the entrance of the cage system. Single-mode delivery and beam-quality preservation are critical here, because any divergence introduced upstream of the objective propagates directly into a degraded focal spot at the sample, which would reduce both Raman signal generation and the system's ability to discriminate small microplastic particles within the cuvette volume.

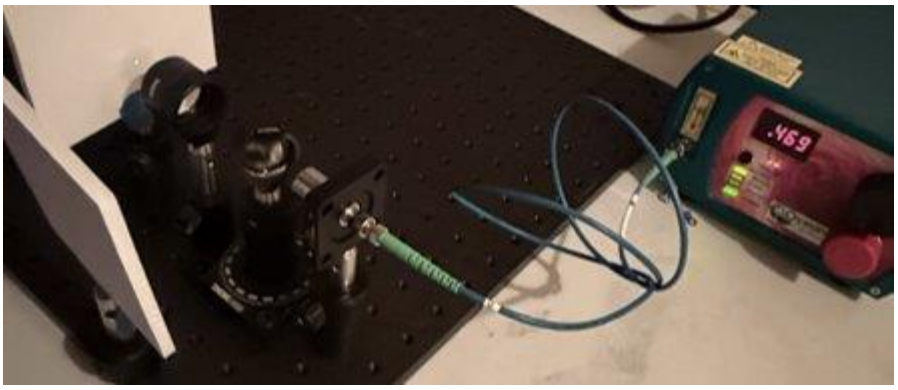

Figure 53 Beam Expander Demo

The original V2 design called for a 6x beam expander between the collimator and the dichroic, intended to fill approximately 80% of the rear aperture of the larger objectives that were under consideration at that stage, specifically the Olympus and Newport M-10x units, both of which present a comparatively large rear aperture that benefits from an expanded input beam to achieve full NA utilization. The migration to the Nikon CF160 family changed this tradeoff. Both the 20x and 50x CF160-ELWD variants present a substantially smaller rear aperture than the Olympus or Newport candidates, and the unexpanded collimated beam from the Ocean Optics tip already approximates an appropriate fill at the new pupil. The beam expander was therefore removed from the build, simplifying the optical path, reducing the part count and the cumulative Fresnel and absorption losses associated with two additional AR-coated achromats, and shortening the cage system overall. The choice of objective within the Nikon family then becomes a tradeoff between focal-spot size and depth of focus rather than rear-aperture fill: the 50x produces an approximately 1 micron diffraction-limited spot at the sample, while the 20x produces an approximately 2.5 micron spot with a correspondingly larger depth of focus, which is more forgiving of cuvette positioning errors and gives a higher probability of intersecting a polymer particle within the focal volume of an aqueous microplastic sample.

Following the collimating tip, the beam passes through a polarization-conditioning stack consisting of a linear polarizer, a 785 nm notch filter, and a quarter-wave plate. The polarizer and quarter-wave plate together act as an optical isolator. Linearly polarized light is converted to circular polarization on the forward path, and any specular back-reflection from the dichroic, the objective, or the cuvette walls returns through the quarter-wave plate as the orthogonal linear polarization, which is then rejected by the polarizer rather than allowed to propagate back into the laser fiber. The 785 nm notch filter in this same stack performs the function that a dedicated laser-line clean-up bandpass would otherwise serve, suppressing the broadband ASE pedestal and the silica fiber Raman background generated within the delivery fiber that would otherwise appear as a structured ghost spectrum near 813 nm in the detection band.

The conditioned beam is then incident on a 785 nm short-pass dichroic mirror oriented at 45 degrees. The dichroic reflects the excitation wavelength toward the objective and transmits Raman-shifted Stokes light above the edge wavelength toward the collection optics, establishing the standard epi-illumination geometry in which excitation and

collection share the same objective. Reflection of the laser into the objective is then focused onto the sample by the 20x Nikon CF160-ELWD infinity-corrected microscope objective. The infinity-corrected design is essential to the architecture, because it places the dichroic and any downstream filters in a collimated beam path between the objective and the tube lens, where flat optics introduce minimal chromatic and spherical aberration regardless of their thickness or insertion order.

The sample is held in a quartz cuvette mounted in a custom 3D-printed sample holder that locates the cuvette at the focal plane of the objective. Quartz is selected for its very weak intrinsic Raman response, ensuring that the dominant signal originates from the polymer particles in the aqueous sample rather than the cuvette walls. The 3D-printed holder is designed to provide repeatable kinematic seating so that the cuvette can be exchanged between measurements without disturbing the alignment between the sample volume and the objective focus, preserving the geometric throughput of the system across runs.

Backscattered Raman light returns through the objective, recollimates in the infinite-conjugate space, and propagates back to the dichroic, where Stokes-shifted wavelengths above the dichroic edge transmit through toward the collection arm. Immediately downstream of the dichroic, a long-pass filter further attenuates any residual 785 nm laser light that leaked through the dichroic edge, providing the additional optical density needed to prevent Rayleigh scatter from saturating the detector or masking low-wavenumber Raman peaks. The filtered Raman beam is then focused by an AR-coated achromatic doublet, which substitutes for the Nikon tube lens at roughly an order of magnitude lower cost while retaining adequate aberration correction across the 800 to 1020 nm band of interest.

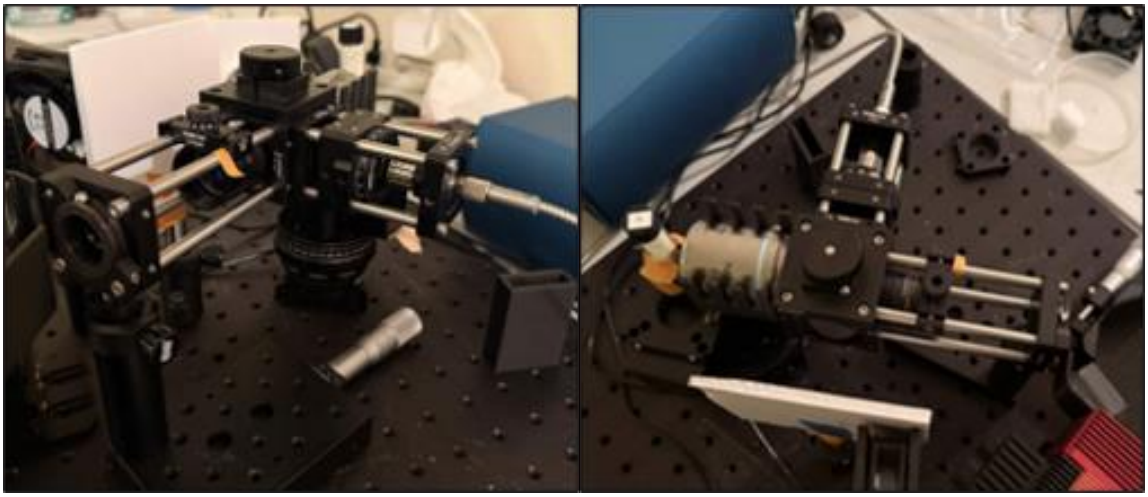

Figure 54 Final Probe Optics

The original architecture focused this achromat directly onto the entrance slit of the Czerny-Turner spectrometer. During integration testing, this configuration produced unacceptable power loss at the slit plane. Alignment tolerances between the freely-mounted achromat focus and the fixed slit were tight enough that small mechanical disturbances translated into large throughput swings, and a significant fraction of the focused cone fell

outside the slit aperture. To resolve this, the achromat was redirected to focus the collected light into a multimode collection fiber, which then routes the signal directly to the spectrometer entrance. Fiber coupling at this interface decouples the probe optics from the spectrometer mechanically, allows the spectrometer to be aligned and maintained as an independent subassembly, and provides a stable, repeatable optical interface that survives the routine handling expected of a portable instrument. The achromat-to-fiber focus marks the terminus of the probe optics subsystem; downstream signal handling is described in the spectrometer section.

8.3. Spectrometer Prototype

Our spectrometer prototyping began on an optical breadboard, where the system has the capacity to be assembled, adjusted, and debugged in a flexible, open layout. The breadboard provides vibration dampening and a grid-like surface that allows for optical posts, post holders, and kinematic mounts to be positioned with high precision. The modular environment is ideal for performing alignment, evaluating component performance, and experimenting with different optical geometries before committing to a final compact enclosure. Our plan for spectrometer prototyping includes using a variable entrance slit that is mounted to a lens tube that contains a pin hole aperture, that is then attached to an SMA adapter. This SMA adapter enables our fiber-coupled halogen light source to be integrated into our spectrometer prototype for testing. Using the variable slit is effective in demonstrating how slit width affects spectral resolution, throughput, and signal-to-noise ratio. The ability to manually adjust the slit in real time is extremely useful during early system development.

The tungsten-halogen lamp, HL-2000 from Ocean Optics, was chosen due to its stability and smooth nature. Its extended visible spectra make it easy to visualize the grating performance, identify alignment errors, and check spectral dispersion on the detector end. It also helps to start with a visible light source, for alignment, rather than jumping right ahead to the Raman signal Its continuous spectrum makes it straightforward to gain details on our grating performance, verify that the dispersion is linear across the detector plane, and check for any aberration-driven distortions in the re-imaged line, such as chroma or astigmatism. Using a bright visible source during initial alignment is also more practical and safer than attempting to align directly with the weak Raman-scattered signal. The halogen source creates well-defined spectral features and uniform illumination that is recognizable, and that can help identify misalignments, focus errors, or incorrect mirror positioning long before the system is tested with the Raman excitation wavelength. In combination with the ACROS SWIR CQD detector and its GUI software—which allows live monitoring of intensity profiles, wavelength registration, and noise characteristics—the breadboard prototype provides a controlled and highly adaptable platform to refine the optical design.

Figure 55 Spectrometer Prototype V1

.

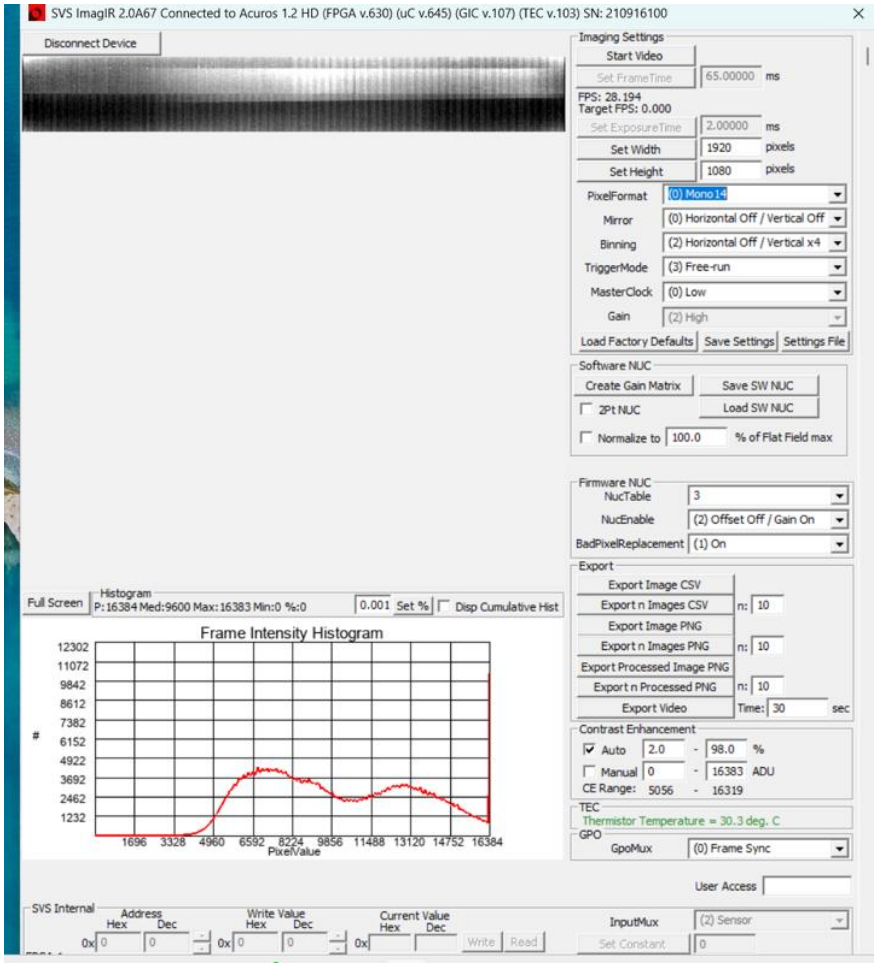

Figure 56 ACUROS software showcasing broadband spectra.

Specifically, we constructed our prototype using a mechanical slit from Thorlabs (VA100CP), our gold-coated collimating mirror from Torrent, the matching gold focusing mirror from Torrent, our 830 grooves/mm diffraction grating, and our ACROS SWIR CQD detector. Aligning these components on the breadboard required a process of positioning, fine adjustment, and continuous feedback from the detector GUI, specifically the intensity histogram and the image of the intensities on the camera detector The slit assembly was first aligned so that the fiber-coupled halogen source illuminated the pinhole and variable slit uniformly. Ensuring that the beam emerging from the slit was centered and traveling level relative to the breadboard surface was needed before introducing any powered optics. The collimating mirror was then positioned at its nominal focal distance from the slit, approximately 101.6 mm, using a combination of translation and rotation stages, along with tube mounts and les mounts to hold the mirror stable while still allowing for small x and y adjustments, along with height. Achieving a clean, well-collimated beam required gradually refining the mirror angle while observing the beam footprint on a temporary viewing card placed at multiple distances. Once collimation was established, the beam was directed onto the diffraction grating. The grating alignment involved carefully adjusting its rotation to place the first-order diffracted beam onto the expected optical axis and ensuring that the beam illuminated the correct region of the grating surface.

After diffraction, the focusing mirror was aligned by walking the beam onto the detector plane. This step typically required micrometer-level tweaks: small angular adjustments of the focusing mirror, lateral shifts to recenter the dispersed spectrum, and height adjustments to minimize astigmatism or vertical skew. Throughout the alignment process, the ACROS detector GUI was enquired. Real-time readout from the camera enabled me to watch the spectral line shape change has I adjusted components.

Even coarse alignment steps—such as roughly steering the beam between components—were followed by fine corrections, since each mirror's curvature and off-axis positioning directly influenced the final spot size and spectral uniformity. The prototype therefore evolved through repeated cycles of optical tuning, detector feedback, and mechanical adjustment. There is lots more to be done as we continue into Senior Design 2, but with this prototype spectrometer I was able to get a halogen spectrum that is like what would be expected (Fig. 45) with no post processing, or dark correction at all, so it only does not look as neat.

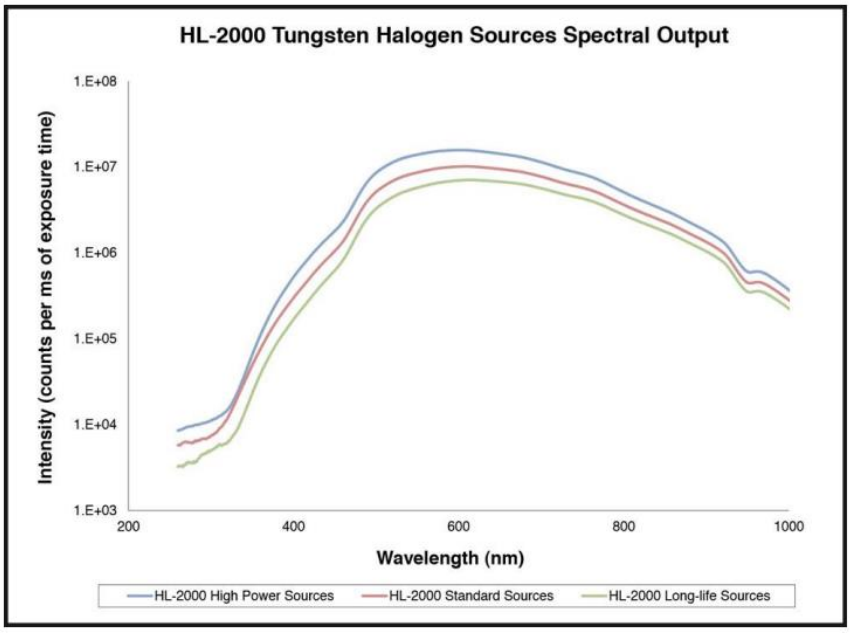

Figure 57 Ocean Optics HL-2000, Tungsten-Halogen Light Source

Our second iteration of our spectrometer included a 3D modeled housing for the grating, mirrors, and slit. After modeling the system on ZEMAX, we decided to switch to a crossed Czerny-turner spectrometer design, in comparison to a standard Czerny-turner layout. Both are compact, but the crossed version results in a massive stray light reduction, which provides useful for our low signal application of Raman spectroscopy. A new housing was modeled to hold the collimating mirror in the same spot and puts the grating on a small rotation stage. A flat edge was included to line the detector up with, and where the slit should be, and the focusing mirror, a notch in the housing was left. The goal of these notches is to make room for the slit and focusing mirror to be mounted on translation stages and left as variable components for better alignment. The detector, and entire housing were both placed on translation stages as well.

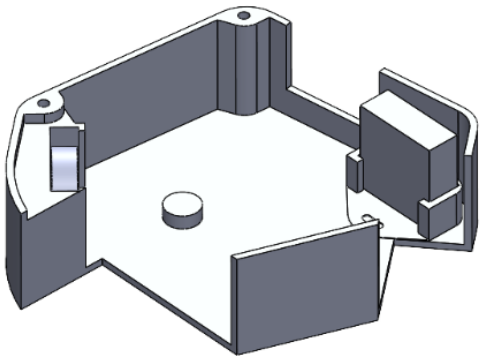

Figure 58 Final Spectrometer housing design.

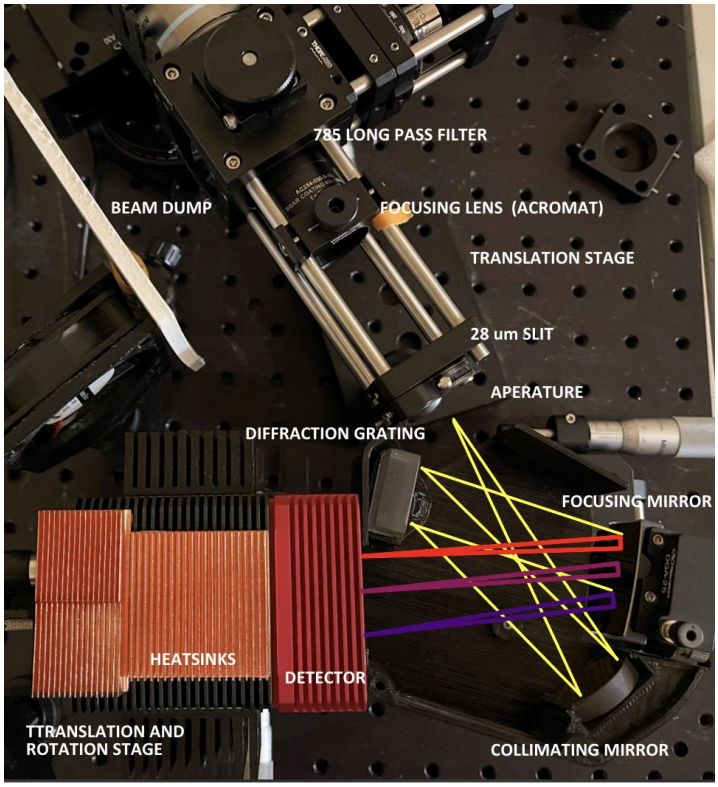

Figure 59 Final Collection Optics.

9. System Testing and Evaluation

9.1. Hardware and Software Testing

9.1.1. Control Systems

In an application such as ECOSpec, which carries with it numerous subsystems required to work together effectively and efficiently, a robust control system is paramount to achieve our goals. The areas of control required can be simply grouped into two sections, safety and acquisition. The safety systems of ECOSpec, such as the laser interlock, allow us to maintain strict operation parameters that ensure consistent and safe usage of the device. With this in mind, we can conclude that the best method of evaluation of these systems is the ability to maintain constant operation of the device with minimal downtime, and no safety incidents while in operation. To test these goals, especially outside of the completed device, we can employ many tools at our disposal from our control MCU, the ESP32. As many of our systems controlled by the ESP32 are handled through GPIO interfaces, we can create simple test scenarios by utilizing LED and numerous input devices to simulate operation of our control systems. With this setup, we can easily and more importantly safely ensure all control systems function as intended without risk for the user or performance of the system.

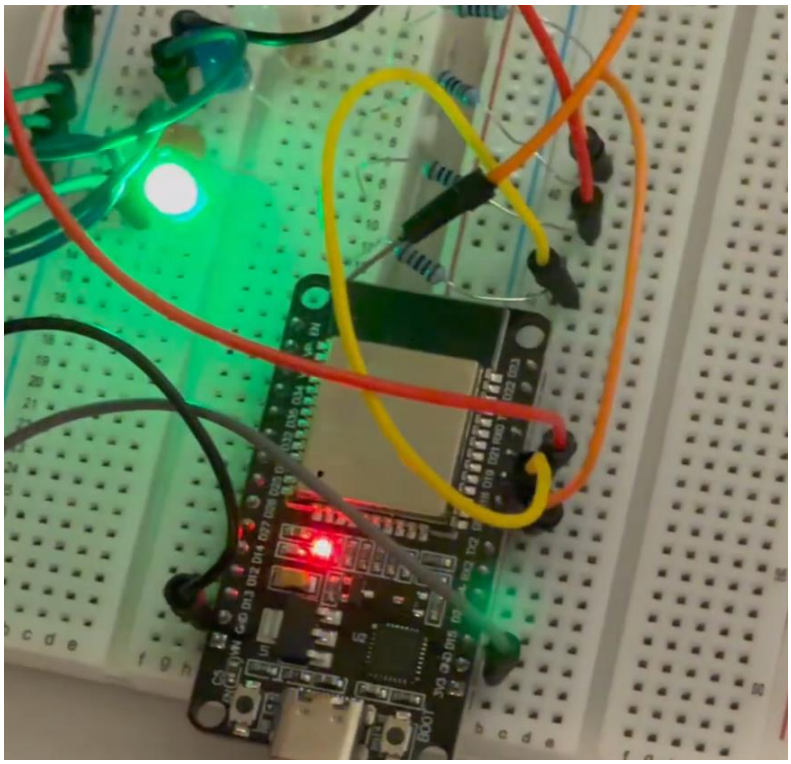

Figure 60 ESP32 GPIO Test Suite

For any control components handled by the control MCU, we once again share a similar goal of safe and consistent operation of the device. In contrast to this however, as the above-mentioned test method focuses entirely on the MCU's ability to interface with external devices, we also must consider testing all control components. To do this, we can utilize the integrated power and data connectors featured on many of the devices used. For those without plug-and-play functionality, a DC power supply can be used to provide appropriate power delivery. With power handled, devices can be tested based on their input and output specifications. For example, to test the DC trigger for the laser, a small pulse can be deployed from a function generator. Verification of all components allows us to provide the safe and consistent execution every time.

```
Hello World
          I (1279282) UART_LED: Sent message: Hello World

Hello World
          I (1280282) UART_LED: Sent message: Hello World

Hello World
          I (1281282) UART_LED: Sent message: Hello World

Hello World
          I (1282282) UART_LED: Sent message: Hello World

Hello World
          I (1283282) UART_LED: Sent message: Hello World

Hello World
          I (1284282) UART_LED: Sent message: Hello World

Hello World
          I (1285282) UART_LED: Sent message: Hello World
```

Figure 61 ESP32 to Raspberry PI UART vis USB Test Suite

9.1.2. Data Handling

Unlike the control systems of ECOSpec, the data pipeline is something that operates behind the scenes, and therefore has less direct effect on the user, besides the usage of the data itself. A metric of feasibility can be difficult to find. The easiest way to determine the quality of the data pipeline is to ensure the data that is output is high quality and usable by any downstream applications. With a metric on how to ensure data is handled established, selection of a test method is simple. For testing of ECOSpec, we elected to utilize pre-prepared samples of Raman spectra and compare these to our processed spectra. With these comparisons, we can make sure our data is handled in a way that is standard for usage in further applications, such as spectral comparison or storage.

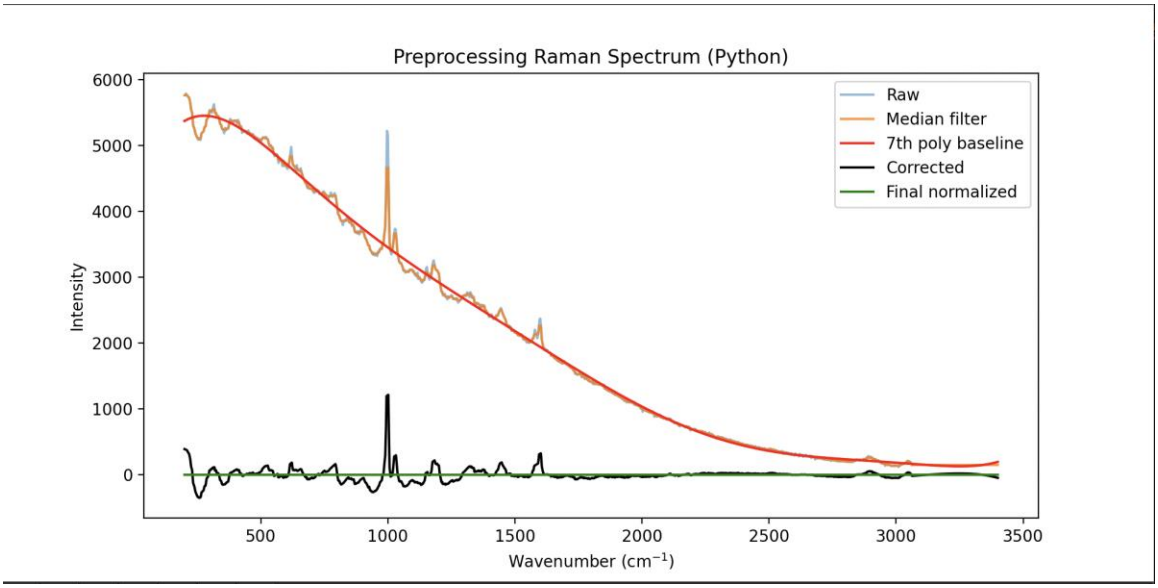

Figure 62 Data Processing Pipeline Performed on a Polystyrene Raman Sample

9.2. Optoelectronics Feasibility Study and Testing

9.2.1. Excitation Source

Raman spectroscopy can be performed with a variety of different wavelengths. The optimal wavelength for detection is material and media dependent. All Raman excitation sources, however, must have narrow linewidths. This is for a variety of reasons: A narrow linewidth reduces fluorescence, narrows the width of the Raman peaks, and increases the spectral resolution of the spectroscopic system. The laser excitation source must be selected with consideration for all these factors, especially in the delicate systems involving Raman spectroscopy.

When taking wavelength into consideration, a balance between Raman peak intensity and fluorescence must be taken into account. The shorter the wavelength, the larger the intensity of the Raman scattered light, as seen in Equation _. However, due to the higher energy in each discrete photon, shorter wavelength light tends to produce larger amounts

of broadband fluorescence. If other contaminants are present in the sample under test, their fluorescent spectra may overpower the target Raman signal. The media which a certain target material is present in may also play a role. Water produces a large fluorescence when illuminated with 532 nm light, so longer wavelengths (IR) are preferred for such purposes. The container in which the sample is illuminated also plays a role. For our purposes, we are using a quartz cuvette, which has a weak Raman response and is common for Raman microscopy and microscopy applications.

This is not to say 532 nm cannot be used for analysis of microplastics in aqueous solutions, as several systems have demonstrated such a feat. (Jung et al., 2024; Luc, 2019) However, with our intention of detecting smaller particles in an aqueous solution, we want to minimize as much fluorescence as possible. An excitation source in the IR, such as a 785 nm or 1064 nm laser, would enable such a response.

Excitation wavelength is largely application dependent. 532 nm light is commonly used for analysis of metals and inorganics. 785 nm is often used for analysis of biological and polymer samples. 1064 nm is best for measurement of samples that have a high fluorescent response, or for more penetrative analysis. (Tuschel, 2016) 532 nm light produces the highest fluorescence but has the strongest Raman peak intensity. 785 significantly reduces fluorescence compared to 532 while maintaining a strong Raman peak intensity. 1064 nm light almost completely negates fluorescence, but the Raman peak intensity is very weak. 1064 nm Raman analysis is typically only viable when a detector with high quantum efficiency in IR, such as InGaAs arrays.

The Ocean Optics LASER-785-IP-ADJ-S is a SMA-coupled 785 nm diode laser source designed for Raman applications. It is a multimode laser that boasts a spectral linewidth of ~0.2 nm. (Ocean Optics, 2009)

However, detection of an IR signal is significantly more challenging than that of a VIS signal. The materials used for traditional CMOS cameras tend to significantly drop off above 800 nm, and CCD sensors are much harder to interface with than CMOS cameras.

9.2.2. Detector

CCDs are a common choice in Raman applications. They offer quantum efficiencies above 50% in the IR region, fast global shutter speeds, and are often sold as line sensors for spectroscopic purposes. They often come with detector heads and controllers which allow precise control of the charge to collect and dump cycles within the CCD.

Scientific CMOS sensors are also popular choices. They have high quantum efficiencies, complex noise reduction circuits, high resolution low-signal amplification circuits, and are easy to interface with. They are common for Raman microscopy, where images of the stokes shifted light provide spatial Raman data. Furthermore, the CMOS camera can easily bin together vertical pixels of the detected spectra to improve SNR. However, their responsivity in the IR region is not as strong as CCDs. They are typically used for 532 nm excitation setups.

Colloidal quantum dot (CQD) short wave infrared (SWIR) detectors are another option. These style of detectors offer a mix between CCD sensitivity and CMOS camera usability. CQD SWIR cameras often use a CMOS style interface to collect information from individual pixels on the sensor, thus allowing CMOS acquisition techniques such as pixel binning. They differ in the fact that instead of the pixels on the sensors being precision fabricated PN junctions, they are (typically film deposited) quantum dots. Not only do they offer higher quantum efficiencies in the IR, they also enable a higher pixel density to be achieved. (onsemi, 2019)

Regardless of the detector's choice, due to the sensitive nature of the detection scheme, cooling of the sensor is a must. Many CCD, CMOS, and SWIR sensors also offer camera modules or detector heads that are prepackaged with TECs. These TECs often come in a stage-1 or stage-2 option, capable of reaching – 15 C and –30 C respectively. Some papers suggest the benefit of cooling below –10 C becomes heavily diminished, especially at shorter integration times (<100 ms). [paper with TEC and SNR graph]

Figure 63 Data Processing Pipeline Performed on a Polystyrene Raman Sample

These modules are very expensive pieces of equipment. And for good reason, they are carefully assembled pieces of technology with high precision electrical and mechanical design. As ECOSpec is a senior design project, the budget for components is limited.

9.2.3. Spectrometer Alingment

The building and aligning of the prototype that the testing was done with is described in chapter 8, but multiple iterations of alignment, and camera images were taken to begin the spectrometer build process. Throughout testing, incremental adjustments to mirror angles, grating orientation, slit position, and detector placement are made to optimize spot shape, minimize aberrations, and ensure consistent, repeatable spectral performance. This iterative process confirms that the optical design functions as expected and provides a

baseline for future refinements. The spectrometer prototype was tested with a Tungsten-Halogen light source, and an indium-gallium white LED flashlight.

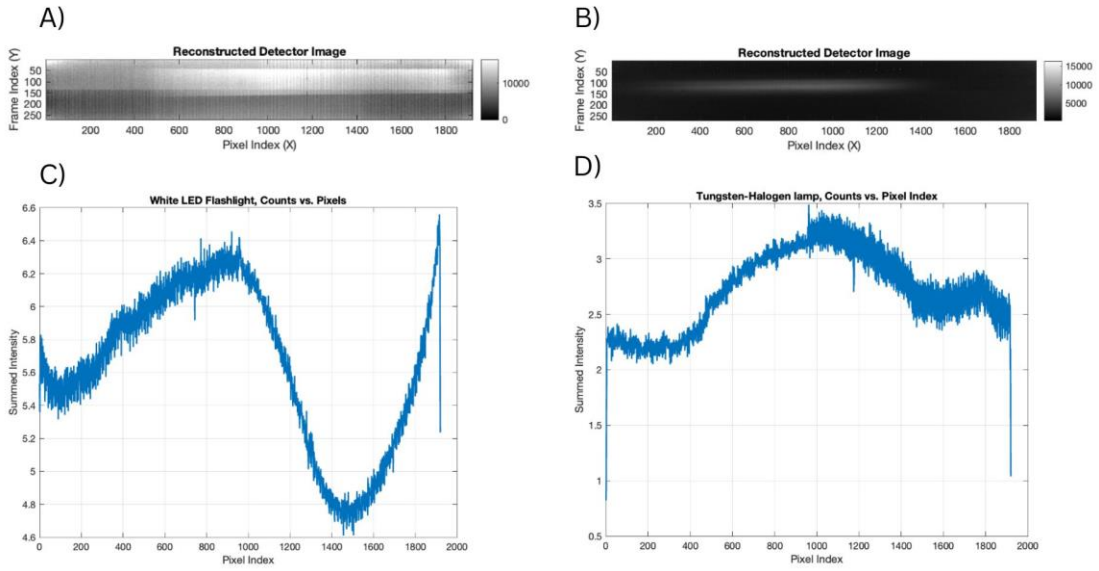

Figure 64 Prototype Spectrometer Testing with White Light Sources.

A and B describe the reconstructed image of what is captured by the ACROS camera, and A and C are the captured spectra with the white LED flashlight, and B and D are captured with the Tungsten-halogen light source. Both C and D are not dark corrected or processed, this is raw data.

The reconstructed detector images in A and B from Figure 49 reveal the spatial distribution of light intensity across the ACROS camera sensor. A shows the white LED flashlight illumination pattern after passing through the spectrometer, and B displays the tungsten-halogen lamp response. In both A and B, it is clear in the image that the light is being dispersed consistently across the spectral axis. But there is some blurring at the edges of the detector field, which could be problematic, and needs to be characterized.

C and D present the raw, uncorrected spectral data extracted from the detector images. The white LED flashlight spectrum demonstrates a characteristic broad emission peak around pixel 800, with a second sharp peak near pixel 1800. This dual peak structure is typical for indium-gallium white LEDs, where the primary peak is from the blue LED emission. The sharp dip around pixel 1400 could possibly represent a spectral gap in the LED's emission spectrum. In comparison, D illustrates a smoother, more continuous distribution, which is characteristic feature of that type of lamp. The broad peak extends from pixel 400 to 1400, with a maximum at around 1000. The spectral shape follows a thermal emission profile, with intensity gradually decreasing towards longer wavelengths. The higher noise level could possibly be attributed to the overall intensity of the tungsten-halogen lamp being lower compared to the LED, and the longer integration times. Longer integration times typically result in more noise being captured. Therefore, the difference between the signal-

to-noise ratio between the two sources can be attributed to both the inherent brightness of the LED and its more concentrated spectral output. Additionally, in B, there is horizontal striping visible in the reconstructed detector images. This could possibly suggest some spatial non-uniformity in the optical path. This could occur because of grating alignment or slit positioning, but it is not known for sure until further experimentation can occur.

After broadband light was shown to pass through the spectrometer, the rainbow image of the visible light that shown onto the detector was aligned by grating rotation so that the edge of the red aligned with the right side of the detector- to make sure that the laser light will disperse to the right side of the detector. Next, the 785 nm laser light source was sent through the system, to gain an understanding of where the wavelength dispersion would start across the detector, and how it will align with our goal wavelength range of 785 – 1100 nm. An image was collected of the 785 nm slit location. The fine alignment was also adjusted until the slit image came into focus. Following the 785, a 980 nm laser diode was sent through the system. For alignment purposes, the 980 nm source was aligned to be slightly past the center of the detector, taken an image, and fine-tuned for the slit image. This not only sets the spectrometer up for wavelength calibration, by noting the laser wavelength and pixel location, but also proves that the detector is sensitive enough in the NIR.

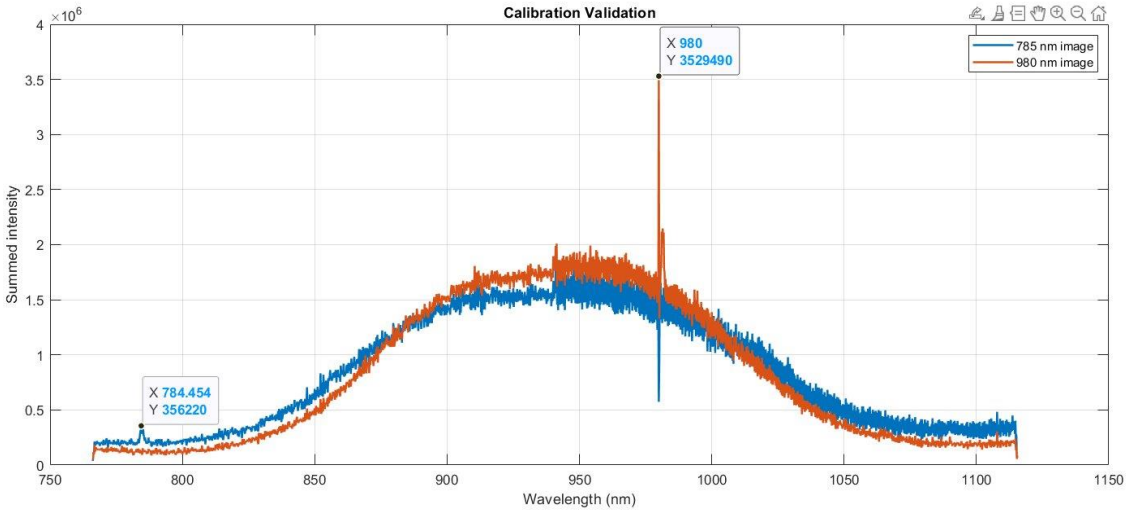

Figure 65 785 nm and 980 nm peak location across the detector.

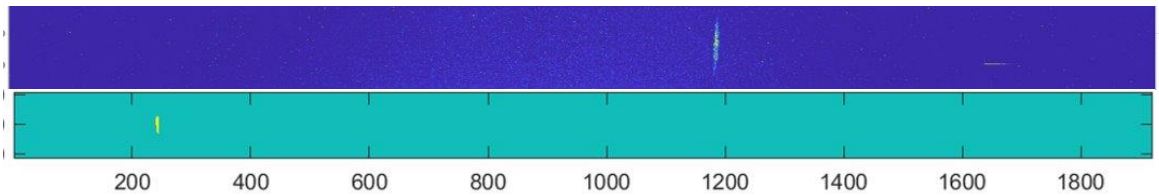

Figure 66 The top image is 980 nm, bottom is 785 nm slit image onto the detector.

This calibration produced an experimental wavelength range of 766–1115.462 nm, compared to the target range of 785–1050 nm. While the calibrated range extends beyond

the intended limits, this does not negatively impact the measurement. In fact, the broader coverage ensures that all relevant spectral features are captured.

For Raman analysis, the more meaningful metric is the shift in wavenumber, defined relative to the excitation source (785 nm). Converting the calibrated wavelength range to wavenumber confirms that the system comfortably spans the region required to detect the Raman peaks of interest. Therefore, despite the discrepancy in absolute wavelength bounds, the calibration is sufficient and appropriate for the intended measurements.

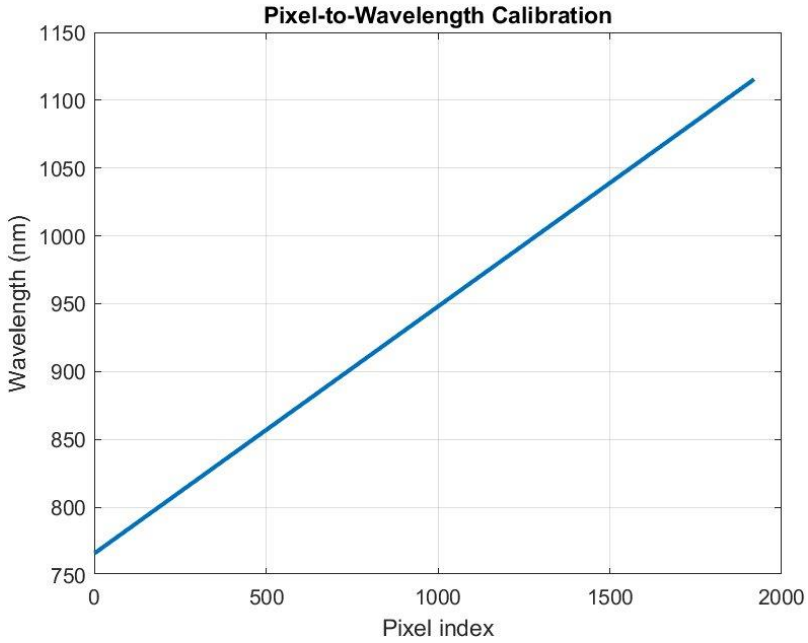

Figure 67 Calibration Curve.

To further prove the alignment of the spectrometer, and confirm the dispersion of light, NIST standard light sources, Ag, and Hg, were used to align and determine the resolution of the spectrometer. The known NIST standard lines of Hg, starting at 766 nm, can be seen in the graph below.

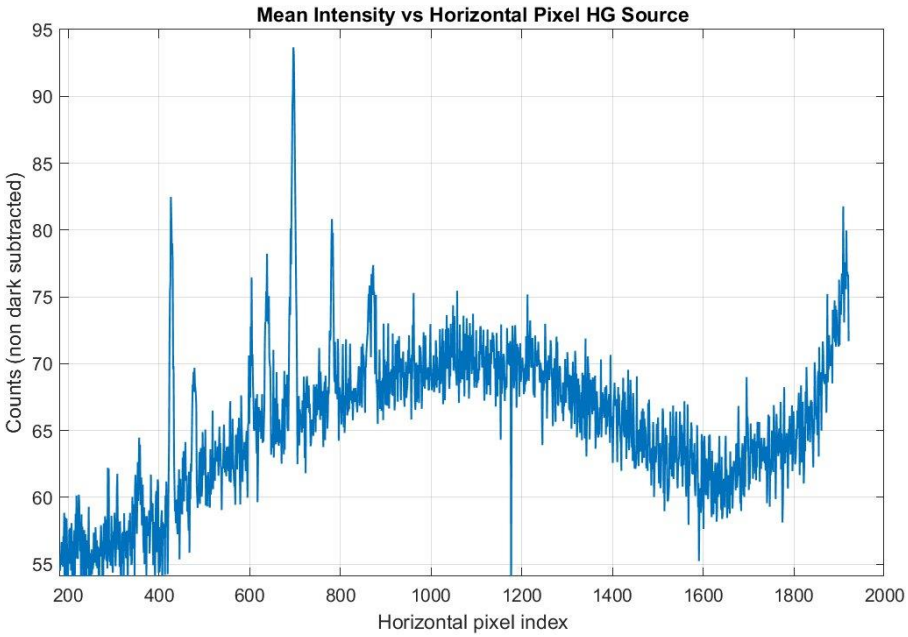

Figure 68 Hg NIST standard lines across spectrometer.

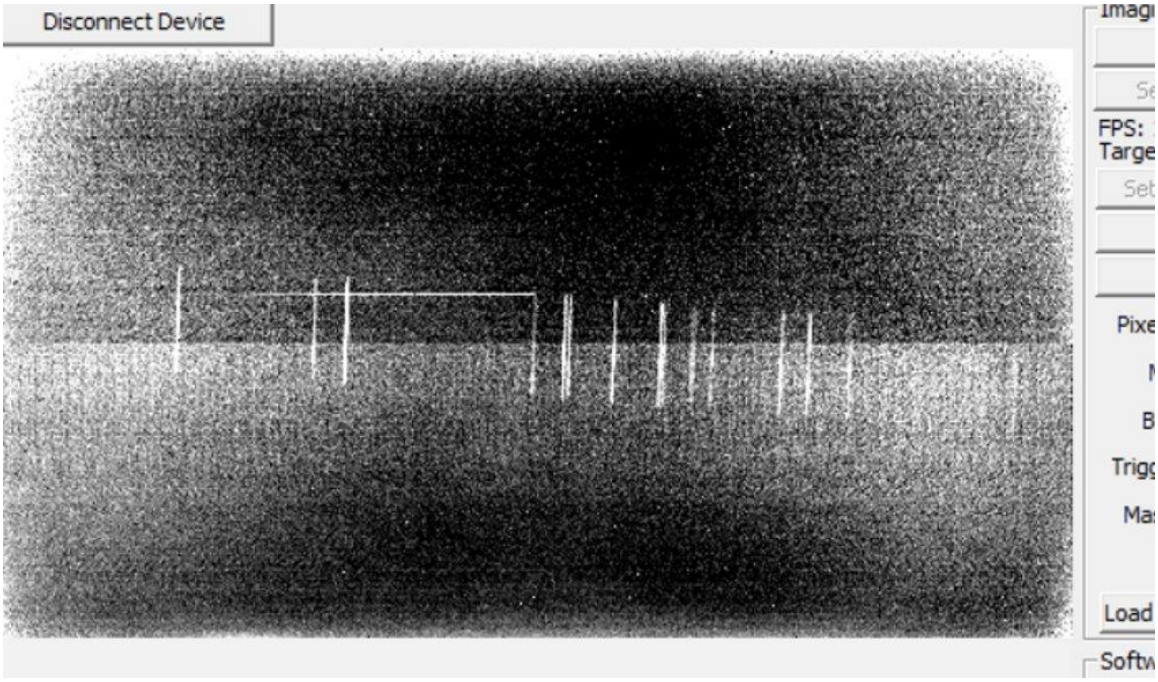

Figure 69 Slit image on detector of Argon NIST spectral lines.

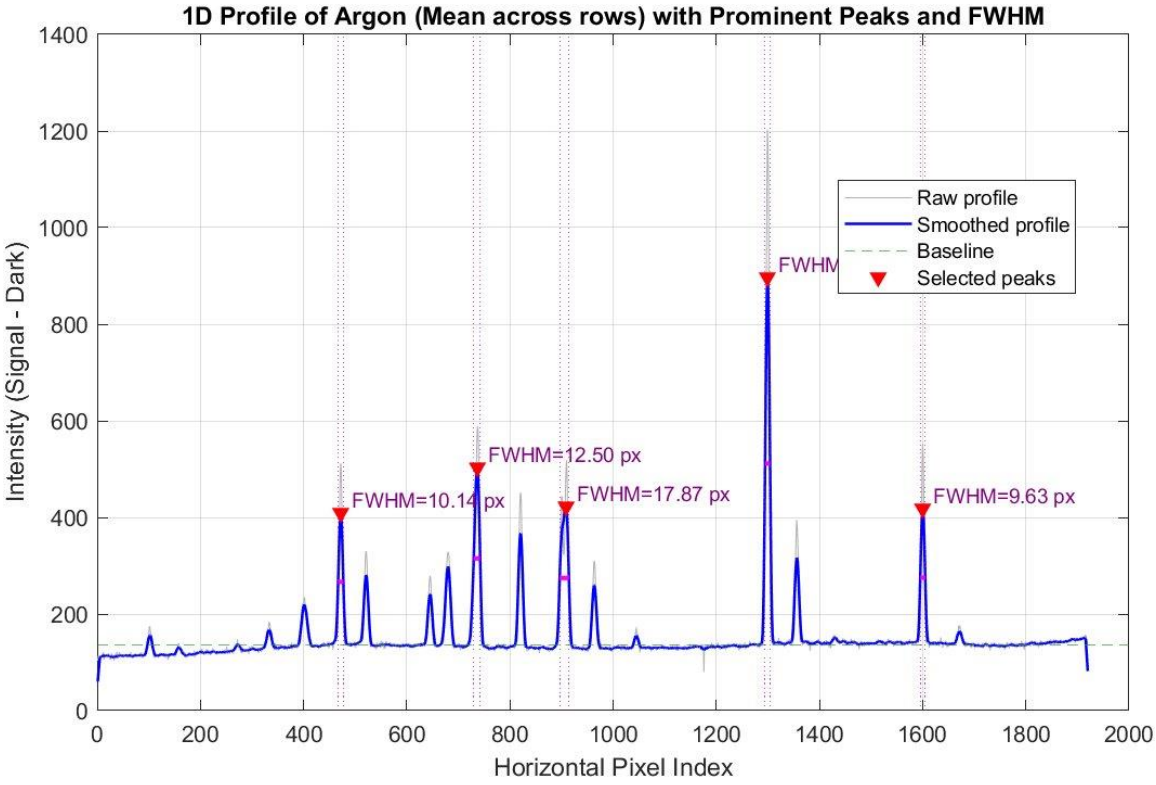

Figure 70 Resolution testing with Argon.

In terms of resolution, after multiple tests with many sources, an average FWHM of 15 pixels was found. An example would be at 980 nm, the average resolution was 9.8 pixels, which equates to 1.49 nm, and a FWHM of 15 wavenumbers.

9.2.4. Preemptive Testing

Prior to designing the system, we tested the feasibility of obtaining Raman spectra of plastic samples with premade spectrometer systems. We used an Ocean Optics QE Pro spectrometer, the Ocean Optics LASER-785-IP-ADJ-S, an Ocean Optics Raman Probe, and the Ocean Optics spectrometer software. This can be seen in Figure 50 and Figure 51, displaying the Raman spectra of a clear water bottle and expanded polystyrene. This testing was performed while our group was streamlining our idea, as a way to make sure that the spectra from the plastics we choose would have a strong response at 785 nm. We were able to borrow all of the equipment listed above, the 785 nm laser, an Ocean Optics QEPro Raman spectrometer, and a Raman probe made for a 785 nm excitation source, along with the fibers needed to connect between the laser, the probe, and the probe back to the spectrometer. This preliminary testing was done before we collected proper chemical samples of our 3 plastics of choice, nylon, polystyrene, and polyethylene terephthalate, so we used our resources and chose plastics around us to perform our preliminary testing. We chose a piece of clear plastic water bottle, and a piece of Styrofoam, and as expected, the

plastic water bottle had a peak around 1600 wavenumbers, similar to polyethylene terephthalate, and the Styrofoam had a peak at around 1000 wavenumbers, similar to polystyrene. Our preliminary testing proved that not only do we obtain Ranan signal from different types of plastic, but we were also able to do it in a lab setting with minimal prep, and the signal at the fingerprint peaks for each plastic is strong, so that further supports our laser and plastic choice.

To ensure that using Raman spectroscopy for microplastic detection is truly a viable project for senior design, basic initial testing was conducted to determine the ease of the task with premade tools and plastic materials on hand. An Ocean Optics QEPro Raman Spectrometer, Ocean Optics Raman Probe, and 785 nm fiber laser was employed to obtain the Raman signal of various macro plastic samples. The Raman probe contains filtering to remove the laser signal and fluorescence. Raman shifted frequencies were able to be detected and plotted accordingly.

One scan was used with an integration time of 10 seconds. The integration time of a spectrometer is the amount of time the sensor is exposed to a light signal for data collection. The number of scans is the number of times that period of data collection is repeated. If multiple scans are taken, the multiple intensity values for each pixel are averaged together and then plotted. [Fig. 50 and 51]. Both images contain spectra that was both dark corrected and fluorescence corrected after obtaining the signal. This post-processing was performed in MATLAB using a 4^{th} polynomial fit, and a background dark subtraction from each pixel intensity. To further explain, a scan of the spectrometer was taken with no illumination light, to obtain the dark noise level, which is then subtracted from the raw Raman signal.

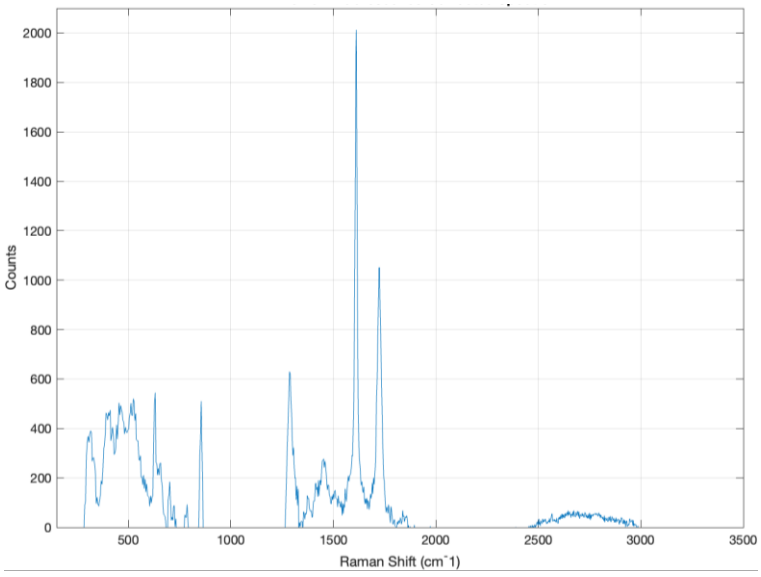

Figure 71 Collection Raman Spectra of Dasani Clear Water Bottle

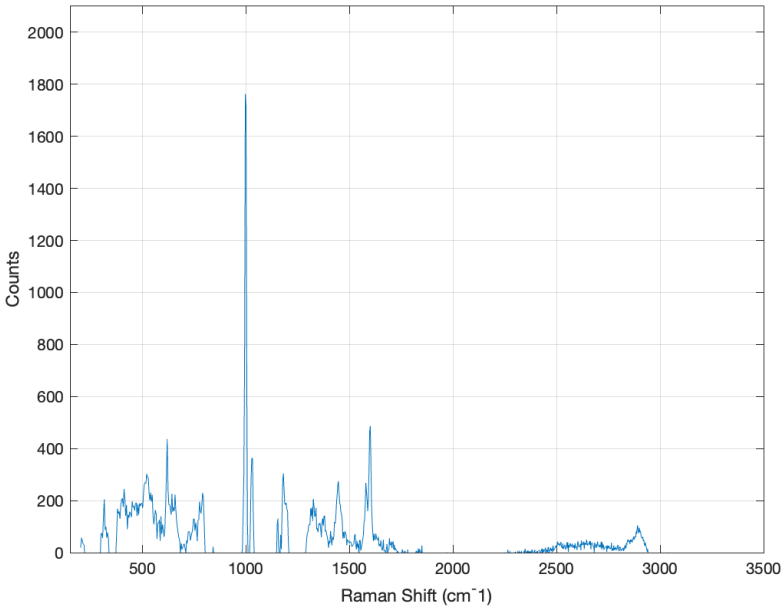

Figure 72 Collected Raman Spectra of Expanded Polystyrene (Styrofoam)

We also tested the quality of the response of the 785 nm laser on the ACUROS CQD SWIR and obtained promising results. To expand further, the ACUROS CQD detector had its highest efficiency in the visible wavelength range, so our team wanted to make sure that this detector would still be responsive at 785 nm. Previously, the ACROS CQD detector had previously showed excellent efficiency in the visible range and demonstrated high quantum efficiency and low noise characteristics based on its data sheets that made it an attractive choice for our application. However, our team wanted to ensure this detector would perform well at 785 nm. Our testing, Figure 52 revealed that the ACROS detector maintains good responsivity at 785 nm, but further testing should be done at alternate power levels from the 785 nm Ocean Optics laser.

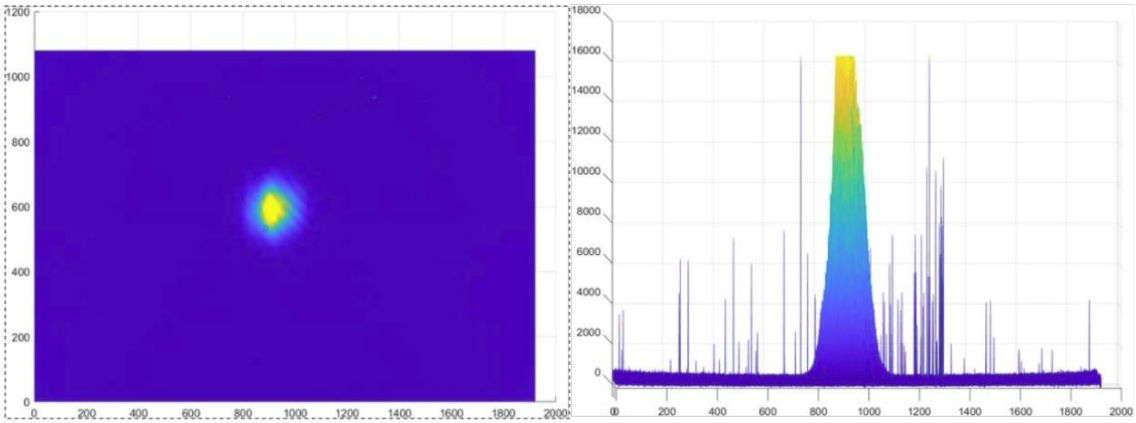

Figure 73 Testing 785 nm Laser Response on the CQD SWIR camera

We also tested the probe optics standalone with an Ocean Optics QEpro spectrometer. We verified its ability to collect Raman spectra with sulfur and polystyrene. Sulfur has a very strong Raman emission within 200 nm

10. Results

Due to lack of a Nikon tube lens, coupling loss between subsystems, low quantum efficiency of the detector, the TEC limit of the camera module set to +15 °C, and lack of adequate noise filters for the detector, we were unable to Raman spectra with the fully integrated optical system.

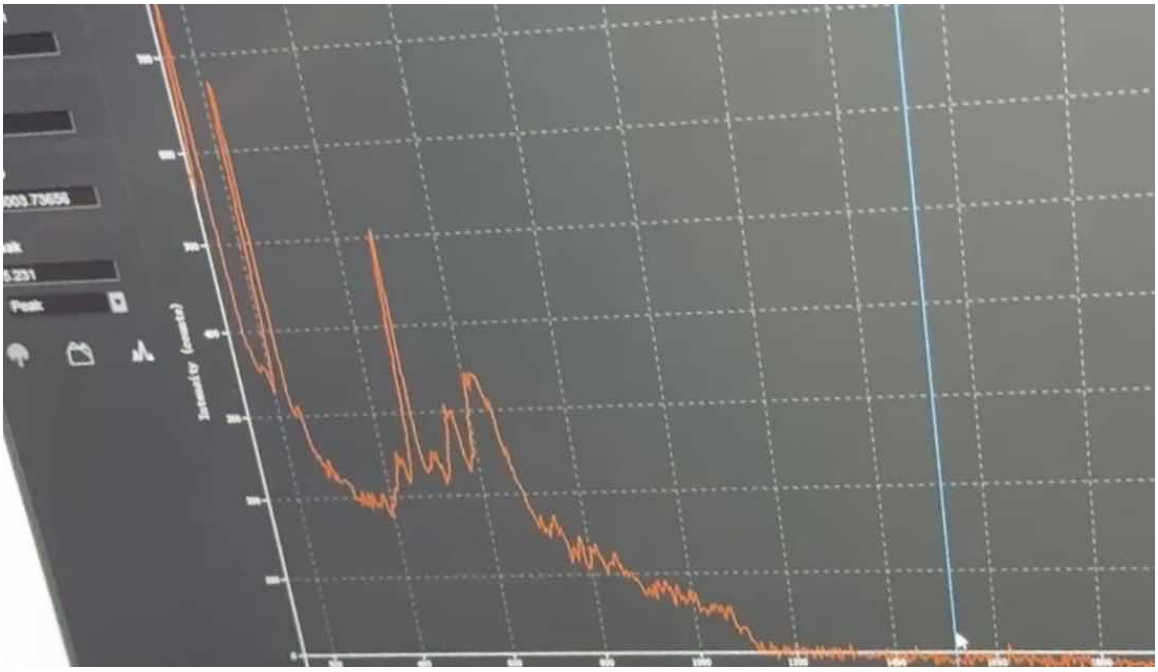

Figure 74 Raman Spectra of Sulfur Collected with QEPro

Electrically, the voltage regulators were able to supply current at max loads of 3 A and 5 A for over 10 minutes without problem. The laser modulation board, while slow, allowed for ultra precise control of power output from the laser. The digital potentiometer allows for a 256 positions, which correlates to 0.004 V steps, which 0.4% precision. The laser could be fully controlled externally through the ESP32 taking input from a touchscreen LCD connected to the Raspberry Pi.

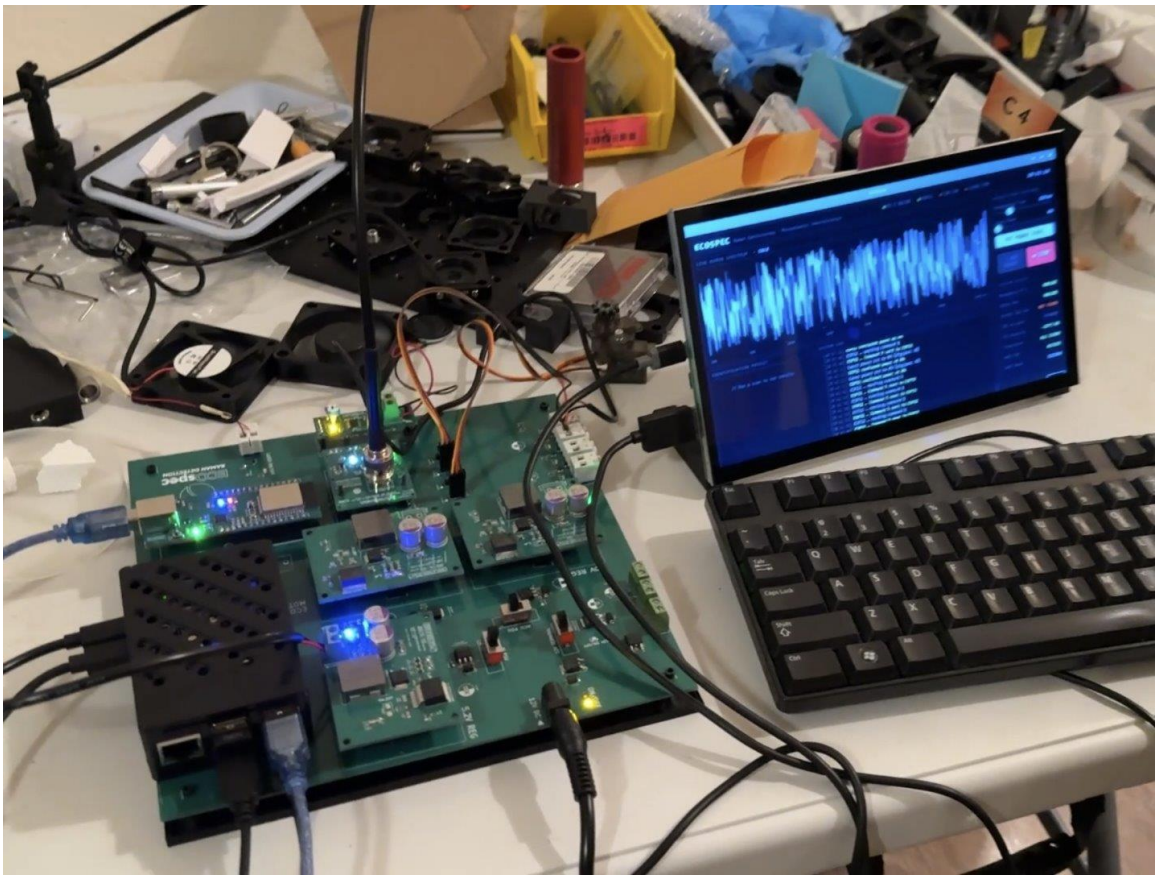

Figure 75 Custom Electrical System Under Full Load

Although we could not collect Raman with our inital system, we were able to meet our 3 main engineering specifications. To begin with, using both the FWHM measurements of the 785 nm, 980 nm laser, and the Argon NIST standard line source, our FWHM measurement met our specification of less than 10 nm. In terms of resolution, after multiple tests with many sources, an average FWHM of 15 pixels was found. An example would be at 980 nm, the average resolution was 9.8 pixels, which equates to 1.49 nm, and a FWHM of 15 wavenumbers. A repeated test was done with the 785 nm line source, demonstrating an average linewidth of 0.273 nm- resulting at a wavenumber resolution of 4.44.

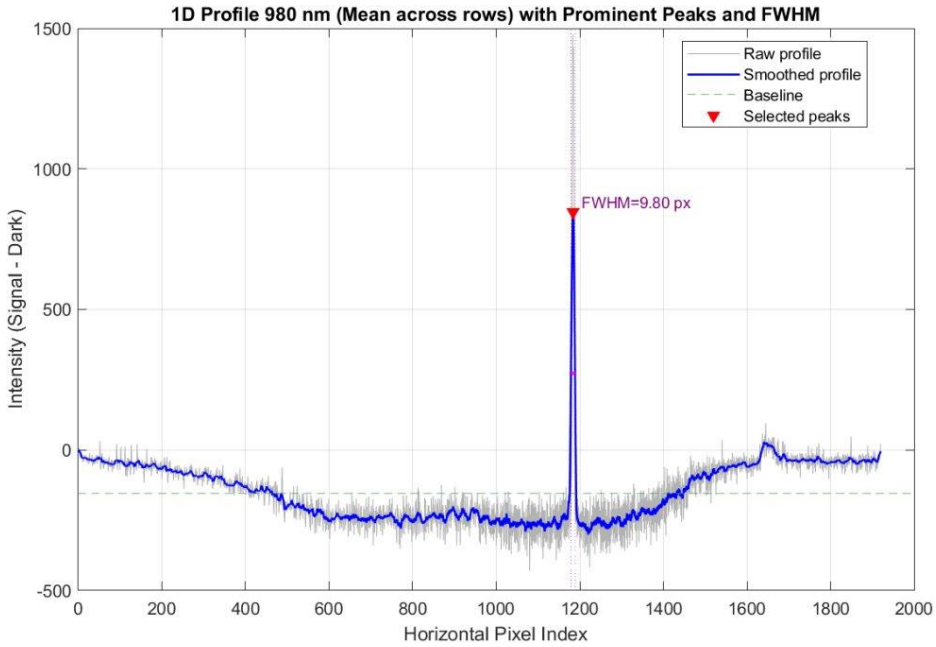

Figure 76 FWHM of 980 nm laser source.

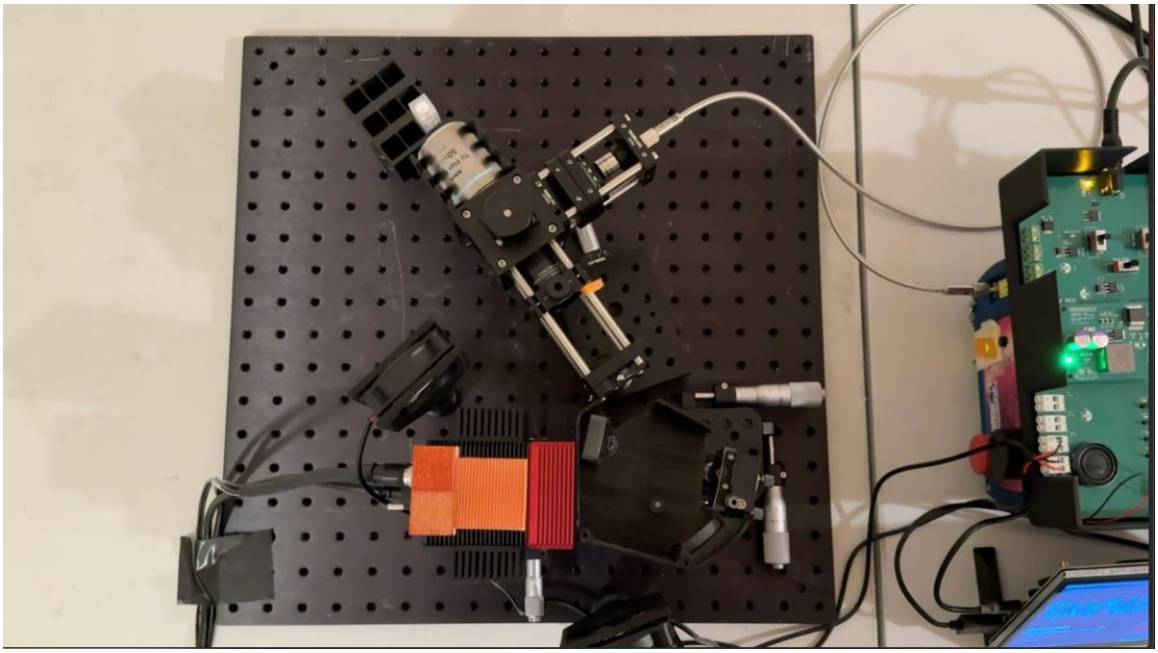
Figure 77 Final Optical Layout, full integration.

11. Administrative Content

11.1. Bill of Materials

Table 47 Project Bill of Materials

Component	Part Name	Count	Unit Price	Total Price
Laser				
785 nm Laser	Ocean Optics LASER-785-IP-ADJ-S	1	Borrowed	Borrowed
BNC Cable	2x Generic Male-Male BNC Cables	1	$10.99	$10.99
RJ11 Connector	25x Generic RJ11 Connectors	1	$6.99	$6.99
30 AWG Wire	25 FT Generic 30 AWG Wire	1	$11.99	$11.99
Fiber	FC-PC/SMA Metal NIR Fiber	2	Borrowed	Borrowed
Optical Components				
1" Mirror Mounts	Thorlabs KM100	2	Borrowed	Borrowed
Translation Stage	Generic Translation Stage	6	Borrowed	Borrowed
Rotation Stage	Generic Rotation Stage	3	Borrowed	Borrowed
Cage Mounted Rotation Stage	ThorLabs	1	Borrowed	Borrowed
Cage Mounts	Thorlabs	3	Borrowed	Borrowed
Quarter Wave Plate	Generic	1	Borrowed	Borrowed
Notch Filter	ThorLabs NF785-33	1	Borrowed	Borrowed
Dichroic Mirror	Semrock RazorEdge 785 nm	1	Borrowed	Borrowed
Long Pass Filter	ThorLabs DMLP805	1	Borrowed	Borrowed
Microscope objective	Nikon 20x CF160 TU Plan Epi ELWD inf.	1	Borrowed	Borrowed
Collection Lens	30 mm	1	Borrowed	Borrowed
Diffraction Grating	830 nm Blaze	1	Borrowed	Borrowed
Curved Gold Mirrors	Generic	2	Borrowed	Borrowed
Detector				
Detector	onsemi ACUROS CQD SWIR 1920-USB3	1	Borrowed	Borrowed
Heatsink	Copper Heatsinks	3	$23.99	$23.99
Heatsink	Aluminum Heatsinks	4	$13.99	$13.99
Thermal Tape	Generic	1	$7.99	$7.99

Fans	4x Generic 60 mm	1	$15.99	$15.99
Sample Preparation				
Quartz Cuvette	Ocean Optics VIS-NIR Quartz Cuvette	1	Borrowed	Borrowed
Sulfur Sample	Soil Acidifier	1	$34.99	$34.99
Sulfur Sample	Pure Poweder Sulfur	1	Borrowed	Borrowed
Processing Systems				
Processing Computer	Raspberry Pi 5	1	$120.00	$120.00
LCD	GeeekPi 10.1” Touchscreen LCD	1	$56.99	$56.99
USB B Cable	Generic	1	$9.99	$9.99
USB C Cable	4x Split Wire USB C	1	$8.99	$8.99
Mini HDMI	Insignia Mini HDMI Cable	1	$27.99	$27.99
PCB Order				
PCB Order 1	JLCPCB Order (02-13-2026) 5x5 Boards + Stencil w/ Shipping	1	$294.53	$294.53
PCB Order 2	JLCPCB Order (03-23-2026) 5x5 Boards + Stencil w/ Shipping	1	$393.25	$393.25
Motherboard				
DC Barrel Jack	Tensility 5.5x2.5 mm Barrel Jack	1	$0.91	$0.91
TVS Diode	SMAJ15A, 15VWM 24.4 VC	1	$0.24	$0.24
Schottkey Diode	MBRD1035CTLT4G	2	$0.61	$1.22
Switches	EG5137-ND 24V 5A DC	4	$3.29	$13.16
PMOS FETs	AO21357	4	$1.13	$4.52
Zener Diode	SMAZ15	4	$0.15	$0.60
Transistors	DMN2056	5	$0.21	$1.05
Flyback Diodes	1N4448W	4	$0.14	$0.56
Side Screw Terminals	Wurth 691137710002 TERM BLK 2POS SIDE ENTRY 5MM	3	$0.34	$1.02
Top Screw Terminals	Wurth 691132700002 TERM BLK 2POS TOP ENTRY 5MM PCB	5	$1.48	$7.40
Gold-Plated Pin Headers	Chanzon 200x Gold Pins	1	$11.99	$11.99
Gold-Plated 2-Pin Sockets	Chanzon 20x 2-Pin Gold-Plated Sockets	1	$8.99	$8.99
Gold-Plated 3-Pin Sockets	Chanzon 20x 3-Pin Gold-Plated Sockets	1	$8.99	$8.99
Gold-Plated 15-Pin Sockets	Chanzon 10x 15-Pin Gold-Plated Sockets	1	$8.99	$8.99
MCU Board				
MCU	ESP32-WROOM-32E-N4	1	$4.84	$4.84

USB Bridge	CP2102QFN28	1	$4.32	$4.32
USB-B Socket	Wurth CONN RCPT USB2.0 TYPEB 4POS	1	$1.29	$1.29
Button	Generic	2	N/A	N/A
Voltage Regulator Board				
Voltage Regulator	TI LM2679SX TO263	3	$9.02	$27.06
Inductor	VSAB1770-220M FIXED IND 22uH 10A 28 mΩ SMD	3	$3.54	$10.62
Output Capacitors	50PZJ180M10X11 - CAP ALUM HYBRID 180uF 20% 50V	6	$1.56	$9.36
Schottkey Diode	MBRD1035CTLT4G	3	$0.61	$1.22
Screw Terminal	Wurth 691137710002TERM BLK 2POS SIDE ENTRY 5MM	1	$0.34	$0.34
Laser Modulation Board				
Digital Potentiometer	TPL0501 100KΩ, 256 positions	1	$2.03	$2.03
LDO	AP7366EA-10W5	1	$0.32	$0.32
Female BNC Connector	Digikey CONBNC001 Generic Female BNC Socket	1	$1.88	$1.88
Transistor	DMN2056	1	$0.21	$0.21
Speaker Board				
Audio Amplifier	TI LM386	1	$1.08	$1.08
Speaker	CLS0281-L152 SPEAKER 8OHM 1W TOP PORT 82DB	1	$5.19	$5.19
Power System Components				
PSU	SUPERNIGHT 12V 30A Switching Power Supply	1	$21.99	$21.99
Power Strip	TBD	1	$14.99	$14.99
Misc				
Servos	4x Miuzei MG90S 9G Micro Servo	2	$13.98	$27.96
3D Printing Filament	ELEGOO 1kg 1.75 mm Black PLA	2	$11.98	$23.96
ESP32 Devkit	3x ESP32 Devkit V1	2	$16.79	$33.58
Crimping Tool	WGGE WG-015 Wire Stripper/Crimping Tool	1	$9.89	$9.89
Spectrometer	Ocean Optics QEPro	1	Borrowed	Borrowed
Halogen	Generic Halogen Lamp	1	Borrowed	Borrowed
Argon	NIST Standard Argon Lamp	1	Borrowed	Borrowed
Mercury	NIST Standard Merucry Lamp	1	Borrowed	Borrowed
Expense Breakdown				
Optical Components		$0.00		

PCB Orders	$687.78
PCB Components	$137.79
Raspberry Pi + UI	$223.96
Detector Cooling	$61.96
Misc	$95.39
System Power	$36.98
Grand Total	**$1308.82**

11.2. Senior Design Milestones

Table 48 Senior Design 1 Milestones

Task	Start Date	End Date	Notes
Group Formation	8/19/25	8/28/25	Form project group on Webcourses.
Project Idea	8/19/25	8/28/25	Brainstorm and finalize project idea.
Committee Formation	8/28/25	9/5/2025	Find a minimum of 2 ECE and 1 PSE faculty members.
D&C Completion	8/28/25	9/5/25	Make a meeting time to meet with necessary advisors.
D&C Meeting	9/10/25 9:00 A.M.	9/10/25 9:30 A.M.	Meet with Dr. Sundaresh & Dr. Kar.
D&C Document Revision	9/10/25	9/12/25	If needed revise D&C document.
Research Components	9/12/2025	TBD	Begin research on potential components for use.
Begin PCB Design	TBD	TBD	Start CAD for PCB.
Optical Midterm Demo		10/07/25	Physical optical demo in undergrad lab
Midterm Milestone Report	9/13/25	10/31/25	Complete Midterm Report.
Midterm Meeting	11/5/2025 9:00 AM		Meet with advisors
Midterm Report Revision	11/3/25	11/7/25	If needed revise Midterm Report.
Final Report		11/25/25	Complete Final Report.
Mini Demo Video		11/25/25	Complete Demo Video.

Table 49 Senior Design 2 Milestones

Task	Start Date	End Date	Notes
Order PCB	1/12/25	1/12/25	Initial order for first rendition.
Fabricate PCB	1/12/25	1/30/25	Begin fabrication of the PCB.

Complete UI	1/12/25	3/15/25	Complete final touches on User Interface.
Finalize Optics	1/12/25	TBD	N/A
Begin fabrication of housing	3/10/25	4/15/25	N/A
PCB design revision	1/12/25	TBD	If necessary, revise the PCB design and order a new one.
Calibration of spectrometer			N/A
Finalize housing	1/12/25	TBD	N/A
Testing	1/12/25	4/22/25	Testing will be done throughout the entire process of fabrication.
Final Adjustments	3/30/25	Week before demo	N/A
Final Live Demo	4/23/25	4/23/25	Present device in front of reviewers and advisors.

12. Conclusion

The development of ECOSpec has shown how a multidisciplinary engineering effort can be organized around a pressing environmental challenge. Microplastics have become a widespread contaminant in water systems worldwide, yet the tools available for identifying their presence remain limited, slow, or inaccessible outside specialized laboratories. This project aimed to investigate whether a compact Raman spectroscopy device could offer a practical and scientifically reliable method for detecting and identifying common microplastic types in aqueous samples. The work completed throughout this phase demonstrates that the foundational research, component selection, system architecture, and feasibility studies are aligned with that goal and that the design has progressed into a stage where continued development will lead toward a functioning prototype.

The project began with extensive research into microplastic pollution, its environmental implications, and the limitations of current detection methods used in academic and industrial settings. This research clarified that traditional analysis techniques often require destructive testing or manual evaluation that depends heavily on operator expertise. Raman spectroscopy emerged as a clear alternative due to its ability to identify materials through their molecular vibrational signatures without destroying the sample. This understanding guided the team to pursue a system architecture that integrates optical excitation and filtering, spectrometer collection, detection, and spectral comparison to known plastic fingerprints. Establishing this scientific grounding early in the project ensured that future engineering decisions remained tied to a justified analytical approach rather than convenience alone.

The project also required evaluating related research efforts, commercial equipment, and previous senior design projects. These comparisons made it possible to identify recurring

engineering challenges such as fluorescence interference, detector noise, optical alignment sensitivity, cooling requirements, laser safety practices, cost constraints, and user handling considerations. Learning from these examples allowed the team to avoid repeating common mistakes while still adapting ideas that have been proven in laboratory environments. This stage also highlighted the value of selecting a 785-nanometer excitation source, long-pass Raman filtering, infinity corrected microscope optics, and a crossed Czerny Turner spectrometer layout. Each of these choices supports better signal clarity, lower fluorescence response in aqueous media, and more reliable material identification within the expected Raman shift range for common plastics such as PET, polystyrene, and nylon.

The engineering design effort required tight coordination across optical, electrical, and software subsystems. The optical subsystem was tasked with delivering a clean and focused excitation beam, filtering out Rayleigh scatter, and capturing Raman-shifted light with sufficient resolution and intensity. The electrical subsystem ensures safe laser operation, detector control, power regulation, thermal stability, and data acquisition. The software subsystem established a complete spectral processing pipeline that handles noise reduction, fluorescence removal, normalization, scaling, comparison algorithms, and user interface presentation. Each subsystem was designed to operate independently while still integrating into a cohesive system, reflecting a deliberate engineering structure suitable for long-term refinement.

Safety and compliance were central throughout the design. The project evaluated and aligned with IEC laser safety classifications, along with IEC standards governing laboratory electronic equipment. These considerations affected enclosure design, interlocks, indicator signaling, thermal protections, and emergency controls. The project also included an analysis of ethical, political, sustainability, and scalability constraints. Recognizing that environmental testing devices may be used by vulnerable communities, regulatory agencies, industrial facilities, or citizen researchers reinforced the importance of transparency, data credibility, and responsible communication of results. These considerations expanded the project beyond a technical exercise and demonstrated awareness of the real-world implications of deploying a pollution detection device.

The feasibility testing completed to this point gives confidence that the system design is moving in the right direction. Laser selection research confirmed that the chosen wavelength supports microplastic identification while reducing fluorescence from water. Detector evaluations helped establish requirements for sensitivity, cooling, and signal integrity. Preemptive measurements and optical alignment evaluations supported the capability of the proposed optical train. These early tests did not represent full system operation but served as validation checkpoints that will reduce technical risk as the project transitions into fabrication and integration.

Administrative planning has also contributed to the likelihood of successful completion. Budget estimates, procurement planning, timeline milestones, prototype fabrication sequencing, and testing schedules have been established. These logistics ensure that the project remains grounded in realistic expectations and can progress through the remaining

phases of senior design without unnecessary delays. The use of collaborative tools and documentation management supports continuity as subsystem work continues in parallel.

As the project moves forward, several key efforts will define the next stage of development. The optical system will be fully assembled and aligned to allow Raman scattering collection in a controlled test environment. The detector and data acquisition hardware will be installed and tested to ensure signal accuracy and noise performance. The software pipeline will be connected to live data rather than simulated spectra, allowing validation of identification accuracy against known samples. The housing will be fabricated to support safety, ergonomics, and component protection. The graphical user interface will be refined to provide intuitive operation for non-technical users while maintaining access to diagnostic information for engineering evaluation. Comprehensive testing will be conducted to evaluate repeatability, sensitivity, specificity, environmental robustness, and system reliability.

The impact of ECOSpec extends beyond the boundaries of a classroom project. If successfully developed, the system could become a valuable tool for water quality monitoring, laboratory verification, industrial compliance, field research, community science programs, and environmental policy support. The modular structure of the design allows for future improvements such as additional polymer classifications, lower detection limits, automated sampling, cloud data integration, or portability for field deployment. The work completed so far demonstrates that the project has a credible scientific foundation, a realistic engineering plan, and a meaningful social purpose.

In summary, the ECOSpec project has progressed from concept to a well-defined and technically justified system design supported by research, feasibility analysis, standards compliance, engineering planning, and multidisciplinary collaboration. The continued development of this work has the potential to produce a functional Raman spectroscopy system capable of identifying microplastics in water in a way that is accessible and informative. The team has laid a strong foundation and is positioned to continue toward prototype fabrication, integrated testing, and demonstration of performance in the next phase of the senior design. The project reflects both engineering capability and environmental responsibility, and it stands as an example of how student innovation can contribute to broader scientific and societal goals.

13. Appendix A Works Cited

[1] M. Co., "In 2024, The Global Plastic Production Will Exceed 400 Million Tons - MARKET NEWS - News," Kitechrecycle.com, Feb. 12, 2025. https://www.kitechrecycle.com/news/in-2024-the-global-plastic-production-will-ex-84661069.html

[2] United States Environmental Protection Agency, "Impacts of Plastic Pollution," www.epa.gov, 2024. https://www.epa.gov/plastics/impacts-plastic-pollution

[3] H. Ritchie, M. Roser, and V. Samborska, "Plastic Pollution," Our World in Data, 2023. https://ourworldindata.org/plastic-pollution

[4] A. R. Aves et al., "First evidence of microplastics in Antarctic snow," The Cryosphere, vol. 16, no. 6, pp. 2127–2145, Jun. 2022, doi: https://doi.org/10.5194/tc-16-2127-2022.

[5] E. Winiarska, M. Jutel, and M. Zemelka-Wiacek, "The potential impact of nano- and microplastics on human health: Understanding human health risks.," Environmental Research, vol. 251, no. 118535, pp. 118535–118535, Mar. 2024, doi: https://doi.org/10.1016/j.envres.2024.118535.

[6] S. Ullah et al., "A review of the endocrine disrupting effects of micro and nano plastic and their associated chemicals in mammals," Frontiers in Endocrinology, vol. 13, Jan. 2023, doi: https://doi.org/10.3389/fendo.2022.1084236.

[7] Y. Lee, J. Cho, J. Sohn, and C. Kim, "Health Effects of Microplastic exposures: Current Issues and Perspectives in South Korea," Yonsei Medical Journal, vol. 64, no. 5, pp. 301–308, Apr. 2023, doi: https://doi.org/10.3349/ymj.2023.0048.

[8] HORIBA Scientific, "What is raman spectroscopy? - HORIBA," www.horiba.com. https://www.horiba.com/usa/scientific/technologies/raman-imaging-and-spectroscopy/raman-spectroscopy/

[9] E. S. Jung et al., "Quantitative Raman analysis of microplastics in water using peak area ratios for concentration determination," npj Clean Water, vol. 7, no. 1, Oct. 2024, doi: https://doi.org/10.1038/s41545-024-00397-4.

[10] I. Chakraborty, S. Banik, R. Biswas, T. Yamamoto, H. Noothalapati, and N. Mazumder, "Raman Spectroscopy for Microplastic Detection in Water sources: a Systematic Review," International Journal of Environmental Science and Technology, vol. 20, Sep. 2022, doi: https://doi.org/10.1007/s13762-022-04505-0.

[11] "How to Choose your Lasers for Raman spectroscopy - Edinburgh Instruments," Edinburgh Instruments, Jul. 13, 2021. https://www.edinst.com/resource/how-to-choose-your-lasers-for-raman-spectroscopy/

[12] AZoM, "AZoM," AZoM, Mar. 30, 2015. https://www.azom.com/article.aspx?ArticleID=11871

[13] "Focusing and Collimating," Newport.com, 2025. https://www.newport.com/n/focusing-and-collimating

[14] R. Keim, "Understanding CCD Output Signals," Allaboutcircuits.com, Apr. 09, 2020. https://www.allaboutcircuits.com/technical-articles/understanding-ccd-output-signals/

[15] P. Whiteaker, "How to calibrate and validate Raman spectroscopy data," ELODIZ, https://www.elodiz.com/calibration-and-validation-of-raman-instruments/ (accessed Sep. 5, 2025).

[16] C. F. Araujo, M. M. Nolasco, A. M. P. Ribeiro, and P. J. A. Ribeiro-Claro, "Identification of microplastics using Raman spectroscopy: Latest developments and future prospects," Water Research, vol. 142, pp. 426–440, Oct. 2018, doi: https://doi.org/10.1016/j.watres.2018.05.060.

[17] M. Naeem, N. Fatima, M. Hussain, T. Imran, and A. S. Bhatti, "Design Simulation of Czerny–Turner Configuration-Based Raman Spectrometer Using Physical Optics Propagation Algorithm," Optics, vol. 3, no. 1, pp. 1–7, Jan. 2022, doi: https://doi.org/10.3390/opt3010001.

[18] S. Schiavi *et al.*, "Plasmonic nanomaterials for micro- and Nanoplastics detection," *Applied Sciences*, vol. 13, no. 16, p. 9291, Aug. 2023. doi:10.3390/app13169291

[20] summary of regional regression results | download table https://www.researchgate.net/figure/Summary-of-Regional-Regression-Results_tbl1_23730322 (accessed Sep. 12, 2025).

[21] Ronald J. Clarke, Anna Oprysa, "Fluorescence and Light Scattering", *Journal of Chemical Education* 2004 81 (5), 705, DOI: https://pubs.acs.org/doi/abs/10.1021/ed081p705#

[22] Brani Vidakovic and Peter Mueller, *Wavelets for Kids: A Tutorial Introduction*, Duke University, 1991. Available from: http://gtwavelet.bme.gatech.edu/wp/kidsA.pdf

[23] "IEC 60825-1:2014," *webstore.iec.ch*. https://webstore.iec.ch/en/publication/3587

[24] "Safety of laser products - Part 1: Equipment classification, requirements and user's guide." Available: https://shop.textalk.se/shop/ws26/40626/files/full_size_-_for_start_page_banner/iec60825-1%7Bed1.2%7Den.pdf

[25] IEC, "IEC 61010-1:2010," *Webstore.iec.ch*, 2016. https://webstore.iec.ch/en/publication/4279

[26] J. Ballato, P. D. Dragic, and M. J. F. Digonnet, "Prospects and challenges for all-optical thermal management of fiber lasers," *Journal of physics. D, Applied physics*, vol. 57, no. 16, pp. 162001–162001, Jan. 2024, doi: https://doi.org/10.1088/1361-6463/ad1ddc.

[27] Occupational Safety and Health Administration, "Laboratory safety guidance," 2011. Available: https://www.osha.gov/sites/default/files/publications/OSHA3404laboratory-safety-guidance.pdf

[28] W. Xu, M. C. Kotecha, and D. A. McAdams, "How good is ChatGPT? An exploratory study on ChatGPT's performance in engineering design tasks and subjective decision-making," *Proceedings of the Design Society*, vol. 4, pp. 2307–2316, May 2024, doi: https://doi.org/10.1017/pds.2024.233

[29] M. Bernabei, S. Colabianchi, A. Falegnami, and F. Costantino, “Students’ use of large language models in engineering education: A case study on technology acceptance, perceptions, efficacy, and detection chances,” *Computers and Education: Artificial Intelligence*, vol. 5, p. 100172, Jan. 2023, doi: https://doi.org/10.1016/j.caeai.2023.100172

[30] M. Cardona, R. Rodríguez, and K. Ishmael, “Artificial Intelligence and the Future of Teaching and Learning Insights and Recommendations,” Office of Educational Technology, May 2023. Available: https://www.ed.gov/sites/ed/files/documents/ai-report/ai-report.pdf

14. Appendix C Raman Fingerprint Peaks of Plastic

Table 6: Known Raman Peaks of PET, PS, and Nylon.

Polymer	Wavenumber (cm^{-1})
PET	633
	854
	1116
	1178
	1288
	1308
	1414
	1452
	1613
	1724
	2895
	2960
PS	616
	795
	1003
	1030
	1150
	1205
	1310
	1352
	1410
	1455
	1527
	1583
	1600

Nylon	2915 3060 880 953 1061 1083 1112 1134 1213 1257 1300 1380 1440 1634 2850 2907 2922 3298

15. Appendix E AI Prompts and Outcomes

[1] https://chatgpt.com/share/69039308-3930-800a-a325-ab593377c8cd